Single and Multiple Wavelength DFB Fiber Lasers

Sigurd Weidemann Løvseth

June 27, 2001

Der theoretisch arbeitende Naturforscher ist nicht zu beneiden, denn die Natur, oder genauer gesagt: das Experiment, ist eine unerbittliche und wenig freundliche Richterin seiner Arbeit. Sie sagt zu einer Theorie nie *ja* sondern im günstigsten Falle *vielleicht*, in den meisten Fällen aber einfach *nein*. Stimmt ein Experiment zur Theorie, bedeutet es für letztere *vielleicht*, stimmt es nicht, so bedeutet es *nein*. Wohl jede Theorie wird einmal ihr *nein* erleben, die meisten Theorien schon bald nach ihrer Entstehung.

Albert Einstein, November 11th, 1922

Abstract

Single mode and multiple mode distributed feedback fiber lasers (DFB-FLs) are analyzed and experimentally investigated, with emphasis on properties that have importance for sensor applications.

It is experimentally found that optical feedback from discrete reflectors and Rayleigh backscattering is a serious challenge for remotely pumped DFB-FL sensors. Strong and long DFB-FL gratings are therefore desired to reduce feedback sensitivity in some sensor applications. Unfortunately, higher order modes can be induced if the DFB-FL grating strength is too high. The threshold grating strength of DFB-FL higher order modes is calculated and compared with the fundamental mode threshold as a function of gain, background loss and various types of grating errors. Higher order modes are found to be greatly enhanced by quadratic chirp. It is proposed to reduce the problem of higher order mode operation by spatially window the gain. The spatial overlap between the fundamental and higher order modes is small, and windowing the gain around the former therefore dramatically increases the threshold of the latter.

A large part of the thesis is devoted to multiple wavelength DFB fiber lasers and gratings. These gratings can be viewed as superpositions of multiple Bragg gratings with different periodicity. A static analysis of multiple wavelength DFB fiber lasers (MW-DFB-FLs) is performed, and the modal powers are calculated as a function of individual grating strength, gain parameters, relative phase and frequency separation between the superimposed gratings, grating phase shift errors, and saturation level of the UV induced refractive index change. Due to spatial hole burning in the form of saturation induced gain gratings, MW-DFB-FLs can operate in multiple modes even if the strengths of the superimposed gratings are not equal. However, both phase shift errors and saturation of the UV induced refractive index could lead to imbalance between the modal output powers.

A comprehensive dynamic model of multimode DFB-FLs is also presented. The dynamics of the spatial distributions of gain, gain gratings, and spontaneous emission is taken into account. The relative intensity noise (RIN) is found for several types of lasers and laser modes, and for some of the lasers as a function of pump RIN and spontaneous lifetime quenching. The modes of MW-DFB-FLs have somewhat more noise than corresponding

single wavelength DFB-FLs, but the RIN of the total output is similar in the two types of lasers. Higher order modes could have several orders of magnitude higher RIN than the fundamental mode.

Further, a distributed sensor based on either an active or passive phase shifted multiple wavelength fiber Bragg grating with novel design is proposed. Depending on the fiber type, a maximum spatial resolution in the range 0.1 - 5 mm is predicted.

Finally, the use of DFB-FLs as acoustic sensors in air is discussed. Two uncoated DFB-FLs are investigated, and the sensitivities vary between 0.61 MHz/Pa at an acoustic frequency of 100 Hz and 0.34 kHz/Pa at an acoustic frequency of 15 kHz. The larger sensitivity at lower frequencies is explained by adiabatic temperature shifts associated with the acoustic wave.

Acknowledgments

Many people deserve my deepest gratitude for helping me complete this work.

First, I would like to thank Kjell Bløtekjær, Jon Thomas Kringlebotn, and Erlend Rønnekleiv. These three people helped me away from murky AlGaAs devices and into the crystal clear world of fiber optics. My supervisor Kjell Bløtekjær has always been there when I needed him, and with his clear mind, helpfulness, and long experience he has given me excellent guidance. Jon Thomas Kringlebotn was essential in defining the original scope of this project, and with his experience with lasers and the fiber optics industry, he has given me many ideas and valuable feedback along the way. Erlend Rønnekleiv has always been a stimulating discussion partner. With his deep understanding of fiber lasers he has never let me off the hook when I came with hasty arguments, and he has been an invaluable source of knowledge for a poor physicist lost in the lab.

I would also like to thank my other colleagues at the Department of Physical Electronics for a stimulating working environment, in particular I would like to thank Helge Engan, Johannes Skaar, Ole Henrik Waagaard, Joar Sæther, and Dag Roar Hjelme for fruitful discussions, and Erik Poppe and Per Gunnar Kjeldsberg for being such great roommates who have accepted my noisy computer and messy desk all these years. I would also like to thank the staff of the department, especially Steinar Smistad and Kolbjørn Lindgjerdet, who have been of help in the lab work.

Parts of the work described in the thesis were performed during a year-long visit to the Optical Fibre Technology Centre (OFTC) at The University of Sydney, Australia. I would like to thank Dmitrii Yu. Stepanov for letting me into his group and sparking my interest for multiple wavelength lasers. I also really appreciated Dima's friendly nature, help through red tape, and the long discussions about international politics. I would also like to express my gratitude to Zourab Brodzeli for the long hours we spent together trying to fabricate lasers, and discussing everything from Sydney giant cockroaches to French women and daily life in Georgia and Russia. Zourab was also very helpful in advising me how to overcome practical problems in the new city, but was unsuccessful in trying to transfer his affection for hanging out at Bondi Beach. Maybe we can take that 24 hour walk (or was it run?) next

time we meet somewhere in the world? With Mark(us) Englund I have shared both the interest in DFB fiber lasers and the destiny of having a thesis to strive with. I really appreciate our friendship and have truly enjoyed our many discussions both during and after my stay in Sydney, and hope to make it to your beloved NT some day! I would also like to thank Director Simon Fleming for inviting me to OFTC. It was a great year in an exciting scientific environment and wonderful country.

Without the support of my family this work would not have been possible. I am especially grateful for the patience and help I have been granted by my wife Siri, particularly during the past year. I also want to thank my children Solveig and Jørgen for help me keeping the right perspective on life. I think we are all looking forward to a postdoctoral life...

Many people have helped me in the editing of this work. Kjell Bløtekjær has read and commented almost all chapters (except this one). Also Erlend Rønnekleiv, Jon Thomas Kringlebotn, Dmitrii Yu. Stepanov, and my wife Siri have read several chapters and been of great help in pointing out completely incomprehensible passages, halting arguments, and grammatical errors. Thank you very much to you all.

Finally, I would like to thank Optoplan AS, my employer since March 2001, for showing such flexibility and generosity during the final stages of this work.

This work was financed by the Norwegian Research Council. I also gratefully acknowledge support from the scholarships Torstein Erbos Gavefond, Marie Bachkes Reiselegat for Ungdom, and Høgskolefondet.

Contents

Chapter 1

Introduction

1.1 DFB Fiber Lasers

The distributed feedback (DFB) laser was first proposed and demonstrated by Kogelnik and Shank [1] in 1970. The cavity boundaries in a DFB laser are not sharply defined by discrete mirrors as in most lasers, but by distributed feedback from a periodic perturbation of either gain or refractive index that runs along the whole laser length, as illustrated in Figure 1.1. This feedback will be wavelength selective, with a maximum at the so-called Bragg wavelength given by:

$$\lambda_B = \frac{n_{\text{eff}}\Lambda_g}{2}. \tag{1.1}$$

Here, Λ_g is the pitch of the periodic structure, or Bragg grating, and n_{eff} is the effective refractive index of the waveguide. The optical frequency corresponding to λ_B is called the Bragg frequency. However, in a uniform index grating, the round trip phase at the Bragg wavelength will be π [2], prohibiting any laser oscillation. Instead two laser modes at each side of the main reflection peak will have the lowest threshold, which could lead to a rather unstable dual-mode operation. This problem was solved by adding a phase shift of π in the center of the grating [3], which results in stable single longitudinal mode lasing at the Bragg frequency. As illustrated in the figure, the power distribution is confined around the center, with the power falling almost exponentially with increasing distance from the phase shift.

DFB fiber lasers (DFB-FLs) [4] have a refractive index grating induced by a holographic UV pattern [5], and gain is provided by doping the fiber with a rare earth element, typical Er^{3+}-ions, and optical pumping. Because of their intrinsic fiber compatibility, relative ease of fabrication, and narrow linewidths in the order of 1-10 kHz, DFB-FLs are promising candidates for a range of applications in sensing and optical communications. An interesting property of DFB-FLs compared with semiconductor DFBs is that they have quite strong hole burning in the form of saturation induced gain gratings.

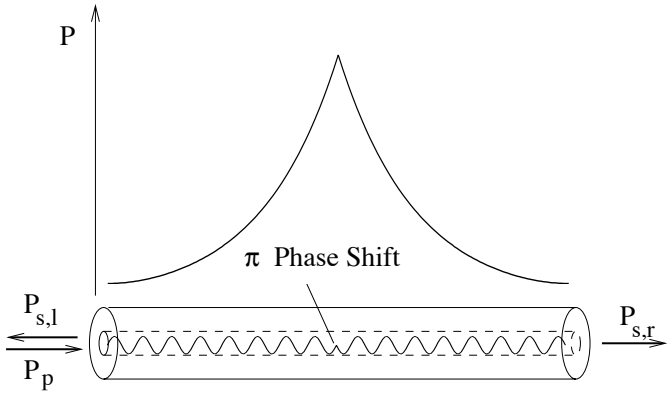

Figure 1.1: Schematic illustration of a distributed feedback fiber laser, with the modal power distribution shown on top. The figure is grossly out of scale, as there are typically $\sim 10^5$ periods of the refractive index modulation in a real DFB-FL. P_p is the power of the incoming pump, whereas $P_{s,l}$ and $P_{s,r}$ are the left and right traveling output powers.

Thus, by superimposing several gratings with different periodicity, multiple wavelength DFB-FLs can be fabricated.

1.2 Outline of the Thesis

The aim of this study is to present numeric models and results that could increase the understanding of single and multiple mode DFB-FL operation, to point out particular challenges for DFB-FLs in optical fiber sensor systems, and propose ways of meeting these challenges.

The thesis is divided in 10 chapters. All chapters, except Chapters 1, 2, 8, and 10, are reproductions of work that is either published, accepted for publishing, or submitted for publishing in scientific journals or conference proceedings, and all chapters, except the current chapter and Chapter 10, can be read independently. Since the chapters are written one by one, there is some variation in notation from article to article. Therefore, a table with definitions of the symbols and acronyms used in the thesis are given in Appendix B.

Chapter 2 contains a review of DFB-FL technology and theory. Specifically, an introduction to the two most important building blocks of the DFB-FL, the fiber Bragg grating and rare earth doped fiber, will be given, and also DFB-FL characteristics, applications, and analysis will be discussed.

In Chapter 3, the effect of exposing DFB-FLs to optical feedback is investigated experimentally. When used as a sensor, especially in offshore

applications, it is likely that an array of DFB-FL sensors will be remotely pumped from a lead fiber that could be several km long. In such systems, the DFB-FL sensors will be exposed to Rayleigh back-scattering from the lead fiber and in some cases discrete reflections from the sidebands of other DFB-FL gratings in an in-line sensor array. The effects of optical feedback to semiconductor DFBs have been well documented, but compared with DFB-FLs, important laser parameter differ by orders of magnitude, as will be discussed in Chapter 2.

In order to get better noise performance and decrease the detrimental effects of optical feedback, high DFB-FL grating strengths are often desirable. Unfortunately, as observed in for instance Chapter 3, DFB-FLs with moderately high grating strengths often operate with one or more higher order modes in addition to the fundamental one. As will be discussed in Chapter 7, these modes see a rather low finesse and are thus particularly noisy. However, for a uniform grating with normal gain parameters, simulations show that such modes should only get close to threshold at very high grating strengths. In order to better understand why higher order mode operation is still seen in practice, Chapter 4 presents a calculation of the threshold margin between fundamental and higher order modes as a function of gain, background loss, and various grating errors.

Chapter 5 proposes a novel solution to the higher order mode problem of high finesse DFB-FLs. By windowing the gain of DFB-FL to fit the fundamental mode, the higher order mode threshold may be substantially increased.

In Chapter 6 a static analysis of multiple wavelength DFB lasers is given. The importance of saturation induced gain gratings for stable multimode lasing is discussed, and modal powers of a dual mode DFB-FL are calculated as functions of a range of parameters, including the strength of each superimposed grating, Bragg frequency separation and phase difference between the gratings, phase shift errors, and saturation level of the UV-induced refractive index change.

Chapter 7 presents a dynamic analysis of single and multiple mode DFB-FLs. The model includes spontaneous emission and the dynamics of the mean gain and gain gratings. The relative intensity noise (RIN) resulting from spontaneous emission and various degrees of pump RIN is presented for various laser structures, such as single mode lasers, lasers with higher order mode operation, and multiple wavelength DFB-FLs with up to 5 superimposed Bragg gratings.

Chapter 8 proposes a new type of distributed fiber grating sensor. The sensor consists of superimposed phase shifted gratings, where the phase shifts of the individual gratings are spatially separated. This type of multi-wavelength grating can either be interrogated as a passive sensor, or, if written in a rare earth doped fiber, it can be used as a multi-wavelength laser. In any case, this type of sensor may have high resolution both in

space and the measurand.

In Chapter 9, theory and measurements of the response of two DFB-FLs exposed to acoustic fields in air are presented. The motivation of this work was both to explore the potential of using DFB-FLs as acoustic sensors, and, perhaps more importantly, to understand the influence of acoustic noise on a DFB-FL used as a source for optical communication or fiber sensor networks. It was found that adiabatic temperature shifts associated with the acoustic fields were more important than the pressure wave itself at lower frequencies.

Finally, in the last Chapter 10 some concluding remarks and suggestions for further studies will be given.

References

[1] H. Kogelnik and C. V. Shank, "Stimulated emission in a periodic structure," *Appl. Phys. Lett.*, vol. 18, pp. 152–154, Feb. 1971.

[2] H. Kogelnik and C. V. Shank, "Coupled-wave theory of distributed feedback lasers," *J. Appl. Phys.*, vol. 43, pp. 2327–35, May 1972.

[3] H. A. Haus and C. V. Shank, "Antisymmetric taper of distributed feedback lasers," *IEEE J. Quantum Electron.*, vol. 12, pp. 532–539, Sept. 1976.

[4] J. T. Kringlebotn, J. Archambault, L. Reekie, and D. N. Payne, "Er^{3+}:Yb^{3+}-codoped fiber distributed feedback laser," *Opt. Lett.*, vol. 19, pp. 2101–2103, Dec. 1994.

[5] G. Meltz, W. W. Morey, and W. H. Glenn, "Formation of Bragg gratings in optical fibers by a transverse holographic method," *Opt. Lett.*, vol. 14, pp. 823–825, Aug. 1989.

Chapter 2

Background

The emergence of distributed feedback fiber lasers (DFB-FLs) [1] is a result of the rapid development of fiber optics technology during the last decades involving multiple disciplines of physics and chemistry[1].

In 1974, only a few years after the DFB laser was reported [3], a patent for DFB fiber lasers was filed [4]. However, practical demonstration of DFB-FLs proved difficult. It was only after the development of high power and low cost pump lasers, techniques for writing fiber Bragg grating utilizing the photosensitivity of some optical fibers, and, not least, rare earth doped single mode fibers with low loss and high photosensitivity, that the first realization of a DFB-FL was reported as much as 20 years later [1].

In this chapter we will give a short introduction to fiber Bragg gratings and erbium doped fibers, and discuss some of the characteristics, applications and analysis methods of DFB-FLs. Hopefully this chapter, and the many references cited herein, will ease the reading of the following chapters.

2.1 Fiber Bragg Gratings

Fiber Bragg gratings were first introduced by Hill et al., who discovered that extremely wavelength selective mirrors could be formed in germanosilicate fibers by letting the fiber guide intense counter-propagating light from an argon ion laser [5]. Either the 488 or 514 nm Ar line could be used, and the original setup is illustrated in Figure 2.1(a). The wavelength selective reflectivity was attributed to periodic perturbation of the refractive index in the fiber created by the standing wave pattern of the light. Such fiber index gratings are today usually called fiber Bragg gratings (FBGs), since the center wavelength of the main reflection peak satisfies the Bragg law known from crystallography, but gratings produced using guided counter-propagating waves are still usually named after Hill. Although some tuning

[1] Readers interested in the fascinating history of fiber optics, will find an excellent starting point in [2].

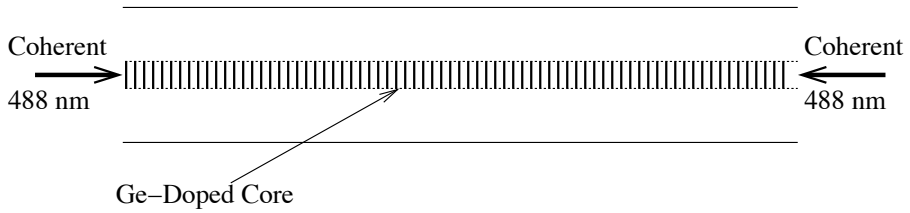

(a) Historic self-induced technique by Hill et al. [5]

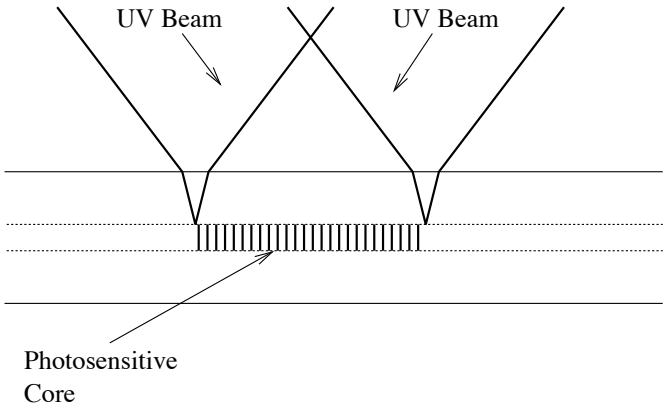

(b) Side-writing technique by Meltz et al. [6]

Figure 2.1: The two principal techniques for FBG fabrication

of the Hill grating periodicity could be achieved by applying strain, the use of counter-propagating guided waves offered little flexibility, since the Bragg wavelength had to be close to the wavelength that wrote the grating. Since the fiber was not photosensitive to infrared light, this ruled out extensive use in for instance telecommunications. An additional problem was that a rather high intensity of light was needed, since the change of refractive index required a two-photon process [7].

Thus, there was relatively little interest in FBGs until Meltz et al. [6] demonstrated the side-writing technique using two coherent UV beams with wavelength 244 nm, as illustrated in Figure 2.1(b). With such a setup, the period of the interference pattern, and thus the Bragg wavelength of the grating, can be increased without limit by changing the angles between the UV beams. In addition, the refractive index increase using UV light is a one-photon effect, and thus much less power is needed to write a grating

with a given strength than when using 488 nm.

UV photosensitivity has been demonstrated for silica fibers with a range of different dopants in addition to Ge, including Sn, B, and Al, and for UV wavelengths other than 244 nm. In order to increase the photosensitivity of the fiber further, hydrogen [8] or deuterium loading can be used. For Ge doped silica fibers, a refractive index shift in the order of $5{\cdot}10^{-4}$ can be achieved, whereas a refractive index shift ~ 0.01 can be made in a hydrogen-loaded fiber. This corresponds to transmission at the Bragg wavelength of only -38 and -876 dB, respectively, for a 1 cm long grating. In all cases, and especially for hydrogen-loaded fibers, the grating strength will decay somewhat over time [9], but long time stability of the grating can be achieved by annealing the gratings at high temperatures. The physical mechanisms behind the UV induced refractive index change are still an area of debate and active research. Examples of popular explanations are that the index change is caused by color center absorption [10], release of built-in tension in the fiber core [11], or local densification [12, 13]. It is not the scope of this thesis to discuss this complicated question in detail, but reviews can be found in [14–16].

Initially, the side-writing technique was implemented by using a beam splitter and an interferometer, for instance a Talbot-interferometer as illustrated in Figure 2.2. In this setup, the Bragg frequency of the grating can be changed by adjusting the mirror angles. In its simplest form, such interferometric setups are only capable of writing gratings with length equal to the UV spot size diameter D_s. However, by moving the fiber relative to the UV spot a grating period Λ_g [17] or steps of multiples of Λ_g [18, 19] between each exposure, longer gratings can be made. Moreover, by controlling the phase between subsequent writing steps, the discrete phase shifts needed for stable single longitudinal mode DFB-FL operation can be included in the structure. Using the same method, also grating with complex profiles including chirp and, through phase dithering, amplitude modulation can be fabricated.

Although highly flexible, the interferometric techniques generally require quite tedious aligning procedures, are sensitive to vibrations and other environmental disturbances, and for writing longer gratings using the step writing technique sophisticated opto-mechanics and opto-electronics are needed. Most commercial FBG manufacturers therefore use the simpler phase mask technique [20] illustrated in Figure 2.3. In this technique, the UV beam is diffracted by a periodic phase mask, and by placing the fiber immediately behind the mask, the -1 and +1 order diffracted beams will produce an interference pattern on the fiber with a pitch Λ_g equal to half the phase mask period Λ_{pm}. By scanning the beam across, gratings can quite easily be made as long as the phase mask. Phase shifts, chirp and amplitude modulation can either be achieved by imprinting the desired grating profile in the phase mask [21], or by moving and dithering the mask relative to the

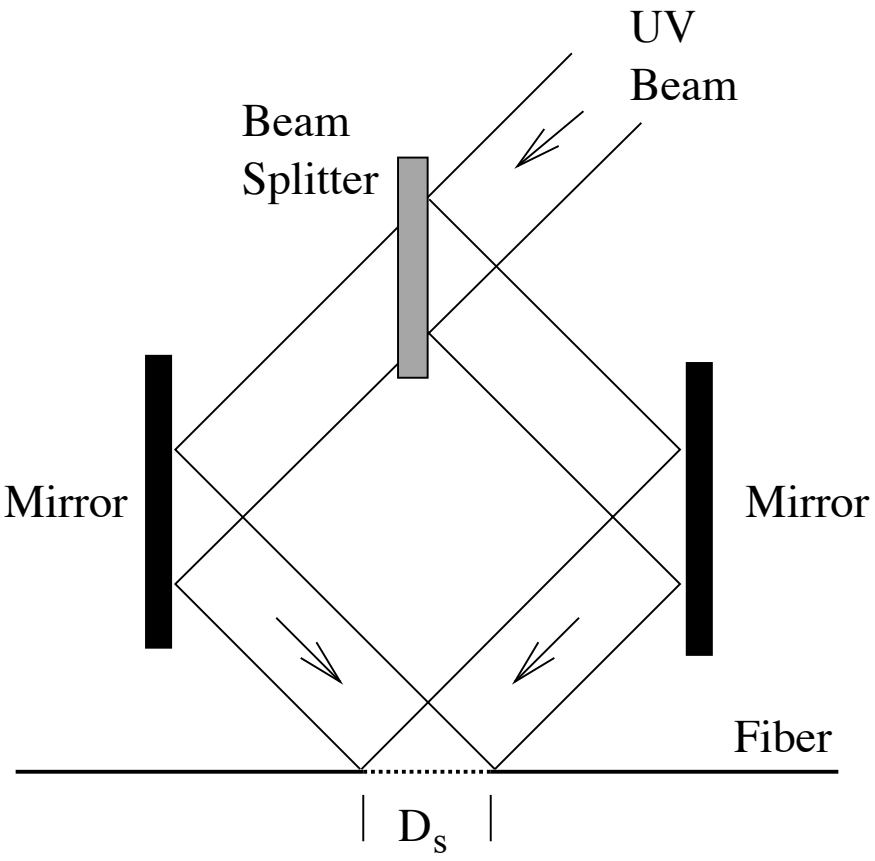

Figure 2.2: Typical interferometric setup for FBG fabrication

fiber [22]. However, when using this direct writing method, each mask offers little wavelength tunability, so in some setups the phase mask is combined with an interferometer [23–25].

2.2 Erbium Doped Fiber Amplifiers

The first optical fiber laser was reported as early as 1964 using Nd^{3+} doped glass [26], and the first erbium doped glass laser was demonstrated shortly thereafter [27]. However, the interest in such devices was small until 1985 when Poole and coworkers managed to fabricate low-loss optical fibers doped with Er^{3+} and Nd^{3+} [28]. Soon the first fiber laser [29] made in single transversal mode erbium doped fiber was reported, and the potential of erbium doped fibers as an optical repeater in the "third telecommunication

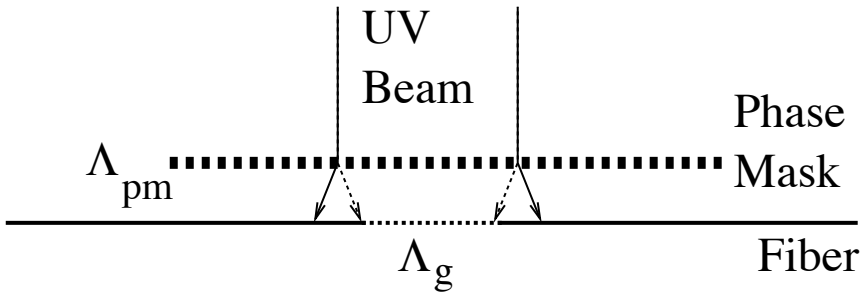

Figure 2.3: Fabrication of FBGs with the phase mask technique

window" around 1550 nm was pointed out [30].

Erbium ions have, like most stable rare earths elements, a multitude of atomic transitions that have been used in experimental glass lasers. However, the 1530 nm transition between the $^4I_{13/2}$ and $^4I_{15/2}$ energy levels has lately received the most attention both from scientific and commercial interests, because of its importance in telecommunications. Today, erbium doped fiber amplifiers (EDFAs) using this transition are used extensively instead of electrical repeaters in long haul fiber optic communication links. With one exception [31], this is also the transition that has been utilized for all reported DFB-FLs. It is beyond the scope of this chapter to discuss the properties of EDFAs in detail[2], but a few important points will be mentioned.

In addition to having a convenient wavelength, the $^4I_{13/2}$ - $^4I_{15/2}$ transition in erbium doped fibers has two properties that make it very favorable for use in optical amplifiers. Firstly, the spontaneous emission lifetime of this transition is quite long, typically around 10 ms. This means that it is possible to invert the gain medium of an EDFA using an optical source with relatively small power, and that there is little cross talk if several signals are amplified simultaneously when their modulation frequency is $\gtrsim 10$ kHz. Secondly, the $^4I_{13/2}$ - $^4I_{15/2}$ transition in EDFAs has a rather broad linewidth. The linewidths of the absorption and gain peaks are broadened due to the splitting of the 7 and 8 Stark levels of the $^4I_{13/2}$ and $^4I_{15/2}$ energy levels, respectively. This splitting is caused by the crystal field of the glass host, and leads to a full width half maximum (FWHM) linewidth that depends on the silica fiber composition. Thus, although the center wavelength of the absorption peak at full inversion is very close to 1531.5 nm for most fibers, the FWHM linewidth varies from 8 nm for a pure silica glass host

[2] A thorough discussion of EDFAs is given in [32–34], in the latter two references also other transitions and rare earth elements are discussed.

to 43 nm for Al-P doped silica [35]. However, the line is shifted to longer wavelengths and widened further if the gain medium is saturated by the signal. Gain flattening of EDFAs remains a very active area of research.

Note that the different Stark levels of the $^4I_{13/2}$ and $^4I_{15/2}$ manifolds are both inhomogeneously and homogeneously broadened. The inhomogeneous broadening is caused by the differences in crystal field seen by the Er^{3+} ions. The homogeneous broadening is a lifetime broadening caused by the rapid phonon-induced transitions between the Stark levels within the $^4I_{13/2}$ and $^4I_{15/2}$ manifolds for a given Er^{3+} ion. Both the homogeneous and inhomogeneous linewidths are of the same order as the Stark splittings at room temperature, and energy can be transferred between different ions through phonon interactions. In practice, the $^4I_{13/2}$ and $^4I_{15/2}$ energy levels therefore have the saturation characteristics of quasi-homogeneously broadening [35].

A consequence of the wide, homgenously broadened bands of the $^4I_{13/2}$ and $^4I_{15/2}$ manifolds is that the absorption and gain peaks of the transition are shifted relative to each other. This could be understood from a detailed balancing approach [36,37], since the bandwidth of both manifolds is larger than kT at room temperature, and the relaxation within each manifold is much faster than the spontaneous emission rate between them. Thus, at a given population inversion level, the EDFA can have net absorption at the low wavelength edge of the transition band, while it has gain at higher wavelengths. This is why the gain spectra of EDFAs shift to higher wavelengths under saturation. The mismatch between the gain and absorption spectra also makes population inversion possible with pumping directly into the $^4I_{13/2}$ manifold at the edge of the transition around 1480 nm [38]. In addition to 1480 nm, 980 nm is today the most popular pump wavelength for EDFAs. As opposed to 1480 nm pumping, full inversion is possible with 980 nm, and the absorption is larger. However, more power is dissipated, and since the erbium absorption peak at 980 nm is quite narrow, pump laser frequency noise could easily lead to noise in the absorption process. Because of the high absorption, it is also difficult to uniformly pump long amplifier structures or arrays with 980 nm. With both pump solutions, the non-radiative decay from the pump-level to the meta-stable laser level is so fast that the gain medium can be modeled as a quasi two-level system [39].

Although the spontaneous emission lifetime of the $^4I_{13/2}$ energy level is quite long for solitary Er^{3+} ions, the effective lifetime can be shortened by a factor of more than 1000 if two or more ions are close to each other. This is caused by a process called cooperative upconversion [40–42], where two or more excited Er^{3+} ions interact. In this process, one ion is de-excited and transfers it excitation energy to another ion, which is upconverted to the higher $^4I_{9/2}$ energy level. Unfortunately, upconverted ion decays quickly and non-radiatively back to the meta-stable $^4I_{13/2}$ level and the excitation energy is lost. The decrease in excited state lifetime eventually leads to a

decrease in the achievable gain if the Er^{3+} concentration increases beyond a certain level. To worsen the problem, the Er^{3+} ions tend to cluster in pure and Ge-doped silica, since Er^{3+} ions are very much larger than the Ge and Si atoms and thus fit poorly in the glass matrix. Cooperative upconversion has thus been identified as the main source of performance degradation of EDFAs [42–45]. However, the degree of clustering can be significantly reduced by doping the fiber core with other dopants than Ge, like Al, P, or Yb. In addition to decreasing the degree of clustering, a combination of the latter dopants increases the absorption of 980 nm [27]. Perhaps the highest gain reported in an EDFA to date was 120 dB/m achieved with a silica core codoped with Lu, P, and Al in addition to Er [46].

2.3 DFB Fiber Laser Characteristics and Applications

2.3.1 Characteristics

Since the demonstration of the first DFB-FL [1], which used a heat induced phase shift to ensure single mode operation, the DFB-FL technology has reached reasonable maturity, and today three manufacturers market DFB-FLs. Permanent center phase shifts are included in the DFB-FL structure either by UV post-processing [47] or during writing [31, 48]. DFB-FLs are for most fibers inherently operating in dual polarization modes. The polarization beat frequency is dependent on the birefringence of the fiber, but is usually in the range 0.5 - 2 GHz. Dual polarization DFB-FLs can be forced to operate in single polarization by twisting [49–51] or injection locking [52], and can be made permanently single polarization by writing a polarization dependent grating [53] or adding a polarization dependent phase shift during post processing [54, 55]. Lasers can be made with either bidirectional or close to unidirectional output by adjusting grating asymmetry [53, 56]. By superimposing DFB gratings with different pitch, it is also possible to fabricate multiple wavelength DFB-FLs [57].

As mentioned in Section 2.2, clustering of Er^{3+} ions in glass may lead to a drastic reduction of the lifetime of the excited state. Under normal conditions, clustered Er^{3+} will therefore act as saturable absorbers with short time constants compared with the other gain atoms. In addition to lowering the gain, it is well known that even a small amount of fast saturable absorbers in a laser cavity leads to a reduced stability margin and even self-pulsing [58–60]. Thus clustering should be avoided at all cost, and normally the maximum gain of a DFB laser fiber is less than 30 dB/m. At the laser wavelength, which normally is above the gain peak for larger output powers and higher lasers stability, the maximum gain could be only fractions of this value. Since the highest feasible Er^{3+} concentration is limited, DFB-

FLs typically have a rather low slope efficiency, often less than 1 % for a 4 cm long laser when pumped with 1480 nm [61], but almost 20 % slope efficiency has been reported for a Er-Yb doped DFB-FL using a 980 nm pump [53].

Because of the rather low gain, quite strong gratings are needed to reach threshold, typically with a mirror round trip transmission loss in the range between -13 dB and -35 dB. For a symmetric and phase-shifted, but otherwise uniform, grating, this corresponds a κl value ranging from 5 to 10, where κ is the coupling coefficient to be defined in Section 2.4, and l is the total grating length. In contrast, semiconductor DFB lasers usually have κl values ranging between 0.5 and 4 [62]. The threshold grating strength depends on the DFB-FL gain and length, which typically is 4 to 10 cm. Fabricating longer DFB-FLs is in principle possible, but maintaining the required grating quality becomes increasingly difficult. Unfortunately, Al or P is needed instead of germanium in the core of erbium-doped fibers in order to reduce clustering, and alumino- and phosphosilicate fibers have low photosensitivity. For Er^{3+} fibers without ytterbium, this problem may be partly solved by codoping aluminum with large fractions of germanium ($> 20\%$) [63], giving a fiber with reasonable photosensitivity and low clustering.

However, often Yb/Er codoping is desired. Not only does Yb increase the 980 nm pump absorption and thus slope efficiency of the laser, but Yb also acts as a buffer that filters out some of the pump-induced noise [64]. A phosphosilicate host is needed for efficient energy transfer between the Yb^{3+} and Er^{3+} [65]. Unfortunately, phosphorus is known to bleach the UV absorption around 240 nm, and strong gratings using this wavelength have only been possible with a high degree of hydrogen loading [66]. Although some photosensitivity in phosphosilicate has been observed using an ArF excimer laser at 193 nm [67], these sources are generally not stable enough to write high quality gratings needed for DFB-FLs. However, the problem of low photosensitivity of phosphosilicate fibers can be avoided by codoping a ring around the fiber core with Ge and B [63]. Strong gratings can then be made in the Ge-doped ring, which overlaps with the fundamental fiber mode and gives sufficient reflectivity levels. Boron is needed to cancel the average refractive index shift otherwise provided by the germanium.

A thorough analysis of the frequency and intensity noise properties of single mode DFB-FLs is given in [60]. The linewidth of DFB-FLs is in the range $\sim 1-10$ kHz [48,60], and DFB-FLs with linewidths of 1 kHz are commercially available. Because of the long cavity and photon life times of DFB-FLs, this linewidth is normally not determined by the spontaneous emission seeding, but rather by thermal fluctuations in the cavity [68]. Thus, unlike many semiconductor lasers, the linewidth of DFB-FLs, although small compared with most lasers, is usually significantly larger than the modified Schawlow-Townes limit [69,70]. Still, it is important to note that the DFB-

FL frequency stability against temperature fluctuations is good, typically 1 GHz/K [71]. The noise spectra of DFB-FLs are characterized by a sharp relaxation oscillation resonance at a few hundred kHz with a rather high Q-value.

Short single mode distributed Bragg reflector (DBR) fiber lasers, where a piece of erbium doped fiber separates two FBGs [72, 73], share many of the favorable properties of DFB-FLs. In fact, these lasers might operate with even narrower linewidths, since the effective cavity length is longer and the relative thermal noise becomes smaller from the central limit theorem. They are also in some ways easier to fabricate, because the FBGs can be made in an ordinary photosensitive fiber without erbium. However, these lasers have lower side mode suppression, and can be subject to mode hopping and multimode behavior for small physical perturbations. However, the side-mode suppression is enhanced with shorter spatial separation between the FBGs until the distance is zero, when the DBR laser becomes a DFB-FL.

2.3.2 Applications

Because of their inherent fiber compatibility, low noise, high stability, and easy selectivity of the laser wavelength, DFB-FLs are promising candidates for a number of telecommunication and sensor applications. In optical communications, most works have focused on the use of DFB-FLs as sources in wavelength division multiplexing (WDM) systems [74–77]. Although the signals from DFB-FLs need to be externally modulated for satisfactory bit-rates, the number of pump lasers and thus system costs can be substantially decreased by multiplexing several DFB-FL channels, either in the same fiber [75], in parallel [77], or by using multimode DFB-FLs [57]. When the pump signal passes through several DFB-FLs the slope efficiency of the system also increases. In either case, high reliability can be ensured by addressing several pump lasers to the same DFB-FL array [77]. Since the modes of a dual polarization or longitudinal mode DFB-FL share essentially the same cavity, the beat frequency between the two modes will be extremely stable, and such DFB-FLs are therefore promising candidates for micro and millimeter wave [78] and soliton generation. Other possible telecom applications include the use of DFB-FLs as a pump for optical phase conjugation [79] and as an absolute wavelength reference [80].

In this thesis, the primary focus is on limitations and possibilities of DFB-FLs in optical fiber sensor systems. Utilizing breakthroughs in optical fiber communications, optical fiber sensor technology has had a tremendous development over the last decades. Several rather recent reviews [81, 82] and books [83–85] are written on this diverse subject. Fiber optic sensors have been developed to measure a range of different physical properties like temperature, strain, static and acoustic pressure, electric current, acceleration, and concentrations of chemical substances. These measurands lead

to changes in the effective index, length, birefringence, Faraday rotation, rare earth gain, and/or Raleigh, Raman, or Brillouin scattering of the fiber, and these shifts are sometimes enhanced for instance by special fiber design, winding the fiber on a mandrel, or using a chemical sensitizer. Advantages of fiber optic sensors compared with traditional sensors include their small size, their immunity to electromagnetic noise, potential for distributed sensing, and that the interrogation electronics can be placed far away from the sensor, which can thus be placed in quite hostile environments. Typically, the changes in fiber properties are measured by use of some kind of optical frequency (OFDR), time (OTDR), or coherence (OCDR) domain reflectometry, or by interferometric means. Perhaps the biggest commercial success of optical fiber sensors so far is the optical fiber gyro [86–88], which makes use of a Sagnac interferometer. Fiber optic gyros are now routinely installed in modern passenger and transport aircrafts [89, 90].

The development of FBGs was a major breakthrough for optical fiber sensor technology [91, 92]. When the effective index or periodicity of the grating is changed by a physical measurand, this can be measured as a shift in the Bragg frequency. FBGs can easily be wavelength multiplexed. The width of the main reflection peak of a uniform FBG is quite broad, typically $\gtrsim$ 20 pm or $\gtrsim$ 2 GHz, corresponding to >2 K or 20 $\mu\epsilon$ resolution in temperature or strain, respectively, but this is sufficient for many purposes. Higher resolution can be achieved by resolving the finer details of the reflection spectrum, and especially high resolution can be achieved by using phase shifted FBGs, which have a narrow notch in the middle of the main peak of the reflection spectrum [93–96].

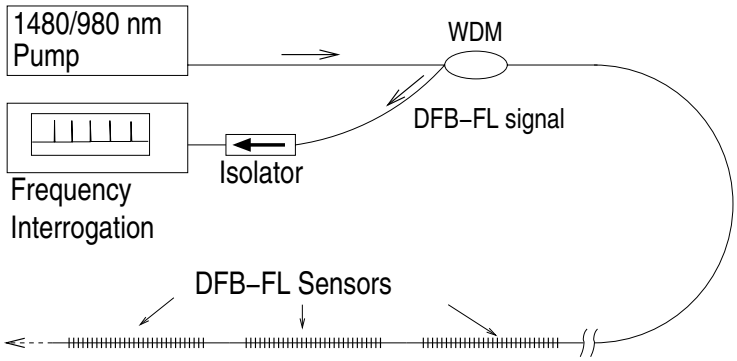

Figure 2.4: Typical DFB-FL sensor array. WDM: Wavelength division multiplexer that separates DFB-FL and pump signal.

A DFB-FL sensor has the same wavelength shift from a physical measurand as a FBG sensor in a similar fiber, but since the linewidth is very narrow, typically 1-10 kHz, high resolution is easily achieved. Just like

FBGs, DFB-FLs can be wavelength multiplexed, as shown in Figure 2.4. In that typical setup, the pump light passes through a wavelength division multiplexer (WDM) and a lead fiber to the DFB-FL sensors. The DFB-FL laser signal could be interrogated at the other end of the fiber, or fed back through the lead fiber and into the 1550 nm arm of the WDM coupler, as illustrated in the figure. Although a 980 nm pump will lead to a higher absorption by the DFB-FL sensors, a 1480 nm pump is preferred in most sensor applications. When pumping with 980 nm, more heat is generated by the DFB-FLs [97], which could perturb the measurements and lead to additional laser noise. In addition, because of the high losses at 980 nm in the silica fiber, serial multiplexing becomes more difficult. In offshore applications the lead fiber could be several km long, in which case the pump light could be seriously attenuated before even reaching the first DFB-FL sensor in an array. Demonstrated sensor applications of single polarization DFB-FLs in the literature include measurements of temperature distribution [97], and sound in water [98, 99] and air [100], the latter results will be presented in Chapter 9. For dual polarization lasers, the beat frequency, which is proportional to the birefringence of the laser, and laser frequency, which is proportional to the optical path length in the grating, do not scale proportionally for different measurands, and this has been utilized for simultaneous measurements of temperature and force [101] and strain [102], respectively. In addition, a simultaneous measurement of strain and temperature employing only two beat frequency measurements has been reported for a dual polarization and longitudinal mode DFB-FL [103].

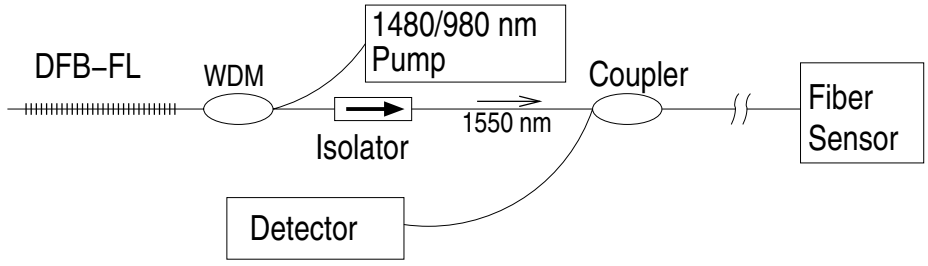

Figure 2.5: Typical setup for a fiber sensor system using a DFB-FL source. WDM: Wavelength division multiplexer that separates DFB-FL and pump signal.

The wavelength of DFB-FLs can be tuned several nm by applying tensile or compressive strain to the fiber. Because of their narrow linewidth compared with conventional tunable lasers, DFB-FLs are also an attractive alternative for interrogating passive fiber sensors based for instance on FBGs or interferometric principles, as illustrated in Figure 2.5. This was clearly demonstrated in [104], where an interrogating system with a relative

accuracy of 30 kHz over a bandwidth of 800 GHz was presented.

2.4 Numerical analysis of DFB-FLs

A large portion of this thesis is devoted to numerical analysis of DFB-FLs, and a short introduction to modeling of single mode waveguides with quasi-periodic structures will therefore be given here.

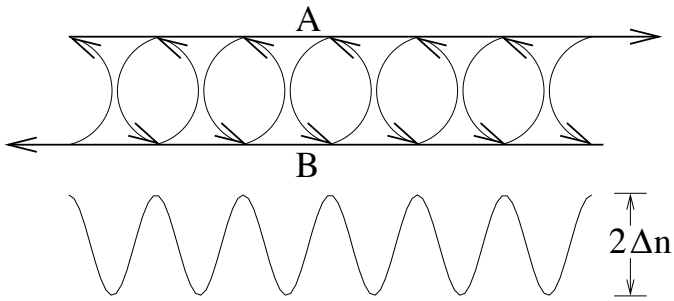

Figure 2.6: Illustration of the interaction between counter-propagating waves in a single mode waveguide with periodic coupling.

The interaction between the counter-propagating waves in a single mode waveguide with a periodic index modulation is illustrated in Figure 2.6. Although other methods exist, for instance the Rouard method adapted from thin film theory [105, 106], the most popular analysis tool for FBGs is the coupled mode theory, which is sometimes also called the coupled wave theory. It was originally developed by Miller [107] to describe coupling between co-propagating waves in transmission lines, but was later extended to waveguides with periodic coupling [108, 109]. Numerous works have since been published that use the coupled mode theory to analyze waveguides with periodic and quasi-periodic index modulation [110–112]. With the addition of gain and gain gratings to the model [113, 114], the coupled mode equations describing the interaction between the forward and backward propagating waves of a single mode waveguide can be written:

$$\begin{aligned} \frac{\partial A}{\partial z} &= (g_0 - j\delta)A + (j\kappa + g_2^*)\,B, \\ -\frac{\partial B}{\partial z} &= (g_0 - j\delta)B + (j\kappa^* + g_2)\,A. \end{aligned} \tag{2.1}$$

Here, A and B are the slowly varying complex amplitudes of the right and left propagating waves, while g_0 is the amplitude gain coefficient. $\delta = \beta - K$ is the detuning of the propagation constant β of the optical waves from the Bragg wave number K, given by $K = \pi/\Lambda_g$, where Λ_g is the

periodicity of the grating. κ and g_2 are the refractive index coupling coefficient and gain-grating coefficient, respectively, of the periodic structure, and the superscript $*$ indicates complex conjugation. These parameters are proportional to the modulation amplitude in refractive index and gain, respectively, as long as the modulation amplitudes are small [113]. Note that the gain grating can be either permanent or saturation induced by the counter-propagating waves [114]. A chirped grating, i.e. a grating with a spatial varying Λ_g, can be modeled either by using a spatial varying δ or by varying the phase of κ and g_2. Equations (2.1) are only valid for a strictly single transverse mode guide, and thus ignores coupling to cladding modes which typically induce some transmission loss a few tens nm below the Bragg wavelength. In addition, higher diffraction orders of the grating are ignored, and it is also required that the relative reflection over a grating period is small. This is true for most FBGs.

In the general case, equation (2.1) can be solved by integration, for instance by first transforming the problem to a Riccati differential equation with only one unknown [110]. However, for uniform gratings exact solutions exist [107, 108]:

$$\begin{bmatrix} A(l) \\ B(l) \end{bmatrix} = T \begin{bmatrix} A(0) \\ B(0) \end{bmatrix} \tag{2.2a}$$

where

$$T = \begin{bmatrix} T_{11} & T_{12} \\ T_{21} & T_{22} \end{bmatrix} = \begin{bmatrix} \cosh\gamma l - j\delta\frac{\sinh\gamma l}{\gamma}, & j\kappa\frac{\sinh\gamma l}{\gamma} \\ -j\kappa^*\frac{\sinh\gamma l}{\gamma}, & \cosh\gamma l + j\delta\frac{\sinh\gamma l}{\gamma} \end{bmatrix}, \tag{2.2b}$$
$$\gamma = \sqrt{|\kappa|^2 - \delta^2}.$$

Here l is the grating length. The gain parameters are omitted for pedagogic reasons, but the full matrix including the gain parameters is given in Chapter 6. T is called the transfer matrix of the grating. A popular method for solving the coupled mode equations for a spatially varying grating is to divide the grating into small sections, and assume that the grating parameters are reasonably constant within each of them. The transfer matrix for each segment is then given in equation (2.2b), and the solution for the whole structure can be found by multiplying the transfer matrices of all the different sections. [115–117]. This is commonly known as the transfer matrix method. It is stable and usually more numerically efficient than direct integration of the coupled mode or the Riccati equations for comparable accuracies.

From the transfer matrix, the transmission and reflection coefficients of the grating are easily found. Specifically, the transmission coefficient t of a

uniform grating becomes [116]:

$$t = \left.\frac{B(0)}{B(l)}\right|_{A(0)=0} = \frac{1}{T_{22}} = \frac{1}{\cosh\gamma l + j\delta\frac{\sinh\gamma l}{\gamma}} \tag{2.3}$$

As long as $|\delta| < |\kappa|$, γ is real, and we get a monotonically decreasing t with increasing l, and the decrease in t is close to exponential for $\kappa l \gtrsim 2$. However, if $|\delta| > |\kappa|$, γ is imaginary, and the transmission coefficient will vary periodically with l. Thus, the frequency band limited by $|\delta| < |\kappa|$ is called the stop band of the grating, and the central peak in the reflection spectrum around $\delta = 0$ will never be narrower than $2|\kappa|$. However, for short gratings the central reflection peak may be significantly wider. For DFB-FLs, the gain medium and possible phase shifts perturb the result given in equation (2.3). However, at lasing, the transmission coefficient of the structure at the laser frequency is infinite, i.e. $T_{22} = 0$, and this may be used to find the laser power and wavelength in a model that includes gain saturation. Alternatively, this condition can be used to find the threshold condition of a laser mode [116].

Both from equations (1.5) and (2.1) it can be deduced that the product between the forward and backward reflection coefficient at $\delta = 0$ is a negative number. Since the round trip phase of a lasing mode needs to be a multiple of 2π, no lasing is therefore possible at the Bragg frequency of DFB lasers with a uniform index grating [113]. The modes closest to the Bragg frequency lie just outside the stop band. However, with a π phase shift in the grating [118], which corresponds to a quarter Bragg wavelength, one of these resonances is shifted to the Bragg frequency. Since the reflectivity is at a maximum at $\delta = 0$, this mode, which is called the fundamental mode of the laser, normally has much lower threshold than the other modes of the phase shifted structure.

We have in this section discussed how to calculate the response of a grating, but excellent inverse scattering techniques also exist to synthesize a grating from a desired response [119–122]. However, these inverse techniques break down for $\kappa l \gtrsim 5$, and are therefore not directly applicable for strong DFB-FL gratings.

References

[1] J. T. Kringlebotn, J. Archambault, L. Reekie, and D. N. Payne, "Er^{3+}:Yb^{3+}-codoped fiber distributed feedback laser," *Opt. Lett.*, vol. 19, pp. 2101–2103, Dec. 1994.

[2] J. Hecht, *City of Light - The Story of Fiber Optics.* The Sloan Technology Series, New York, NY, USA: Oxford University Press, 1999.

[3] H. Kogelnik and C. V. Shank, "Stimulated emission in a periodic structure," *Appl. Phys. Lett.*, vol. 18, pp. 152–154, Feb. 1971.

[4] J. C. Fletcher, C. Elachi, G. A. Evans, and C. Yeh, "Fiber distributed feedback laser." US patent US3958188, May 1976.

[5] K. O. Hill, Y. Fuji, D. C. Johnson, and B. S. Kawasaki, "Photosensitivity in optical fiber waveguides: Application to reflection filter fabrication," *Appl. Phys. Lett.*, vol. 32, pp. 647–649, May 1978.

[6] G. Meltz, W. W. Morey, and W. H. Glenn, "Formation of Bragg gratings in optical fibers by a transverse holographic method," *Opt. Lett.*, vol. 14, pp. 823–825, Aug. 1989.

[7] D. K. W. Lam and B. K. Garside, "Characterization of single-mode optical fiber filters," *Appl. Opt.*, vol. 20, pp. 440–445, Feb. 1981.

[8] P. J. Lemaire, R. M. Atkins, V. Mizrahi, and W. A. Reed, "High pressure H_2 loading as a technique for acheiving ultrahigh UV photosensitivity and thermal sensitivity in GeO_2 doped optical fibres," *Electron. Lett.*, vol. 29, pp. 1191–1193, June 1993.

[9] T. Erdogan, V. Mizrahi, P. J. Lemaire, and D. Monroe, "Decay of ultraviolet-induced fiber Bragg gratings," *J. Appl. Phys.*, vol. 76, pp. 73–80, July 1994.

[10] D. P. Hand and P. S. J. Russel, "Photoinduced refractive-index changes in germanosilicate fibers," *Opt. Lett.*, vol. 15, pp. 102–104, Jan. 1990.

[11] D. Wong, S. B. Poole, and M. G. Sceats, "Stress-birefringence reduction in elliptic-core fibers under ultraviolet-irradiation," *Opt. Lett.*, vol. 17, pp. 1773–1775, Dec. 1992.

[12] M. G. Sceats, G. R. Atkins, and S. B. Poole, "Photolytic index changes in optical fibers," *Ann. Rev. Mater. Sci.*, vol. 23, pp. 381–410, 1993.

[13] B. Poumellec, P. Niay, M. Douay, and J. F. Bayon, "The UV-induced refractive index grating in Ge:SiO2 preforms: Additional CW experiments and the macroscopic origin of the change in index," *J. Physics D*, vol. 29, pp. 1842–1856, July 1996.

[14] J. Albert, "Permanent photoinduced refractive-index changes for Bragg gratings in silicate glass waveguide and fibers," *MRS Bulletin*, vol. 23, Nov. 1998.

[15] A. Othonos and K. Kalli, *Fiber Bragg Gratings-Fundamentals and Applications in Telecommunications and Sensing.* Artech House optoelectronics library, Norwood, Massachussets, USA: Artech House, 1999.

[16] R. Kashyap, *Fiber Bragg Gratings.* Optics and Photonics, San Diego, California, USA: Academic Press, 1999.

[17] B. Malo, K. O. Hill, F. Bilodaeu, D. C. Johnson, and J. Albert, "Point-by-point fabrication of micro-Bragg gratings in photosensitive fibre using single excimer pulse refractive index modifications techniques," *Electron. Lett.*, vol. 29, pp. 1668–1669, Sept. 1993.

[18] R. Stubbe, B. Sahlgren, S. Sandgren, and A. Asseh, "Novel techniques for writing long superstructured fiber Bragg gratings," in *Photosensitivity and Quadratic Nonlinearity in Glass Waveguides (Fundamentals and Applications)*, (Portland, OR, USA), Sept. 1995. Postdeadline paper PD1.

[19] A. Asseh, H. Storøy, B. E. Sahlgren, S. Sandgreen, and R. A. H. Stubbe, "A writing technique for long fiber Bragg gratings with complex reflectivity profiles," *J. Lightwave Technol.*, vol. 15, pp. 1419–1423, Aug. 1997.

[20] K. O. Hill, B. Malo, F. Bilodeau, D. C. Johnson, and J. Albert, "Bragg gratings fabricated in monomode photosensitive optical fiber by a UV exposure through a phase mask," *Appl. Phys. Lett.*, vol. 62, pp. 1035–1037, Mar. 1993.

[21] J. Albert, K. O. Hill, B. Malo, S. Thériault, F. Bilodeau, D. C. Johnson, and L. E. Erickson, "Apodisation of the spectral response of fibre Bragg gratings using a phase mask with variable diffraction efficiency," *Electron. Lett.*, vol. 31, pp. 222–223, Feb. 1995.

[22] M. J. Cole, W. H. Loh, R. I. Laming, M. N. Zervas, and S. Barcelos, "Moving fibre/phase mask-scanning beam technique for enhanced flexibility in producing fibre gratings with uniform phase mask," *Electron. Lett.*, vol. 31, pp. 1488–1490, Aug. 1995.

[23] F. Ouellette and P. A. Krug, "Writing ring interferometer for writing gratings." Australian patent AU7686896A1, 1997.

[24] R. Kashyap, "Assessment of tuning the wavelength of chirped and unchirped fibre Bragg grating with single phase-masks," *Electron. Lett.*, vol. 34, pp. 2025–2027, Oct. 1998.

[25] G. W. Yoffe, J. W. Arkwright, and B. C. Smith, "Flexible and stable interferometer for fabricating fiber Bragg gratings," in *BGPP - Topical Meeting on Bragg Gratings, Photosensitivity, and Poling in Glass Waveguides, Stuart, Florida, USA*, 1999 OSA Technical Digest Series, (Washington D.C., USA), pp. 93–95, Opt. Soc. Am., 1999.

[26] C. J. Koester and E. Snitzer, "Amplification in a fiber laser," *Appl. Opt.*, vol. 3, pp. 1182–1186, Oct. 1964.

[27] E. Snitzer and R. Woodcock, "Yb^{3+}-Er^{3+} glass laser," *Appl. Phys. Lett.*, vol. 6, pp. 45–46, Feb. 1965.

[28] S. B. Poole, D. N. Payne, and M. E. Fermann, "Fabrication of low-loss optical fibres containing rare-earth ions," *Electron. Lett.*, vol. 21, no. 17, p. 737, 1985.

[29] R. J. Mears, L. Reekie, S. B. Poole, and D. N. Payne, "Low-threshold, tunable CW and Q-switched fibre laser operating at 1.55 μm," *Electron. Lett.*, vol. 22, no. 3, p. 159, 1986.

[30] R. J. Mears, L. Reekie, I. M. Jauncey, and D. N. Payne, "Low-noise erbium-doped fibre amplifier operating at 1.54 μm," *Electron. Lett.*, vol. 23, no. 19, p. 1026, 1987.

[31] A. Asseh, H. Storøy, J. T. Kringlebotn, W. Margulis, B. Sahlgren, S. Sandgren, R. Stubbe, and G. Edwall, "10 cm Yb^{3+} DFB fibre laser with permanent phase shifted grating," *Electron. Lett.*, vol. 31, pp. 969–970, June 1995.

[32] E. Desurvire, *Erbium-Doped Fiber Amplifiers.* New York, NY, USA: John Wiley & Sons, 1994.

[33] M. J. F. Digonnet, ed., *Rare-Earth-Doped Fiber Lasers and Amplifiers*, vol. 71 of *Optical Engineering.* New York, NY, USA: Marcel Dekker, 2 ed., May 2001.

[34] D. Hewark, ed., *Glass and Rare Earth-Doped Glasses for Optical Fibres.* No. 22 in EMIS Datareviews Series, London, England: INSPEC, IEE, 1998.

[35] W. J. Miniscalco, "Optical and electronic properties of rare earth ions in glasses," in *Rare Earth Doped Fiber Lasers and Amplifiers* (M. J. F. Digonnet, ed.), vol. 37 of *Optical Engineering*, ch. 2, pp. 19–133, New York, NY, USA: Marcel Dekker, 1 ed., 1993.

[36] A. Einstein, "Zur Quantentheorie der Strahlung," *Physik. Z.*, vol. 18, pp. 121–128, 1917.

[37] D. E. McCumber, "Theory of phonon-terminated optical masers," *Phys. Rev.*, vol. 134, pp. A299–A306, Apr. 1964.

[38] E. Snitzer, H. Po, F. Hakimi, R. Tumminelli, and B. C. McCollum, "Erbium doped fiber laser amplifier at 1.55 μm with pump at 1.49 μm and Yb sensitized Er oscillator," in *Proceedings OFC/OFS '88*, (New Orleans, USA), Optical Society of America, 1988. Postdeadline paper PD2.

[39] C. R. Giles and E. Desurvire, "Modeling erbium-doped fiber amplifiers," *J. Lightwave Technol.*, vol. 9, pp. 271–283, Feb. 1991.

[40] F. E. Auzel, "Materials and devices using double-pumped phosphors with energy transfer," *Proc. IEEE*, vol. 61, pp. 758–786, 1973.

[41] J. C. Wright, "Up-conversion and excited state energy transfer in rare earth doped materials," in *Radiationless Processes in Molecules and Condensed Phases* (F. K. Fong, ed.), pp. 239–295, Berlin, Germany: Springer-Verlag, 1976.

[42] P. Myslinski, D. Nguyen, and J. Chrostowski, "Effects of concentration on the performance of erbium-doped fiber amplifiers," *J. Lightwave Technol.*, vol. 15, pp. 112–120, Jan. 1997.

[43] R. R. Wyatt, "Spectroscopy of rare-earth-doped fibers," in *Fiber laser sources and amplifiers; Proceedings of the Meeting* (M. J. F. Digonnet, ed.), vol. 1171 of *Proc. SPIE*, (Boston, MA, USA), pp. 54–64, Sept. 1989.

[44] P. F. Wysocki, J. L. Wagener, M. J. Digonnet, and H. J. Shaw, "Evidence and modeling of paired ions and other loss mechanisms in erbium-doped silica fibers," in Digonnet and Snitzer [123], pp. 66–79.

[45] J. L. Wagener, P. F. Wysocki, M. J. Digonnet, H. J. Shaw, and D. J. Digiovanni, "Effect of concentration on the efficiency of erbium-doped silica fiber lasers," in Digonnet and Snitzer [123], pp. 80–91.

[46] B. N. Samson, L. Dong, J. P. de Sandro, and J. E. Caplen, "1.2 dB/cm gain in erbium: lutecium co-doped Al/P silica fibre," *Electron. Lett.*, vol. 34, pp. 111–113, Jan. 1998.

[47] P. Varming, J. Hübner, and M. Sejka, "Erbium doped fibre DFB laser with permanent $\pi/2$ phase-shift induced by UV post-processing," in *IOOC-95 Tech. Dig.*, vol. 5, June 1995. Post-Deadline Paper PD1-3.

[48] W. H. Loh and R. I. Laming, "1.55 μm phase-shifted distributed feedback fibre laser," *Electron. Lett.*, vol. 31, pp. 1440–1442, Aug. 1995.

[49] Z. E. Harutjunian, W. H. Loh, R. I. Laming, and D. N. Payne, "Single polarisation twisted distributed feedback fibre laser," *Electron. Lett.*, vol. 32, pp. 346–348, Feb. 1996.

[50] E. Rønnekleiv, M. N. Zervas, and J. T. Kringlebotn, "Modeling of polarization-mode competition in fiber DFB lasers," *IEEE J. Quantum Electron.*, vol. 34, pp. 1559–1568, Sept. 1998.

[51] E. Rønnekleiv, M. N. Zervas, and J. T. Kringlebotn, "Corrections to "Modeling of polarization-mode competition in fiber DFB lasers"," *IEEE J. Quantum Electron.*, vol. 35, pp. 1097–1100, July 1999.

[52] S. Yamashita and G. J. Cowle, "Single-polarization operation of fiber distributed feedback (DFB) lasers by injection locking," *J. Lightwave Technol.*, vol. 17, pp. 509–513, Mar. 1999.

[53] M. Ibsen, E. Rønnekleiv, G. J. Cowle, M. O. Berendt, O. Hadeler, M. N. Zervas, and R. I. Laming, "Robust high-power (>20 mW) all-fibre DFB lasers with unidirectional and truly single polarisation outputs," in *Proc. Conf. Lasers and Electro-Optics (CLEO) 1999*, (Baltimore, MD, USA), pp. 245–246, 1999.

[54] H. Storøy, B. Sahlgren, and R. Stubbe, "Single polarisation fibre DFB laser," *Electron. Lett.*, vol. 33, pp. 56–58, Jan. 1997.

[55] J. I. Philipsen, M. O. Berendt, P. Varming, V. C. Lauridsen, J. H. Povlsen, J. Hübner, M. Kristensen, and B. Pálsdóttir, "Polarisation control of DFB fibre laser using UV-induced birefringent phase-shift," *Electron. Lett.*, vol. 34, pp. 678 – 679, Apr. 1998.

[56] V. C. Lauridsen, J. H. Povlsen, and P. Varming, "Design of DFB fibre lasers," *Electron. Lett.*, vol. 34, pp. 2028–2030, Oct. 1998.

[57] M. Ibsen, E. Rønnekleiv, G. J. Cowle, M. N. Zervas, and R. I. Laming, "Multiple wavelength all-fibre DFB lasers," *Electron. Lett.*, vol. 36, pp. 143–144, Jan. 2000.

[58] A. E. Siegmann, *Lasers.* Mill Valley, CA, USA: University Science Books, 1986.

[59] F. Sanchez, P. Le Boudec, P.-L. François, and G. Stephan, "Effects of ion pairs on the dynamics of erbium-doped fiber lasers," *Phys. Rev. A*, vol. 48, pp. 2220–2228, Sept. 1993.

[60] E. Rønnekleiv, "Frequency and intensity noise of single frequency fiber Bragg grating lasers." To appear in Opt. Fiber Technol., vol. 7, 2001.

[61] E. Rønnekleiv, O. Hadeler, and G. Vienne, "Stability of an Er-Yb-doped fiber distributed-feedback laser with external reflections," *Opt. Lett.*, vol. 24, pp. 617–619, May 1999.

[62] J. Carrol, J. Whiteaway, and D. Plumb, *Distributed feedback semiconductor lasers*, vol. 10 of *IEE Circuits, Devices and Systems series*. London, United Kingdom: The Institution of Electrical Engineers, 1998.

[63] L. Dong, W. H. Loh, J. E. Caplen, J. D. Minelly, K. Hsu, and L. Reekie, "Efficient single-frequency fiber lasers with novel photosensitive Er/Yb optical fibers," *Opt. Lett.*, vol. 22, pp. 694–696, May 1997.

[64] S. Taccheo, P. Laporta, O. Svelto, and G. DeGeronimo, "Theoretical and experimental analysis of intensity noise in a codoped erbium-ytterbium glass laser," *Appl. Phys. B*, vol. 66, pp. 19–26, Jan. 1998.

[65] V. P. Gapontsev, S. M. Matitsin, A. A. Iseneev, and V. B. Kravchenko, "Erbium glass lasers and their applications," *Opt. Laser Technol.*, vol. 14, no. 8, pp. 189–196, 1982.

[66] B. Malo, J. Albert, F. Bilodeau, T. Kitagawa, D. C. Johnson, K. O. Hill, K. Hattori, Y. Hibino, and S. Gujrathi, "Photosensitivity in phosphorus-doped silica glass and optical wave-guides," *Appl. Phys. Lett.*, vol. 65, pp. 394–396, July 1994.

[67] T. Kitagawa, K. O. Hill, D. C. Johnson, B. Malo, J. Albert, S. Theriault, F. Bilodeau, K. Hattori, and Y. Hibino, "Photosensitivity in P_2O_5-SiO_2 waveguides and its applications to Bragg reflectors in single-frequency Er^{3+}-doped planar waveguide," in *Proc. Optical Fiber Communication Conference, OFC'94*, 94. Post deadline paper PD17-1.

[68] K. H. Wanser, "Fundamental phase noise limit in optical fibres due to temperature fluctuations," *Electron. Lett.*, vol. 28, pp. 53–54, Jan. 1992.

[69] A. L. Schawlow and C. H. Townes, "Infrared and optical masers," *Phys. Rev.*, vol. 112, pp. 1940–1949, Dec. 1958.

[70] K. Petermann, *LASER DIODE MODULATION AND NOISE*, vol. 3 of *Advances in Optoelectronics (ADOP)*, ch. 7. Dordrecht, The Netherlands: Kluwer Academic Publishers, 1988.

[71] S. Takahashi and S. Shibita, "Thermal variation of attenuiation for optical fibers," *J. Non-Crystalline Solids*, vol. 30, pp. 359–370, 1978.

[72] G. A. Ball and W. H. Glenn, "Design of a single-mode linear-cavity erbium fiber laser utilizing bragg reflectors," *J. Lightwave Technol.*, vol. 10, pp. 1338–1343, Oct. 1992.

[73] J. L. Zyskind, V. Mizrahi, D. J. DiGiovanni, and J. W. Sulhoff, "Short single frequency erbium-doped fibre laser," *Electron. Lett.*, vol. 28, pp. 1385–1387, July 1992.

[74] M. Sejka, J. Hübner, P. varming, M. Nissov, and M. Kristensen, "Fiber-distributed feedback lasers for high-speed wavelength-division multiplexed networks," in *OFC' 96, Optical Fiber Communication*, vol. 2 of *1996 Technical Digest Series*, (San Jose, CA, USA), pp. 51–52, Opt. Soc. of Am., Feb. 1996.

[75] J. Hübner, P. Varming, and M. Kristiansen, "Five wavelength DFB fiber laser source for WDM systems," *Electron. Lett.*, vol. 33, pp. 139–140, Jan. 1997.

[76] M. Ibsen, A. Fy, H. Geiger, and R. I. Laming, "Fibre DFB lasers in a 4x10 Gbit/s WDM link with a single sinc-sampled fibre grating dispersion compensator," in *Proceedings of ECOC'98-24th European Conference on Optical Communication*, vol. 3, (Madrid, Spain), pp. 109–111, IEEE, Telefonica, Sept. 1998.

[77] M. Ibsen, S. ul Alam, M. N. Zervas, A. B. Grudinin, and D. N. Payne, "8- and 16-channel all-fiber DFB laser WDM transmitters with integrated pump redundancy," *IEEE Photon. Technol. Lett.*, vol. 11, pp. 1114–1116, Sept. 1999.

[78] W. H. Loh, J. P. de Sandro, G. J. Cowle, B. N. Samson, and A. D. Ellis, "40 GHz optical-millimetre wave generation with a dual polarisation distributed feedback fibre laser," *Electron. Lett.*, vol. 33, pp. 594–595, Mar. 1997.

[79] S. Y. Set, S. Yamashita, M. Ibsen, R. I. Laming, D. Nesset, A. E. Kelly, and C. Gilbertas, "High bitrate of a novel optical phase conjugator using inline fibre DFB lasers," in *Proceedings of ECOC'98-24th European Conference on Optical Communication*, vol. 3, (Madrid, Spain), pp. 109–111, IEEE, Telefonica, 1998.

[80] H. Simensen, J. Henningsen, and S. Søgaard, "DFB fiber lasers as optical wavelength standards in the 1.5-μm region," *IEEE Trans. Instrum. Meas.*, vol. 50, pp. 482–485, Apr. 2001.

[81] K. Hotate, "Fiber sensor technology today," *Opt. Fiber Technol.*, vol. 3, pp. 356–402, Oct. 1997.

[82] A. D. Kersey, "A review of recent developments in fiber optic sensor technology," *Opt. Fiber Technol.*, vol. 2, pp. 291–316, July 1996.

[83] J. P. Dakin and B. Culshaw, eds., *Optical fiber sensors*, vol. 1-4. Boston, MA, USA: Artech House, 1988-1997.

[84] E. Udd, ed., *Fiber optic smart structures.* Wiley series in pure and applied optics, New York, NY, USA: Wiley, 1995.

[85] E. Udd, ed., *Fiber optic sensors : an introduction for engineers and scientists.* Wiley series in pure and applied optics, New York, NY, USA: Wiley, 1991.

[86] V. Vali and R. W. Shorthill, "Fiber ring interferometer," vol. 15, pp. 1099–1100, May 1976.

[87] H. Lefevre, *The Fiber-Optic Gyroscope.* Boston, MA, USA: Artech House, 1993.

[88] E. Udd, H. C. Lefevre, and K. Hotate, eds., *Fiber Optics Gyros: 20th Anniversary Conference*, vol. 2837 of *Proc. SPIE*, Nov. 1996.

[89] C. R. McClary and J. R. Walborn, "Fault-tolerant air data inertial reference system development results," in *Position Location and Navigation Symposium*, pp. 31–36, IEEE, Apr. 1994.

[90] G. A. Sanders, B. Szafraniec, R.-Y. Liu, C. L. Laskoskie, L. K. Strandjord, and G. Weed, "Fiber optic gyros for space, marine, and aviation applications," in Udd *et al.* [88], pp. 61–71.

[91] W. W. Morey, G. Meltz, and W. H. Glenn, "Fiber optic Bragg grating sensors," in *Fiber Optic and Laser Sensors VII* (R. P. DePaula and E. Udd, eds.), vol. 1169 of *Proc. SPIE*, pp. 98–107, 1989.

[92] A. D. Kersey, M. A. Davis, H. J. Patrick, M. L. K. P. Koo, C. G. Askins, M. A. Putnam, and E. J. Friebele, "Fiber grating sensors," *J. Lightwave Technol.*, vol. 15, pp. 1442–1462, Aug. 1997.

[93] G. P. Agrawal and S. Radic, "Phase-shifted fiber Bragg gratings and their application for wavelength demultiplexing," *IEEE Photon. Technol. Lett.*, vol. 6, pp. 995–997, Aug. 1994.

[94] J. Canning and M. G. Sceats, "π-phase-shifted periodic distributed structures in optical fibres by UV post-processing," *Electron. Lett.*, vol. 30, pp. 1344–1345, Aug. 1994.

[95] M. LeBlanc, S. T. Vohra, T. E. Tsai, and E. J. Friebele, "Transverse load sensing by use of pi-phase-shifted fiber Bragg gratings," *Opt. Lett.*, vol. 24, pp. 1091–1093, Aug. 1999.

[96] D. Y. Stepanov, J. Canning, and Z. Brodzeli, "High-resolution measurements of fibre Bragg grating transmission spectra," in *Proceedings of ECOC'98-24th European Conference on Optical Communication*, vol. 1, (Madrid, Spain), pp. 407–408, IEEE, Sept. 1998.

[97] O. Hadeler and M. N. Zervas, "Application of a DFB fibre laser temperature sensor for characterizing pump induced temperature distributions along another DFB fibre laser," in *14^{th} International Conference on Optical Fiber Sensors* (A. G. Mignani and H. C. Lefèvre, eds.), vol. 4185 of *Proc. SPIE*, pp. 142–145, 2000.

[98] D. Thingbø, E. Rønnekleiv, and J. T. Kringlebotn, "Intrinsic distributed feedback fibre laser high frequency hydrophone," in *Bragg Gratings, Photosensitivity, and Poling in Glass Waveguides*, OSA Technical Digest, (Washington DC, USA), pp. 57–59, Optical Society of America, 1999.

[99] D. J. Hill and P. J. Nash, "In-water acoustic response of a coated DFB fibre laser sensor," in *14^{th} International Conference on Optical Fiber Sensors* (A. G. Mignani and H. C. Lefèvre, eds.), vol. 4185 of *Proceedings of SPIE*, pp. 33–36, 2000.

[100] S. W. Løvseth, E. Rønnekleiv, J. T. Kringlebotn, and K. Bløtekjær, "Fiber distributed-feedback lasers used as acoustic sensors in air," *Appl. Opt.*, vol. 38, pp. 4821–4830, Aug. 1999.

[101] J. T. Kringlebotn and R. I. Loh, W. H. Laming, "Polarimetric Er3+-doped fiber distributed-feedback laser sensor for differential pressure and force measurements," *Opt. Lett.*, vol. 21, pp. 1869–1871, Nov. 1996.

[102] O. Hadeler, E. Rønnekleiv, M. Ibsen, and R. I. Laming, "Polarimetric distributed feedback fiber laser sensor for simultaneous strain and temperature measurements," *Appl. Opt.*, vol. 38, no. 10, pp. 1953–1958, 1999.

[103] O. Hadeler, M. Ibsen, and M. N. Zervas, "Distributed feedback fibre laser sensor for simultaneous strain and temperature measurements in the RF domain," in *14^{th} International Conference on Optical Fiber Sensors* (A. G. Mignani and H. C. Lefèvre, eds.), vol. 4185 of *Proceedings of SPIE*, pp. 588–591, 2000.

[104] E. Rønnekleiv, J. T. Kringlebotn, and D. Thingbø, "800 GHz continously tunable fiber DFB laser for high speed high accuracy spectral characterization." To be presented at *Topical Meeting on Bragg Gratings, Photosensitivity and Poling in Glass Waveguide (BGGP)*, (Stresa, Italy), paper BWB2, July 2001.

[105] M. P. Rouard, "Etudes des proprietes optiques des lames metalliques tres minces," *Annal. Phys II*, vol. 7, no. 20, 1937.

[106] L. A. Weller-Brophy and D. G. Hall, "Analysis of waveguide gratings: Application of Rouard's method," *J. Opt. Soc. Am. A*, vol. 2, pp. 863-871, 1985.

[107] S. E. Miller, "Coupled wave theory and waveguide applications," *Bell Syst. Tech. J.*, vol. 33, pp. 661–719, May 1954.

[108] S. E. Miller, "On solutions for two waves with periodic coupling," *Bell Syst. Tech. J.*, vol. 47, pp. 1801–1822, Oct. 1968.

[109] S. E. Miller, "Some theory and applications of periodically coupled waves," *Bell Syst. Tech. J.*, vol. 48, pp. 2189–2219, Sept. 1969.

[110] H. Kogelnik, "Filter response of nonuniform almost-periodic structures," *Bell Syst. Tech. J.*, vol. 55, pp. 109–126, Jan. 1976.

[111] *Theory of Dielectric Optical Waveguides*, (New York, NY, USA), Academic Press, 1991.

[112] T. Erdogan, "Fiber grating spectra," *J. Lightwave Technol.*, vol. 15, pp. 1277–1294, Aug. 1997.

[113] H. Kogelnik and C. V. Shank, "Coupled-wave theory of distributed feedback lasers," *J. Appl. Phys.*, vol. 43, pp. 2327–35, May 1972.

[114] W. S. Rabinovich and B. J. Feldman, "Spatial hole burning effects in distributed feedback lasers," *IEEE J. Quantum Electron.*, vol. 25, pp. 20–29, Jan. 1989.

[115] H. Kogelnik and R. Schmidt, "Switched directional couplers with alternating $\Delta\beta$," *IEEE J. Quantum Electron.*, vol. 12, pp. 396–401, July 1976.

[116] G. Björk and O. Nilson, "A new exact and efficient numerical matrix theory of complicated laser structures: Properties of asymmetric phase-shifted DFB lasers," *J. Lightwave Technol.*, vol. 5, pp. 140–146, Jan. 1987.

[117] M. Yamada and K. Saduka, "Analysis of almost periodic distributed feedback slab waveguides via a fundamental matrix approach," *Appl. Opt.*, vol. 26, no. 16, pp. 3474–3478, 1987.

[118] H. A. Haus and C. V. Shank, "Antisymmetric taper of distributed feedback lasers," *IEEE J. Quantum Electron.*, vol. 12, pp. 532–539, Sept. 1976.

[119] R. Feced, M. N. Zervas, and M. Muriel, "An efficient inverse scattering algorithm for the design of nonuniform fiber bragg gratings," *IEEE J. Quantum Electron.*, vol. 35, pp. 1105–1115, Aug. 1999.

[120] L. Poladian, "Simple grating synthesis algorithm," *Opt. Lett.*, vol. 25, pp. 787–789, June 2000.

[121] L. Poladian, "Correction to "Simple grating synthesis algorithm"," *Opt. Lett.*, vol. 25, p. 1400, Sept. 2000.

[122] J. Skaar, L. Wang, and T. Erdogan, "On the synthesis of fiber bragg gratings by layer peeling," *IEEE J. Quantum Electron.*, vol. 37, no. 2, pp. 165–173, 2001.

[123] M. J. Digonnet and E. Snitzer, eds., *Fiber Laser Sources and Amplifiers IV*, vol. 1789 of *Proc. SPIE*, Mar. 1993.

Chapter 3

Stability of Distributed Feedback Fiber Lasers with Optical Feedback[1]

Abstract

The tolerance of two fiber distributed feedback lasers to external back-reflection from discrete reflectors and to Rayleigh back-scattering has been investigated. The results show a reduced feedback sensitivity for the longer laser grating.

3.1 Introduction

Fiber distributed feedback (DFB) lasers used as sensor elements with optical frequency interrogation is an attractive high resolution alternative to passive Bragg grating sensors. Remote pumping and interrogation of such sensor lasers without the use of an optical isolator near the sensing point may be required. However, this will introduce Rayleigh back-scattering into the laser from the lead fiber. If in addition several laser sensors at different wavelengths are serially multiplexed along the same fiber [1], each laser may also experience discrete external reflections from the grating side-bands of the other lasers.

It is known that back-reflections into narrow linewidth semiconductor lasers may cause increased frequency noise, or even self pulsing. The tolerable back-reflection level of such lasers has been found to decrease with increasing external cavity length and with decreasing laser mirror reflectivity [2]. However, important laser parameters such as the frequency and relative linewidth (inverse Q-value) of the relaxation oscillation resonance and

[1] This chapter contains a reedited version of [E. Rønnekleiv and S. W. Løvseth, "Stability of distributed feedback fiber lasers with optical feedback," in *13th International Conference on Optical Fiber Sensors* (B. Y. Kim and K. Hotate, eds.), vol. 3746 of *Proceedings of SPIE*, pp. 466–469, 1999.]

the coherence length of the solitary laser differ largely, typically by orders of magnitude, between semiconductor lasers and fiber DFB lasers. Therefore, few quantitative conclusions can be made about the back-reflection tolerance of fiber DFB lasers from existing work on semiconductor lasers.

In this paper we investigate the feedback attenuation required for stable operation of Er^{3+} fiber DFB lasers experiencing Rayleigh back-scattering or discrete end-reflection from fiber lengths ranging from $\sim$ 10 m to 13 km. We also discuss the possibility of improving the tolerance to back-reflections by increasing the DFB grating strength and/or by using a laser with asymmetric output characteristics.

3.2 Experiments and Results

Two Er^{3+} doped fiber DFB lasers, made by IONAS, Denmark, with grating lengths of 5 and 10 cm and nominal $\pi/2$ phase-shifts at the grating center have been investigated. In the following they will be denoted DFB1 and DFB2, respectively. From a heat scan measurement [3], the coupling coefficients were estimated to $\kappa = 170$ m^{-1} for DFB1 and $\kappa = 150$ m^{-1} for DFB2, giving total grating strengths of $\kappa l = 8.5$ and 15, respectively. Fundamental mode operation at the Bragg resonance frequency was verified for DFB1, while it was found that DFB2 could switch from the fundamental to a higher order longitudinal mode, depending on how the fiber was mounted. The higher order mode of DFB2 was found to be highly asymmetric, with a 15.8 dB ratio between the left and the right output power. When operating in the fundamental mode this ratio was 0.9 dB for DFB1 and 6.0 dB for DFB2. Both lasers were operating in only one polarization mode, and the laser wavelengths were 1551.1 nm for DFB1 and 1554.6 nm for DFB2.

The experimental setup is shown in Figure 3.1. The fiber laser was pumped at 1480 nm from the left through a 1480/1550 wavelength division multiplexer (WDM). Both lasers were pumped through their high output power ends. The output from the 1550 branch of the WDM was guided through a 50 dB optical isolator (ISO) and split by a 3 dB coupler, enabling the fiber laser frequency and the output power from the left to be measured simultaneously. The frequency was measured using a Mach-Zehnder interferometer (MZ), having an imbalance of 101.5 m and fringe sensitivity of 321 kHz/rad. A polarization controller (PC2) was used to optimize the interferometer response, and quadrature operation was ensured by feedback from the differential detector (D1 and D2) to a PZT stretcher inside the interferometer through a low-pass filter (LPF). The laser output power to the left was measured with detector D3, and was kept at 121 μW for DFB1 and 313 μW for DFB2 during all the experiments. The relative intensity noise (RIN) and frequency noise of the lasers without back-reflection in the frequency range from 2.4 to 930 kHz were measured to be 5.6 kHz and -36

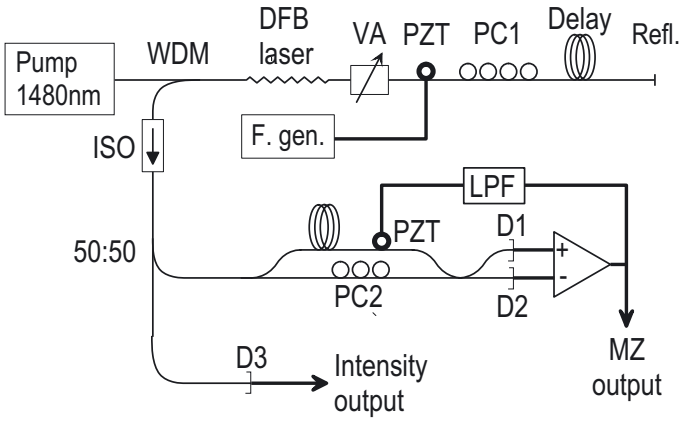

Figure 3.1: Experimental setup for investigation of DFB fiber lasers with optical feedback.

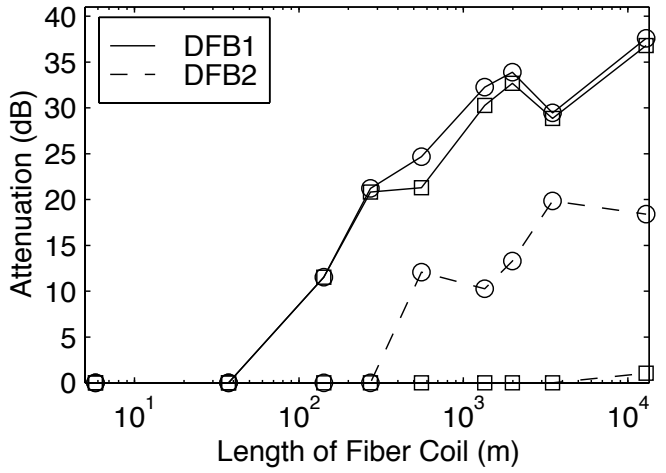

Figure 3.2: Attenuation needed for stable operation in frequency and intensity of DFB1 and DFB2 exposed to Raleigh scattering from fiber delay as a function of delay lengths. Curves with square markers (□) show the smallest attenuation measured to get CW operation (see main text), whereas curves with circular markers (∘) show the smallest attenuation needed for max. ±20 kHz relaxation oscillation amplitude.

dB (RMS values) for DFB1 and 6.5 kHz and -43 dB for DFB2. The 3 dB bandwidth and center frequency of the relaxation oscillations were roughly 8 kHz and 207 kHz for DFB1 and 18 kHz and 238 kHz for DFB2, respectively.

The right end of the fiber laser was connected through a variable optical attenuator (VA) to various fiber delay coils, ranging in length from a few

meters to 13 km. By terminating the ends of the delay coils with bending losses, the effect of Rayleigh back-scattering at different attenuator settings could be investigated. To study the effect of back-reflection from a discrete point, we used a mirror with -0.75 dB reflectivity or a -14.5 dB cleaved fiber end reflector. The PZT phase modulator and the polarization controller (PC1) were used to control the phase and polarization of the feedback signal. Standard telecom fiber of varying fabricates were used in the delay coils, and the back-scattered Raleigh power per unit length may have varied by ± 1 dB between the coils. The lengths and transmission losses were measured with an OTDR. Connector and splice losses were measured, and have been included in the stated attenuation values.

For Rayleigh scattering, one important parameter is the length of back-scattering fiber the laser can tolerate before the noise induced by back-reflection start to dominate over other noise sources. For longer lengths, it is interesting to know the attenuation required to maintain stable operation. The RMS frequency noise of DFB1 seemed unchanged for fiber lengths up to 37 m, but at 142 m the laser was self pulsing with excessive frequency noise. The noise of DFB2 seemed unchanged for lengths up to 273 m. With 13 km of fiber, RMS noise of 37 kHz with bursts of ± 170 kHz could be observed. We also measured the attenuation needed between the delay fiber and the DFB fiber lasers to avoid frequency noise bursts with amplitudes exceeding $\pm$ 20 kHz during a period of 12 s and the attenuation needed for continuous wave (CW) operation for the same duration. By CW operation we mean that the intensity should not have any noise with amplitude larger than 30 % of the DC value.

The results of the Rayleigh measurements are displayed in Figure 3.2. As seen from the figure, DFB2 is considerably more stable than DFB1 for fiber lengths above 100 m. At 13 km, the attenuation needed to avoid excess noise with DFB1 was 19.2 dB higher than with DFB2. DFB2 was only showing small signs of self oscillation at 13 km delay, with only 0.5 dB attenuation required for CW operation. DFB1, on the other hand, started self-oscillations for attenuation levels only slightly below those where the frequency noise started to increase, and at 13 km delay, 36.7 dB attenuation was needed for CW operation. Also note that the attenuation needed seems to approach saturation for the longest fiber delays from 2 to 13 km. This is expected, since the Rayleigh scattering feedback per fiber length levels will be lower far away from than close to the laser due to the fiber transmission losses. In addition, the longest lengths correspond to several relaxation oscillation periods [2].

As discussed by Petermann [2] and others, a discrete reflector will shift both the intensity, frequency, and linewidth of the laser, depending on the phase of the back-reflection. In a real sensor application, the phase of back-reflections may drift at various speeds due to mechanical vibrations in the lead fiber. It is thus interesting to investigate how the laser frequency and

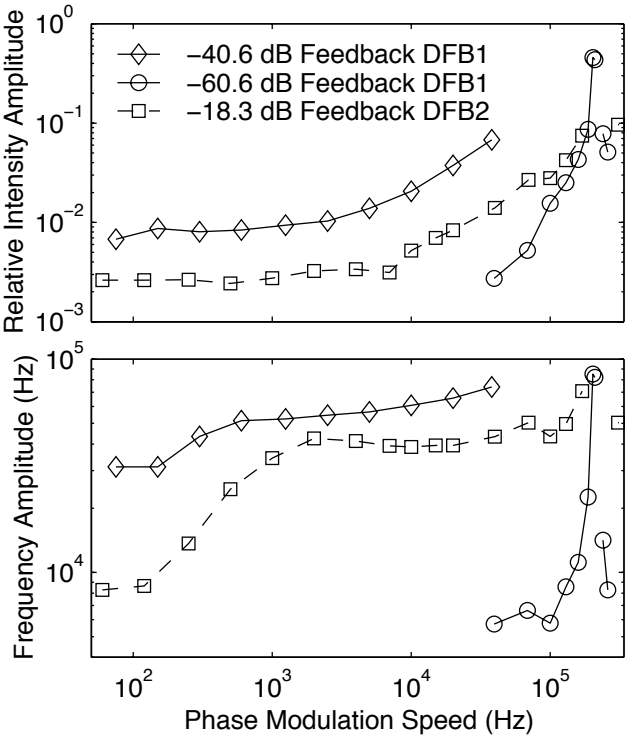

Figure 3.3: Laser intensity (top) and frequency (bottom) response as a function of phase modulation frequency of feedback from a distance of 28.5 m (DFB1) and 29.5 m (DFB2).

intensity amplitudes vary with the phase modulation speed. Setting PC2 to the position of largest possible response, we measured this frequency response for a distance between the reflector and the fiber lasers of 29 meter. Phase modulation was obtained by driving the PZT ring in the delay with a triangular waveform. For phase modulations speeds far below the relaxation oscillation frequencies, this produced fringes in the laser frequency and intensity which easily could be measured with an oscilloscope. For larger phase modulation speeds, large relaxation oscillations were triggered and we had to estimate the frequency response from the Fourier spectra of the oscilloscope traces. The results are shown in Figure 3.3. Note that different feedback levels were used in the measurements, and that DFB1 starts to self-oscillate for modulation speeds close to the relaxation oscillation peak even at a feedback level less than -60 dB.

Similar to the Raleigh scattering case, we measured the largest feedback with less than 6 dB worst case increase in RIN, with less than ± 20 kHz relaxation oscillation amplitude, and with CW laser operation. The two latter results are shown in Figure 3.4. The phase of the feedback was again

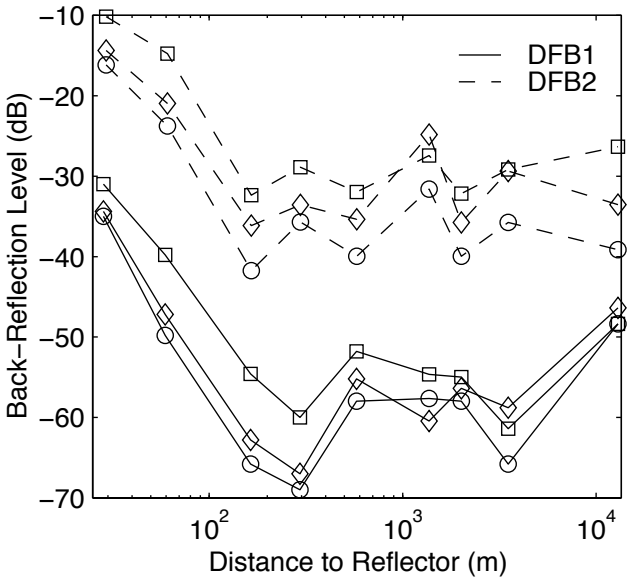

Figure 3.4: Maximum feedback allowed from discrete reflectors for stable operation in frequency and intensity of DFB1 and DFB2. Curves with circular (∘) and square (□) markers show the largest feedback allowed to get a maximum relaxation oscillation amplitude of ± 20 kHz for a back-reflection phase modulation speed of 1 and 10 kHz, respectively. Curves with diamond (⋄) markers show maximum feedback allowed for CW operation for a back-reflection phase modulation speed of 1 kHz

modulated with the PZT, yielding comparable noise bursts at each fringe. The figure shows the feedback level for a phase modulation speed of 1 and 10 kHz for the frequency noise and 1 kHz for the CW limit measurements. The largest feedback levels for 10 kHz are slightly larger than for 1 kHz. The explanation is probably that the laser in the former case are shorter period of time in the unstable regime. The tolerable feedback seems to approach constant levels for delays longer than one relaxation oscillation period, corresponding to a fiber delay of roughly 500 m. This is in agreement with the theory for semiconductor lasers [2].

3.3 Conclusion

We see from the measurements that the 10 cm DFB2 with $\kappa l \approx 15$ can tolerate back-reflection levels that are about 20 dB higher than the 5 cm DFB1 with $\kappa l \approx 8.5$. This is believed to be due to a weaker coupling of the laser modal power of DFB2 to the external cavity [2]. Since the longitudinal mode of operation in this laser during the experiment is not

known, clear conclusions cannot be made about the reason for this weak coupling. If DFB2 was operating in its fundamental mode, an important reason is probably the increased intensity concentration near the phase-shift position for higher κl values [3]. In theory, an increase in κl by 6.5 corresponds to a reduction in coupling efficiency by $e^{-6.5}$, and the tolerable back-reflection level should thus be increased by $20\log_{10}(e^{6.5}) = 56$ dB.[2] Not included in this estimate are possible effects of non-linearities due to the high intensity inside high κl lasers, which may contribute to a reduced stability.

If DFB2 has been operating in the higher order mode, the improved tolerance to back-reflection should rather be explained by the 16 dB output asymmetry of this mode. This corresponds to an external cavity coupling coefficient that is 16 dB lower to the left than to the right, and the tolerable feedback level sho uld thus be higher by 16 dB at the right side. In principle, asymmetric output lasers could be exploited by mounting the laser with the low output end pointing towards the source of back-reflections, i. e. the lead fiber. The expense of such a solution would be a reduced output power returned through the lead fiber.

The maximum length of Rayleigh back-scattering fiber that would give no excess noise without attenuation was found to be around 100 m for DFB1 and around 300 m for DFB2. DFB2 can however be made free from excess noise for all the investigated fiber lengths up to 13 km by introducing a 10 dB attenuator at the laser wavelength near the laser. Again, this would give a 10 dB reduction in output power.

References

[1] K. P. Koo and A. D. Kersey, "Noise and cross talk of a 4-element serial fiber laser sensor array," in *1996 Conf. on Optical Fiber Communications, Technical Digest*, pp. 266–267, 1996.

[2] K. Petermann, "External optical feedback phenomena in semiconductor laser," *IEEE J. of Selected Topics in Q. Elect.*, vol. l, no. 2, pp. 480–487, 1995.

[3] E. Rønnekleiv, M. Ibsen, M. N. Zervas, and R. I. Laming, "Characterization of intensity distribution in symmetric and asymmetric fiber DFB lasers," in *CLEO'98 Tec. Digest*, vol. 6, (San Fransisco), 1998.

[2] In the conference proceeding it was mistakenly written that the tolerable back reflection level is increased by 28 dB.

Chapter 4

”Fundamental and higher order mode thresholds of DFb fiber lasers”

Authors: Lovseth, S.W.; Ronnekleiv, E.;

Published in Journal of Lightwave Technology
Volume 20, March 2002 Page(s):494 – 501

Fundamental and Higher Order Mode Thresholds of DFB Fiber Lasers

Sigurd Weidemann Løvseth and Erlend Rønnekleiv

***Abstract*—Higher order modes are detrimental for distributed feedback (DFB) fiber lasers. The thresholds of these modes are calculated as functions of gain, loss, and various types of grating defects, like harmonic, linear, quadratic, and random chirp, and discrete phase errors. The higher order modes are particularly enhanced by high gain, quadratic chirp, and discrete phase errors close to the center of the grating.**

***Index Terms*—Distributed feedback (DFB) lasers, laser modes, laser stability, optical fiber Bragg gratings (FBGs), optical fiber lasers, optical hole burning.**

I. Introduction

DISTRIBUTED feedback fiber lasers (DFB-FLs) [1] are attractive for a range of optical communications and sensing applications because of their narrow linewidth, short length, and relative ease of fabrication. They are typically made by writing an ultraviolet (UV)-induced Bragg grating in a photosensitive fiber doped with a rare earth element, and externally pumped by a semiconductor source. As with semiconductor DFB lasers [2], stable single-longitudinal-mode operation can usually be achieved by introducing a phase shift in the center of the grating. Permanent single-polarization DFB fiber lasers have been fabricated by writing a polarization-dependent grating [3] or adding a polarization-dependent phase shift during postprocessing [4], [5].

Although DFB-FLs have many similarities with their semiconductor counterparts, many laser parameters differ by orders of magnitude. In particular, DFB-FLs are longer, typically 4–10 cm, and have lower intrinsic loss but also lower gain than semiconductor DFBs. Thus, in order to reach threshold, integrated coupling coefficients κl in the range from five to 10 are usually needed. κ is the coupling coefficient of the grating and l is its length, and the transmissivity of a uniform grating without gain and loss is given by $1/\cosh(2\kappa l)$ at the Bragg frequency. In contrast, semiconductor DFBs usually have grating strengths κl ranging from 0.5 to 4, and typically $\kappa l \approx 2$ [6], which means that their mirror reflectivities are order of magnitudes lower. For DFB-FLs, it is often desirable to be well above the threshold limit in order to reduce sensitivity to backreflection. For sensing applications, backreflection into the cavity can lead to increased frequency noise and even self-pulsing [7]. Unfortunately, if the grating is too strong, DFB-FLs often lase in one or more higher order longitudinal modes in addition to the fundamental, as reported for $\kappa l \gtrsim 14$ in [7], [8]. Typical spatial distributions of a fundamental and higher order mode are shown in Fig. 1. By fundamental mode, we mean a mode with frequency close to the Bragg frequency in the grating stopband and with the power concentrated around the center phase shift. Higher order modes, on the other hand, have a frequency close to the edge of the grating stopband. Such modes are also often called side modes. They have much broader spatial power distributions, and above threshold they will, therefore, usually have larger slope efficiencies than the fundamental modes. The long effective cavity length also means that the thermal noise, which usually is the dominating frequency noise source of the fundamental modes [9], will be lower, and low-finesse distributed backreflection (DBR) fiber lasers with comparable effective cavity length noise experimentally have been found to have a Schawlow–Townes limited linewidth of only 60 Hz [10]. However, because the effective mirror reflectivity for the higher order modes is much lower than that for the fundamental mode, it is far more vulnerable to optical feedback. In addition, the lower cavity finesse also means that the higher order modes have shorter photon lifetimes, leading to much higher intrinsic relative intensity noise (RIN) [11]. Because the higher order modes are spread out in the grating, they are generally also more affected by bending and twisting of the fiber than fundamental modes. Note that even when the side modes have low output power, they will increase the overall RIN and frequency noise by cross-saturation effects. For semiconductor DFBs, it has been found that even when the side modes are suppressed by more than 30 dB, compared with the fundamental modes, they can cause an increase in the laser linewidth [12]–[15]. In DFB-FLs, the mode partition noise will be smaller due to mode selective negative feedback from saturation-induced gain

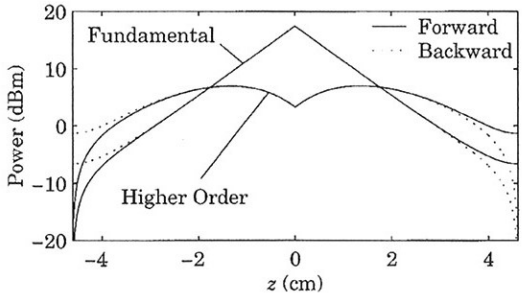

Fig. 1. Power distribution of the forward- and backward-propagating waves of the fundamental and higher order modes of a DFB-FL with $\kappa l = 12.9$ and a quadratic chirp centered at the grating center of 500 GHz/m, corresponding to a detuning between the edge and center of the grating of $\delta_{B,\max} = 1.06$ GHz. Laser parameters are otherwise given in Table I.

Manuscript received May 22, 2001. This work was supported by the Norwegian Research Council.

S. W. Løvseth is with Optoplan A/S, Trondheim N-7448, Norway and also with the Department of Physical Electronics, Norwegian University of Science and Technology, Trondheim N-7491, Norway.

E. Rønnekleiv is with Optoplan A/S, Trondheim N-7448, Norway.

Publisher Item Identifier S 0733-8724(02)01475-5.

gratings [11], and, thus, a somewhat higher side mode level is probably permissible.

The detrimental effect of the higher order modes on the laser performance necessitates an understanding of the physical mechanisms controlling their threshold levels. However, although it has been suggested to increase the threshold of higher order modes by apodization of the laser grating [16] or by winnowing the gain[17], little work has been published that addresses this problem. Despite the strong global spatial hole burning in DFB-FLs, the threshold grating strength for typical fiber gain parameters and grating length is, in theory, as high as $\kappa l \approx 22.5$ for a perfect and uniform grating [18]. The threshold grating strength will, of course, decrease with increasing gain, and will also be affected by other fiber parameters like background loss level. However, it is clear that the relatively low threshold seen experimentally must be caused by grating errors. It is the aim of this work to show to what degree different types of grating defects enhance higher order modes, and what the correlation is between higher order mode threshold and the gain and unbleachable background loss of the laser fiber.

II. Numerical Model and Input Parameters

In order to calculate the modes of the different grating structures, we have solved the coupled mode equation using a transfer matrix method and gain model that are described in detail elsewhere [18]–[21]. The model can calculate the power and frequency of the modes of DFB-FL structures with arbitrary grating amplitudes and phase profiles supporting any number of modes.

The gain model includes local and global spatial hole burning, and in order to account for UV-induced lifetime quenching [22], [21], the model adds the gain contribution from N_{gm} number of gain media, each consisting of a fraction ξ_k of the ions and having a spontaneous emission lifetime quenching by a factor ζ_k, where k is the gain media number. We have assumed that both the fundamental mode and the higher order mode with the lowest threshold are in the same single polarization, implying a polarization dependent grating [3]. The results of a model where polarization effects are taken into account will depend on the type of grating, i.e., if we have a polarization-dependent grating or phase shift. For instance, if only the phase shift were polarization-dependent, the higher order modes would possibly benefit from polarization hole burning. Generally, however, we expect results from a model accounting for polarization effects to be similar to those presented here.

The fiber and laser input parameters of the model include signal (g_s) and pump (g_p) gain at full inversion and signal (a_s) and pump (a_p) absorption at zero inversion, respectively, unbleachable loss (a_0), pump power (P_p), spontaneous emission power before the onset of UV-induced quenching (P_{sp}), and the ratio between the pump and signal wavelengths (r_{wl}). Except where otherwise explicitly stated, the values of the parameters in this work are taken from measurements performed on a codoped erbium–ytterbium DFB-FL presented in [21] and are summarized in Table I. In all calculations, we have assumed a grating length of $l = 9.22$ cm. We have assumed a grating with uniform coupling strength and with a center phase shift of π. All DFB-FLs are pumped from the left with a pump power of $P_p = 140$ mW. The modal threshold coupling coefficient is found by iteration with an accuracy of at least $\Delta\kappa = 0.5\ \mathrm{m}^{-1}$.

TABLE I
Laser Parameters Used in the Calculations

Parameter	Value
g_s	15.9 dB/m
a_s	11.7 dB/m
g_p	3.0 dB/m
a_p	8.9 dB/m
a_0	0.24 dB/m
P_{sp}	4.1 mW/m
P_p	140 mW
N_{gm}	2
$\xi_2 = 1 - \xi_1$	0.38
$[\zeta_1,\ \zeta_2]$	[1, 26]
r_{wl}	1480/1550=0.955
l	9.22 cm

III. DFB-FL Threshold Dependence on Fiber Parameters

A. Gain

In order to obtain higher laser slope efficiency, high gain fibers are preferred for most DFB-FL applications. Phosphosilicate fibers codoped with erbium and ytterbium [23], [3] yield the best results in the 1500-nm telecommunications window because ytterbium increases the absorption of 980-nm pump light and reduces the cooperative upconversion effects of erbium clusters. Unfortunately, high-power DFB-FLs, particularly when pumped with a 980-nm source, are significantly affected by self-heating [24], which leads to grating chirp, lower stability, and excess noise. Thus, in some applications where low linewidth is important, fibers with lower gain but higher photosensitivity are preferred, and 1480-nm pumps are used in order to minimize pump induced heating.

However, if we have higher order modes above threshold, the stability of the fundamental mode is of little interest. Laser thresholds are often expressed in terms of gain or pump power. For a DFB-FL, however, almost maximum gain for a given pump wavelength is obtained for a relatively low pump power. Therefore, we have chosen to look at thresholds in terms of integrated grating strength $\kappa_{\mathrm{th}} l$ instead of gain, because the former remains easier to manipulate for a DFB-FL designer. Yet, the dependence between threshold in gain and in grating strength is of interest, and, in Fig. 2, modal thresholds in integrated coupling coefficient $\kappa_{\mathrm{th}} l$ are plotted as functions of signal gain at full inversion g_s for perfect, uniform gratings. The other gain parameters a_s, g_p a_p, and P_{sp} are scaled proportionally with g_s to simulate the effect of varying the concentration of the gain atoms or their overlap with the fundamental mode of the fiber.

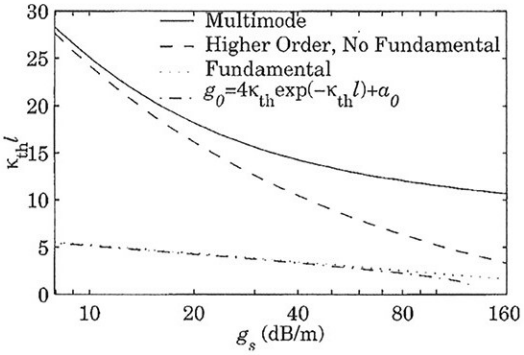

Fig. 2. Threshold integrated coupling coefficient $\kappa_{\rm th}l$ of the fundamental mode and for lasing in higher order modes with and without the fundamental mode present as a function of the signal gain at full inversion g_s. The other gain parameters a_s, g_p, a_p, and $P_{\rm sp}$ are scaled proportionally with g_s from the values given in Table I. Also shown is the analytical estimate of the fundamental mode threshold given in (1), which is valid for $\kappa_{\rm th}l \gg 1$.

Concentration-dependent effects like cooperative upconversion are ignored. The threshold for higher order mode operation with and without the fundamental mode present is shown together with the threshold of the fundamental mode itself. Note, however, that because the fundamental mode threshold is lower than the higher order mode threshold for a uniform π phase-shifted DFB-FL grating, it is not physical to have higher order modes present without the fundamental mode.

For $\kappa l \gg 1$ and reasonably low values of the laser gain g_0, the cavity mirror reflectivity for the fundamental modes in the center of the grating stopband is $R \approx 1 - 4\exp(-\kappa l)$, whereas the effective cavity length is $l_{\rm eff} \approx 1/\kappa$, yielding

$$g_0 \approx 4\kappa_{\rm th}\exp(-\kappa_{\rm th}l) + a_0. \tag{1}$$

At threshold, there is no saturation, and g_0 can easily be calculated from the gain parameters and the value of the pump power [19]. From Fig. 2, we see that we have a good fit between the analytical formula (1) and our numerical model even for relative small values of $\kappa_{\rm th}l$.

Calculations of the threshold of higher order modes are more complex even with large values of κl, and there is no counterpart to (1). However, from Fig. 2, it is clear that the higher order mode threshold in absence of the fundamental mode decreases faster with increasing gain than the fundamental mode threshold. However, the difference in threshold g_s between the two types of modes increases from 87 dB/m at $\kappa_{\rm th}l \approx 5.5$ to 115 dB/m at $\kappa_{\rm th}l = 3.3$. Because the effective cavity length of the fundamental mode equals $1/\kappa$ for $\kappa l \gg 1$, the overlap between the higher order modes and fundamental mode increases with decreasing κ. Thus, the difference in threshold g_s between the fundamental mode and the higher order modes with the fundamental mode present is very large for low values of κl.

In short, it is possible to design stable single-mode DFB-FLs regardless of the fiber gain chosen, but because $\kappa_{\rm th}l$ for the higher order mode threshold decreases with increasing g_s, a compromise between slope efficiency and fundamental mode cavity finesse has to be made in cases where backreflection into the cavity is an issue.

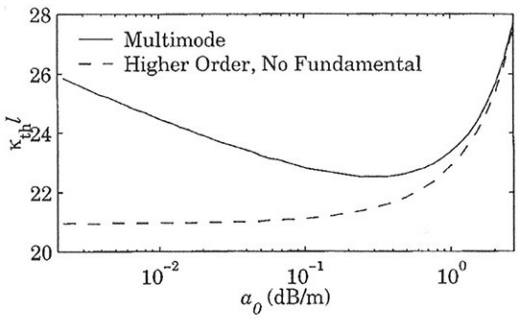

Fig. 3. The threshold κl of the higher order modes as a function of unbleachable loss a_0. $g_s = 15.9$ dB/m, as in Table I. Compared with the higher order mode $\kappa_{\rm th}l$, the fundamental mode thresholds do not vary much in the plotted interval of a_0.

Instead of scaling the gain parameters g_s, a_s, g_p, a_p, and $P_{\rm sp}$, the round-trip gain of the modes could be scaled by changing the device length l. However, the threshold curves of Fig. 2 would then look different because the round-trip background loss a_0 also scales with l. As will be discussed in Section III-B, a_0 is very important for higher order mode thresholds.

B. Unbleachable Loss

The intrinsic unbleachable loss a_0 in DFB-FLs is usually much higher than in standard telecom fibers; commonly assumed major sources of the increase in a_0 are UV exposure [25] and, when used, hydrogen or deuterium loading of the fiber for increased photosensitivity. In Fig. 3, we have plotted the higher order mode thresholds with and without the fundamental mode present as a function a_0. As expected, the threshold without the fundamental mode increases monotonically with increasing loss. More interesting, perhaps, is that the threshold with the fundamental modes present has a minimum near $a_0 \approx 0.2$, i.e., close to the measured value in Table I. The reason that the multimode threshold increases for lower values of a_0 is the increase in the gain saturation power of the fundamental mode. For small values of a_0 and moderate values of κl, the fundamental mode will saturate the gain in most of the grating structure. However, if the grating strength and a_0 became large enough, a_0 would become the dominating loss mechanism [18], [26]. The maximum power of the fundamental mode around the center phase shift will then not increase with increasing κl, and the fundamental mode will saturate the gain at the ends of the structure less effectively because the ratio $l_{\rm eff}/l$ becomes smaller. However, as long as $a_0 \lesssim 0.1$, the higher order modes will not be significantly affected by the intrinsic losses because of their larger mirror losses, but will benefit from the increasing gain left by the fundamental mode with increasing a_0. For lower κl, the fundamental mode has relatively large mirror losses as well, and its threshold, which is not included in Fig. 3, does not change significantly with a_0 in the plotted interval. However, even if the measured value of $a_0 = 0.24$ dB/m is close to the minimum of the higher order mode $\kappa_{\rm th}l$ curve, purposely increasing a_0 further is probably not a good idea because it would decrease the output power and increase the RIN [9] of a DFB-FL written in the fiber. On the other hand, low values of a_0 would ensure both high side-mode suppression and large output power.

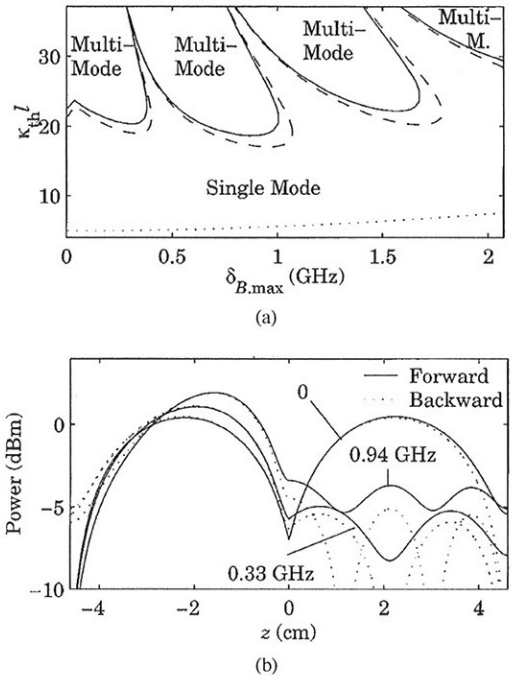

Fig. 4. (a) The thresholds of higher order and fundamental mode operation for a DFB-FL with linear chirp as a function of detuning between the center and edge of the grating. Curve definitions as in Fig. 2. (b) The power distribution of the forward- and backward-propagating waves of the lasing higher order modes of a DFB-FL with linear chirp corresponding to a detuning $\delta_{B,\max}$ of 0, 0.33, and 0.94 GHz in Bragg frequency between the center and the outer edge of the grating, and with κl at 23.0, 19.4, and 17.5, respectively.

IV. Effect of Grating Errors

From Section III it is clear that the low higher order mode threshold of $\kappa_{\text{th}}l \sim 14$ found experimentally cannot be explained from the laser gain and loss parameters alone, but probably by a combination of grating errors and relatively high gain and intrinsic loss. Grating errors can arise from a number of different sources that will produce different types of grating errors, and we will here discuss the most typical ones and their effect on higher order and fundamental mode threshold.

A. Linear and Quadratic Chirp

Unintended linear and/or quadratic chirp is a common problem in grating writing setups and can come from a number of different sources, including drift of the laser power and beam direction, fiber photosensitivity and diameter variations [27]–[29], misalignments of the setup, and, for strong gratings, variation in the degree of coherence between the interfering beams along the fiber grating [18]. Quadratic-like chirp profiles can also be induced by self-heating caused by the fundamental mode and the nonradiative decay from the pump level to the upper laser level, especially for high power DFB-FLs pumped at 980 nm.

In Fig. 4, we have plotted the thresholds of the fundamental mode and higher order modes as functions of linear chirp. The chirp is quantified in terms of detuning in Bragg frequency between the center and edge of the grating, $\delta_{B,\max}$. The power distribution of the higher order mode with the lowest threshold

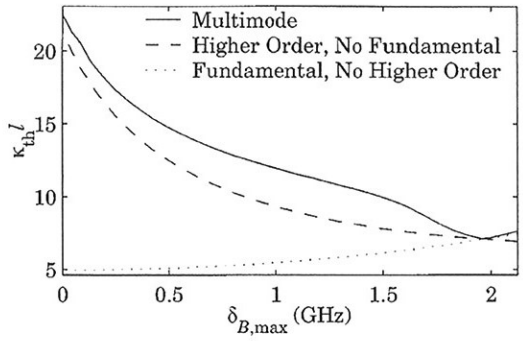

Fig. 5. Thresholds as functions of quadratic chirp quantified by maximum detuning between the center and outer edge of the grating $\delta_{B,\max}$.

is shown in the lower half of the figure for selected values of $\delta_{B,\max}$. As the chirp increases, the side-modes are detuned relative to the grating period in one half of the grating, and will increasingly only be supported by and oscillate in the opposite grating half. The asymmetry of the higher order modes leads to a small difference in $\kappa_{\text{th}}l$ between modes with opposite detuning from the mean Bragg frequency, since the DFB-FL is pumped from the left. The linear chirp also broadens the reflection spectrum and perturbs the round-trip phase of the higher order modes, and this leads to a slightly lower higher order mode $\kappa_{\text{th}}l$ for some values $\delta_{B,\max}$ compared with the uniform grating case $\delta_{B,\max} = 0$. With increasing linear chirp, the effective cavity length, and at some point also the cavity finesse, of a given higher order mode decreases, resulting in a mode hop to the next higher order mode. Each mode hop is associated with the occurrence of an extra lobe in the spatial power distribution, as seen in the lower half of Fig. 4. However, regardless of the value of the linear chirp, the higher order mode threshold remain high, and for $\delta_{B,\max} \gtrsim 1$ GHz the local minimum levels of the multimode $\kappa_{\text{th}}l$ curve seem to increase rapidly with increasing $\delta_{B,\max}$. Thus, linear chirp is probably not a major cause of higher order mode operation. However, linear chirp causes a decrease in the cavity finesse seen by the fundamental mode, leading to an increase of its threshold.

In Fig. 5, we have plotted the threshold for higher order and fundamental modes of DFB-FLs with quadratic chirp symmetric around the center of the grating. In contrast to linear chirp, even a relatively small amount of quadratic chirp leads to a drastic decrease in higher order mode threshold. At a detuning $\delta_{B,\max}$ between the center and outer edge of the grating of 1.95 GHz, corresponding to a quadratic chirp coefficient of 920 GHz/m^2, the higher order mode threshold becomes lower than the fundamental mode threshold. In effect, the outer edges of the grating become mirrors for a DBR-like cavity for the higher order mode. In Fig. 1, the spatial power distribution of the modes of a DFB-FL with quadratic chirp operating above the higher order mode threshold is shown. It is interesting to note that, assuming uniform gain in the structure, linear chirp leads to a symmetric reflection spectrum and asymmetric spatial higher order mode power distributions, whereas quadratic chirp leads to an asymmetric reflection spectrum and symmetric modes.

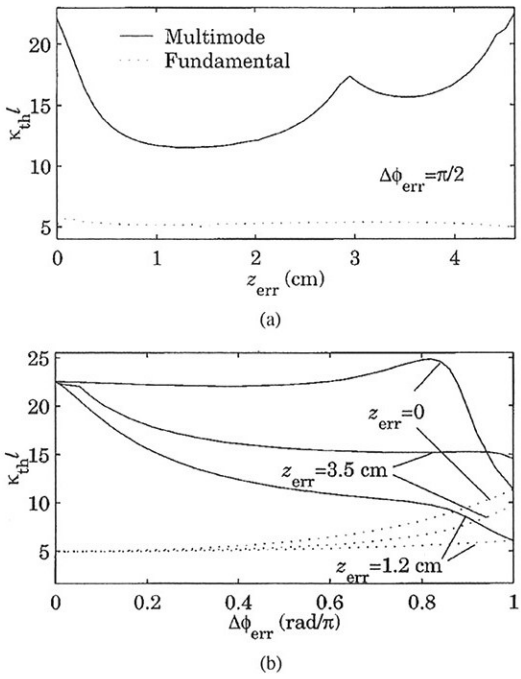

Fig. 6. Threshold κl for single fundamental and multiple mode operation of DFB-FLs with a discrete grating phase error. (a) Thresholds as functions of the position of a phase error $\Delta\phi_{err} = \pi/2$. (b) Thresholds as functions of the value $\Delta\phi_{err}$ of a phase error positioned at $z_{err} = 0$, 1.2, and 3.5 cm.

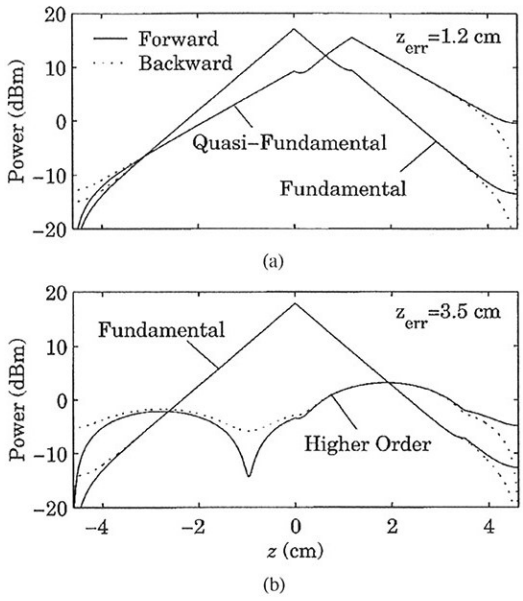

Fig. 7. Power of the modes of DFB-FLs with one discrete phase error of $\Delta\phi_{err} = \pi/2$ and with $\kappa l = 16.1$. Definitions as in Fig. 1. (a) $z_{err} = 1.2$ cm. (b) $z_{err} = 3.5$ cm.

B. Discrete Phase Errors

Discrete phase errors can be induced during grating fabrication for instance due to errors in phase masks or inaccuracies in translation stages. On Fig. 6(a), the two lowest modal thresholds of a DFB-FL with a single rather large discrete phase error of $\Delta\phi_{err} = \pi/2$ is plotted as function of the phase error position z_{err} relative to the central phase shift. It is expected that a number of smaller phase errors distributed over a short length will enable similar laser modes with similar thresholds. As discussed in [30], a grating with multiple phase shifts will have multiple resonances in the stopband. For the asymmetric perturbation modeled in Fig. 7, an extra fundamental-like mode will oscillate around z_{err} at high grating strengths. The extra mode has its lowest threshold when the phase error is in a relative short distance, $z_{err} \approx 1.2$ cm, from the center phase shift. Due to the grating asymmetry, the forward and backward output power of the extra mode will be different, as illustrated in the plot of the modal power distribution on top of Fig. 7. Although this extra mode is fundamental in nature for small values of z_{err}, it also sees a relatively low cavity finesse compared with the fundamental mode, and beat and mode partition noise will make the lasers with two such modes useless for many purposes. Around $z_{err} \approx 3$ cm in Fig. 6(a), there is a mode hop on the multimode threshold curve, leading to another minimum around $z_{err} \approx 3.5$ cm. As illustrated in Fig. 7(b), this mode is similar to more conventional higher order modes, with less asymmetry but larger spread in the power distribution. Note also that this mode seems to have three lobes, indicating a second-order mode.

In Fig. 6(b) the thresholds as functions of the phase error value $\Delta\phi_{err}$ are plotted for $z_{err} = 0$, 1.2, and 3.5 cm. For $z_{err} =$ 1.2 cm, corresponding to the minimum multimode threshold in Fig. 6(a), we see that the major decrease in multimode threshold comes at relatively small values of $\Delta\phi_{err}$. When the value of the phase error equals the center phase shift, $\Delta\phi_{err} = \Delta\phi_{center} = \pi$, the two modes with lowest threshold become degenerate, in line with the theory for passive multiple phase shifted gratings [30]. The multimode threshold for $z_{err} = 3.5$ cm also decreases fast with increasing $\Delta\phi_{err}$ after an initial mode hop at $\Delta\phi_{err} \approx 0.05\pi$. However, unlike the case $z = 1.2$ cm, we do not observe any degeneration at $\Delta\phi_{err} = \pi$, because a phase error as far as 3.5 cm from the center cannot support a mode in the stopband.

An early technique of fabricating DFB-FLs that remains popular is writing a uniform grating and adding the center phase shift by UV postprocessing [31], [32]. The center phase-shift value $\Delta\phi_{center}$ is often decided by maximizing the output power. However, with background loss a_0 present, the output power actually decreases if the effective cavity finesse seen by the fundamental mode increases above a certain limit [18], [26], and $\Delta\phi_{center}$ found by maximizing the output power will not equal the ideal value for side mode suppression, which for a uniform grating is $\Delta\phi_{center} = \pi$. With more advanced grating writing setups [33], [34] that allow incorporation of the center phase shift during the writing [35], [36], inaccuracies may still cause deviations from $\Delta\phi_{center} = \pi$, but in most cases self-heating [24] would probably be of more concern for the effective value of $\Delta\phi_{center}$. In Fig. 6(b), we have plotted the multimode and single mode thresholds as functions of phase error $\Delta\phi_{err}$ in the center for a uniform grating, with $\Delta\phi_{center} = \pi \pm \Delta\phi_{err}$. With increasing phase-shift error, there is a steady increase in the fundamental mode threshold as the mode is pushed further from the center of the grating stopband. However, because the fundamental mode spreads out in the grating, the increase in cavity finesse that the higher

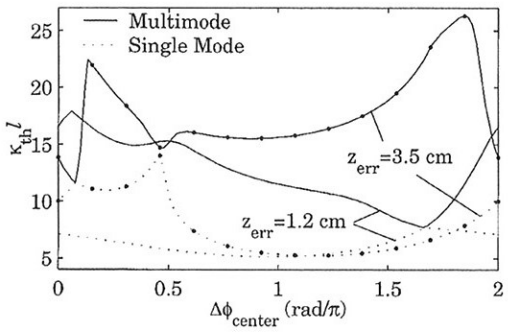

Fig. 8. Thresholds in κl for single and multimode operation of DFB-FLs with a discrete grating phase error of $\Delta\phi_{\rm err} = \pi/2$ positioned at $z_{\rm err} = 1.2$ and $z_{\rm err} = 3.5$ cm as functions of center phase shift value $\Delta\phi_{\rm center}$.

order mode with lowest threshold may see is countered by an increase in modal overlap with the fundamental mode. Thus, there is little change in the multimode threshold until $\Delta\phi_{\rm err}$ reaches 0.8π. When $\Delta\phi_{\rm err} = \pi$, the DFB-FL no longer has a phase shift ($\Delta\phi_{\rm center} = 0$) and there is no longer a fundamental mode in the grating stopband but two higher order modes just outside with equal thresholds [37].

With other grating errors present, a deviation from ideal value of $\Delta\phi_{\rm center}$ is far more serious, as illustrated in Fig. 8; the multiple and single mode thresholds for two DFB-FLs with phase errors of $\Delta\phi_{\rm err} = \pi/2$ located at $z_{\rm err} = 1.2$ and $z_{\rm err} = 3.5$ cm, respectively, are plotted as functions of center phase shift value $\Delta\phi_{\rm center}$. Because $\Delta\phi_{\rm err}$ is not equal to π or zero, the curves are not symmetric around $\Delta\phi_{\rm center} = \pi$, and they are characterized by many mode hops. The slope efficiency is much higher for higher order modes than for the fundamental modes for DFB-FLs with strong gratings. Thus, if the grating strength were $\kappa l = 15$ in the two cases $z_{\rm err} = 1.2$ and $z_{\rm err} = 3.5$ cm, and the center phase shift were tuned by uncritically maximizing the output power, the resulting DFB-FL would probably have $1.5\pi < \Delta\phi_{\rm center} < 1.9\pi$ in the case $z_{\rm err} = 1.2$ cm, and $0 < \Delta\phi_{\rm center} < 0.5\pi$ in the case $z_{\rm err} = 3.5$ cm, with the higher order modes dominating the output.

C. Periodic Chirp

Some types of grating errors, like phase mask stitching errors or inaccuracies in moving parts of the grating writing setup, are likely to be of periodic nature with short periods $\Lambda_{\rm err}$ compared with the DFB-FL length. Other errors, such as those caused by diameter and composition variations along the fiber or variations in UV exposure, are likely to be of a more random character with lower spatial frequencies. As discussed in Sections IV-A and IV-B, more repeatable errors such as those caused by misalignment are also likely to occur with a low spatial frequency compared with the inverse DFB-FL length. In Fig. 9, the thresholds $\kappa_{\rm th}l$ for multimode and fundamental mode operation are plotted as functions of the spatial frequency $\sigma_{\rm err} = 1/\Lambda_{\rm err}$ of a sinusoidal chirp with a maximum [i.e., $\delta\nu_B \propto \cos(2\pi\sigma_{\rm err}z)$] or zero [i.e., $\delta\nu_B \propto \sin(2\pi\sigma_{\rm err})$] detuning $\delta\nu_B$ from the unperturbed uniform grating at the center $z = 0$. As expected from Section IV-A, low-frequency chirp leads to a dramatic decrease in higher order mode

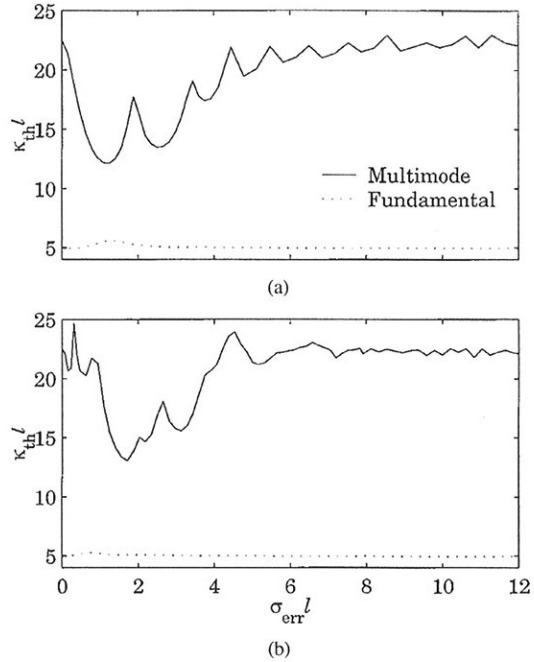

Fig. 9. (a) Thresholds in κl of a DFB-FL with a cosine modulated detuning, with an amplitude of 1 GHz, as functions of spatial frequency of the detuning $\sigma_{\rm err}$ scaled with the grating length l. (b) The same for a sine-modulated detuning.

threshold, with a minimum at $\sigma_{\rm err}l \approx 1$, which is lower in the cosine than the sine case. The reason is that the higher order modes will oscillate between grating sections detuned with the same sign. However, reflections from different periods of the sinusoidal will not be added in phase for these modes, so with higher spatial frequencies the higher order mode threshold is only moderately affected by the periodic chirp, and could even increase if the chirp amplitude were larger. Note that the minimum in $\kappa_{\rm th}l$ for the multimode operation corresponds to a maximum in the fundamental mode threshold, making low frequency chirp particularly detrimental compared with high frequency chirp. As the spatial chirp frequency approaches zero, the sine detuning approaches linear chirp with amplitude decreasing linearly with $\sigma_{\rm err}$, whereas the cosine detuning approaches quadratic chirp with the amplitude proportional to $\sigma_{\rm err}^2$. As expected from Section IV-A, this leads to series of mode hops in the sine case with higher order mode thresholds sometimes higher than a uniform grating, whereas low frequency cosine chirp is always detrimental.

D. Random Spatial Detuning Fluctuations

Many of the aforementioned sources of grating errors have a random character, and the effect of random grating errors are, therefore, investigated. Little work has been published recently on the spectral density distributions in the spatial frequency space of the most likely sources of random detuning. Of the different sources, fluctuations in diameter and composition along the fiber are most difficult to control for the DFB-FL fabricator. We have, therefore, assumed that optical fiber diameter fluctuations are the dominating grating error source, and

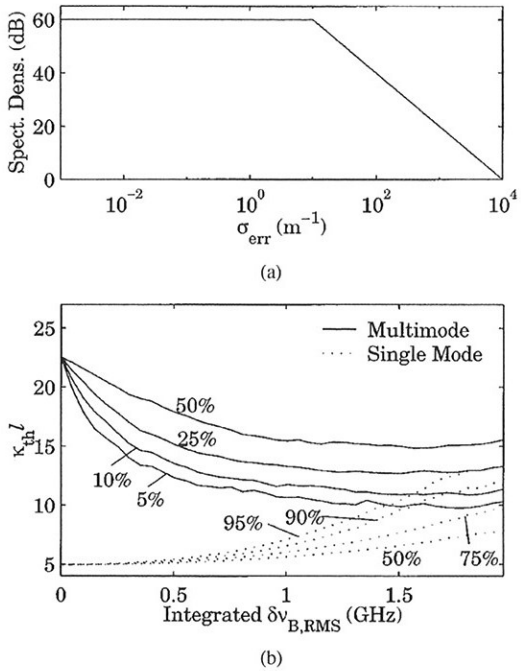

Fig. 10. Multiple and single-mode lasing thresholds $\kappa_{\rm th}l$ for an ensemble of 640 different DFB-FLs with random spatial Bragg wavelength detuning profiles. (a) Spectral density in the spatial frequency space of the expected Bragg wavelength detuning $\delta\nu_{B,\rm rms}$ for the DFB-FL samples. (b) Lower five, 10, 25, and 50 percentiles of $\kappa_{\rm th}l$ for multimode operation and higher 50, 75, 90, and 95 percentiles of $\kappa_{\rm th}l$ for single-mode operation plotted as functions of expected rms amplitude $\delta\nu_{B,\rm rms}$ of the detuning.

that the noise density spectrum of fiber diameter is flat up to a spatial frequency of $\sigma_{\rm err} = 10\ {\rm m}^{-1}$, followed by a decline $\propto 1/\sigma_{\rm err}$ in amplitude, as illustrated in Fig. 10. This is roughly the spectral shape found in some early work [27]–[29] on fiber diameter measurements, and is plausible also for contemporary fiber production facilities, with the cutoff frequency determined by the distance between the preform and fiber diameter monitoring device during fiber drawing. In terms of grating phase noise [38], this corresponds to a decline in root mean square (rms) amplitude $\propto 1/\sigma_{\rm err}$ for $\sigma_{\rm err} < 10\ {\rm m}^{-1}$, and $\propto 1/\sigma_{\rm err}^2$ for $\sigma_{\rm err} > 10\ {\rm m}^{-1}$. We picked 640 random error profile samples from a distribution with an expected detuning spectrum, as shown in Fig. 10(a). Each spectral element has a Gaussian-distributed imaginary and real part. For each DFB-FL sample, the thresholds $\kappa_{\rm th}l$ for multimode and single-mode operation were calculated for varying degree of detuning amplitude. In Fig. 10(b), the resulting lower percentiles of multimode threshold and higher percentiles of single-mode threshold are plotted as functions of expected rms Bragg wavelength detuning $\delta\nu_{B,\rm rms}$. The single-mode thresholds generally seem to have a monotonic increase with increasing grating errors. The five and 10 percentiles of the multimode thresholds decrease rapidly up to $\delta\nu_{B,\rm rms} \approx 0.5$ GHz before flattening out. The multimode threshold five percentile comes down to $\kappa_{\rm th}l \approx 10$ at $\delta\nu_{B,\rm rms} \approx 2$ GHz. At this detuning amplitude, the single-mode 95 percentile has reached $\kappa_{\rm th}l \approx 13.3$. Of course, these extremes are caused by different members of the ensemble, but, still, this is an indication that 2-GHz, or even 1-GHz, integrated rms detuning would make it very difficult to make high quality DFB-FLs with high yield. Note that a 1-GHz rms detuning at 1550-nm wavelength corresponds to an rms diameter variation of approximately 0.04% for a fiber with a numerical aperture of 0.2 and core diameter of approximately 5 μm. However, as discussed in Section IV-C, variations with spatial frequencies much larger or much smaller than the inverse length of the DFB-FL grating will not have much effect.

V. Conclusion

Higher order modes have proven to be a problem for the realization of stable high-finesse DFB-FLs. High-finesse DFB-FLs can be especially useful in sensing applications where high backreflection tolerance is desirable. We have analyzed the dependence of the fundamental and higher order modes thresholds on gain, background loss, and grating defects.

We have confirmed that higher fiber gain leads to lower higher order mode thresholds, making the realization of high-finesse single-mode DFB-FLs more difficult. However, as long as problems like spontaneous lifetime shortening caused by erbium clustering are avoided, higher gain also means that the fundamental modes become more powerful and stable at lower values of cavity finesse, and for many applications where a low cavity finesse is acceptable, high gain is, therefore, very welcome. If the fiber has a high photosensitivity, it is also possible to fabricate high-finesse single-mode DFB-FLs by writing a strong but short grating, thus making the round-trip gain for the higher order modes smaller.

We have also found that although background loss weakens the fundamental modes of high-finesse DFB-FLs, the higher order modes actually can experience an increase in the effective round-trip gain and decrease in threshold in terms of integrated coupling coefficient with increasing loss. Thus, a better understanding of the loss mechanisms of UV-exposed photosensitive fiber is desirable, and known sources of loss, such as hydrogen loading of the fiber, should be eliminated.

Although gain and loss must be controlled and measured in order to predict higher order mode thresholds, grating errors could be far more serious for the threshold margin between the fundamental and higher order modes. Particularly detrimental are grating errors with spatial frequency approximately equal to the inverse laser length. For instance, for quadratic chirp, we have found with our laser parameters that the threshold margin is zero with a quadratic chirp coefficient of 940 GHz/m^2, corresponding to a detuning between the center and outer edge of the grating of only 2 GHz. We have also found that discrete phase errors in the grating reduce the higher order mode threshold significantly, especially if the phase errors are positioned close to the center phase shift, in which case we get two fundamental-like modes operating in the grating stopband.

In many cases, grating errors are not repeatable but have a rather random character. We simulated an ensemble of DFB-FLs picked from a Bragg frequency detuning profile distribution that we believe is realistic when fiber diameter variations is the dominating error source. For many of the samples, it was found that there is a significant decrease in higher order mode

threshold and increase in fundamental mode threshold for a fraction of a GHz in rms Bragg frequency detuning, which corresponds to a few parts per 10^4 in fiber diameter variations. Therefore, tight control of the fiber diameter and other grating error sources is imperative for a repeatable fabrication of high-quality DFB-FLs.

ACKNOWLEDGMENT

The authors would like to thank J. T. Kringlebotn and K. Bløtekjær for helpful advice and discussions.

REFERENCES

[1] J. T. Kringlebotn, J. Archambault, L. Reekie, and D. N. Payne, "Er^{3+} : Yb^{3+}-codoped fiber distributed feedback laser," *Opt. Lett.*, vol. 19, pp. 2101–2103, Dec. 1994.

[2] H. A. Haus and C. V. Shank, "Antisymmetric taper of distributed feedback lasers," *IEEE J. Quantum Electron.*, vol. QE-12, pp. 532–539, Sept. 1976.

[3] M. Ibsen, E. Rønnekleiv, G. J. Cowle, M. O. Berendt, O. Hadeler, M. N. Zervas, and R. I. Laming, "Robust high-power (>20 mW) all-fibre DFB lasers with unidirectional and truly single polarisation outputs," in *Proc. Conf. Lasers Electro-Optics (CLEO) 1999*, Baltimore, MD, USA, 1999, pp. 245–246.

[4] H. Storøy, B. Sahlgren, and R. Stubbe, "Single polarisation fibre DFB laser," *Electron. Lett.*, vol. 33, pp. 56–58, Jan. 1997.

[5] J. I. Philipsen, M. O. Berendt, P. Varming, V. C. Lauridsen, J. H. Povlsen, J. Hübner, M. Kristensen, and B. Pálsdóttir, "Polarisation control of DFB fibre laser using UV-induced birefringent phase-shift," *Electron. Lett.*, vol. 34, pp. 678–679, Apr. 1998.

[6] J. Carrol, J. Whiteaway, and D. Plumb, *Distributed Feedback Semiconductor Lasers*. London, U. K.: Institution of Electrical Engineers, 1998, vol. 10, IEE Circuits, Devices and Systems.

[7] E. Rønnekleiv and S. W. Løvseth, "Stability of distributed feedback fiber lasers with optical feedback," *Proc. SPIE*, vol. 3746, pp. 466–469, 1999.

[8] E. Rønnekleiv, M. Ibsen, M. N. Zervas, and R. I. Laming, "Characterization of fiber distributed-feedback lasers with an index-perturbation method," *Appl. Opt.*, vol. 38, pp. 4558–4565, July 1999.

[9] E. Rønnekleiv, "Frequency and intensity noise of single frequency fiber Bragg grating lasers," Opt. Fiber Technol., vol. 7, pp. 206–235, 2001, to be published.

[10] G. A. Ball, C. G. Hull-Allen, and J. Livas, "Frequency noise of a Bragg grating fibre laser," *Electron. Lett.*, vol. 30, pp. 1229–1230, July 1994.

[11] S. W. Løvseth and D. Y. Stepanov, "Dynamic analysis of multiple wavelength DFB fiber lasers," *IEEE J. Quantum Electron.*, vol. 37, pp. 1237–1245, Oct. 2001.

[12] W. Elsässer and E. O. Göbel, "Spectral linewidth of gain- and index-guided InGaAsP semiconductor lasers," *Appl. Phys. Lett.*, vol. 45, pp. 353–355, Aug. 1984.

[13] T. P. Lee, C. A. Burrus, and D. P. Wilt, "Measured spectral linewidth of variable-gap cleav-coupled-cavity lasers," *Electron. Lett.*, vol. 21, pp. 53–54, Jan. 1985.

[14] U. Krüger and K. Petermann, "The semiconductor laser linewidth due to the presence of side modes," *IEEE J. Quantum Electron.*, vol. 24, pp. 2355–2358, Dec. 1988.

[15] X. Pan, B. Tromborg, and H. Olesen, "Linewidth rebroadening in DFB lasers due to weak side modes," *IEEE Photon. Technol. Lett.*, vol. 3, pp. 112–114, Feb. 1991.

[16] D. Y. Stepanov, J. Canning, L. Poladian, R. Wyatt, G. Maxwell, R. Smith, and R. Kashyap, "Apodized distributed-feedback fiber laser," *Opt. Fiber Technol.*, vol. 5, pp. 209–214, 1999.

[17] M. A. Englund and S. W. Løvseth, "Selective gain tuning in erbium doped fibres," in *Proc. OECC/IOOC'01*, July 2001.

[18] S. W. Løvseth and D. Y. Stepanov, "Analysis of multiple wavelength DFB fiber lasers," *IEEE J. Quantum Electron.*, vol. 37, pp. 70–80, June 2001.

[19] E. Rønnekleiv, M. N. Zervas, and J. T. Kringlebotn, "Modeling of polarization-mode competition in fiber DFB lasers," *IEEE J. Quantum Electron.*, vol. 34, pp. 1559–1568, Sept. 1998.

[20] ——, "Corrections to 'Modeling of polarization-mode competition in fiber DFB lasers'," *IEEE J. Quantum Electron.*, vol. 35, pp. 1097–1100, July 1999.

[21] E. Rønnekleiv, M. Ibsen, and G. J. Cowle, "Polarization characteristics of fiber DFB lasers related to sensing applications," *IEEE J. Quantum Electron.*, vol. 36, pp. 656–664, June 2000.

[22] E. Rønnekleiv, O. Hadeler, and G. Vienne, "Stability of an Er–Yb-doped fiber distributed-feedback laser with external reflections," *Opt. Lett.*, vol. 24, pp. 617–619, May 1999.

[23] L. Dong, W. H. Loh, J. E. Caplen, J. D. Minelly, K. Hsu, and L. Reekie, "Efficient single-frequency fiber lasers with novel photosensitive Er/Yb optical fibers," *Opt. Lett.*, vol. 22, pp. 694–696, May 1997.

[24] O. Hadeler and M. N. Zervas, "Application of a DFB fibre laser temperature sensor for characterizing pump induced temperature distributions along another DFB fibre laser," *Proc. SPIE*, vol. 4185, pp. 142–145, 2000.

[25] G. Meltz and W. W. Morey, "Bragg grating formation and germanosilicate fiber photosensitivity," *Proc. SPIE*, vol. 1516E, pp. 185–199, Dec. 1991.

[26] V. C. Lauridsen, J. H. Povlsen, and P. Varming, "Optimising erbium-doped DFB fibre laser length with respect to maximum output power," *Electron. Lett.*, vol. 35, pp. 300–302, Feb. 1999.

[27] P. H. Krawarik and L. S. Watkins, "Fiber geometry specifications and its relation to measured fiber statistics," *Appl. Opt.*, vol. 17, pp. 3984–3989, Dec. 1978.

[28] L. S. Watkins and P. H. Krawarik, "Spatial power spectrum characteristics of the core diameter of furnace drawn and laser drawn step-index optical fibers," *Appl. Opt.*, vol. 20, pp. 2856–2860, Aug. 1981.

[29] S. G. Akopov, V. N. Korshunov, V. S. Solovyev, and B. N. Fomichev, "Energy characteristics of the irregularity distribution-functions of the geometrical structure of optical fibers," *Telecommun. Radio Eng.*, vol. 47, pp. 54–57, Aug. 1992.

[30] G. P. Agrawal and S. Radic, "Phase-shifted fiber Bragg gratings and their application for wavelength demultiplexing," *IEEE Photon. Technol. Lett.*, vol. 6, pp. 995–997, Aug. 1994.

[31] J. Canning and M. G. Sceats, "π-phase-shifted periodic distributed structures in optical fibres by UV post-processing," *Electron. Lett.*, vol. 30, pp. 1344–1345, Aug. 1994.

[32] P. Varming, J. Hübner, and M. Sejka, "Erbium doped fiber DFB laser with permanent $\pi/2$ phase-shift induced by UV post-processing," in *Proc. IOOC'95.*, vol. 5, June 1995, pp. PD1–PD3.

[33] M. J. Cole, W. H. Loh, R. I. Laming, M. N. Zervas, and S. Barcelos, "Moving fibre/phase mask-scanning beam technique for enhanced flexibility in producing fibre gratings with uniform phase mask," *Electron. Lett.*, vol. 31, pp. 1488–1490, Aug. 1995.

[34] R. Stubbe, B. Sahlgren, S. Sangren, and A. Asseh, "Novel techniques for writing long superstructured fiber Bragg gratings," in *Proc. Photosensitivity Quadratic Nonlinearity Glass Waveguides*, Portland, OR, Sept. 1995, p. PD1.

[35] W. H. Loh and R. I. Laming, "1.55 μm phase-shifted distributed feedback fibre laser," *Electron. Lett.*, vol. 31, pp. 1440–1442, Aug. 1995.

[36] A. Asseh, H. Storøy, J. T. Kringlebotn, W. Margulis, B. Sahlgren, S. Sandgren, R. Stubbe, and G. Edwall, "10 cm Yb^3+ DFB fibre laser with permanent phase shifted grating," *Electron. Lett.*, vol. 31, pp. 969–970, June 1995.

[37] H. Kogelnik and C. V. Shank, "Coupled-wave theory of distributed feedback lasers," *J. Appl. Phys.*, vol. 43, pp. 2327–2335, May 1972.

[38] R. Feced and M. N. Zervas, "Effects of random phase and amplitude errors in optical fiber Bragg gratings," *J. Lightwave Technol.*, vol. 18, pp. 90–101, Jan. 2000.

Sigurd Weidemann Løvseth, photograph and biography not available at the time of publication.

Erlend Rønnekleiv, photograph and biography not available at the time of publication.

Chapter 5

Selective Gain Tuning in Erbium Doped Fibres[1]

Abstract

A new technique for spatially windowing the effective gain in erbium doped fibre is presented. The technique is demonstrated experimentally and an application for this process is described with supporting numerical results.

5.1 Introduction

Erbium doped fibre lasers offer several key advantages that make them attractive for use in remote sensing applications. In 1994, Kringlebotn *et al.* demonstrated the first distributed feedback fibre laser (DFB-FL) [1]. Based on a phase shifted fibre Bragg grating, a short cavity length DFB-FL produces an output with very narrow linewidth and robust single frequency operation.

For remote sensing applications of DFB-FLs, sensitivity to back reflections [2] and noise performance [3] are important considerations. A common dependency to both these characteristics is the product term κL of the fibre Bragg grating, where κ is the coupling coefficient and L is the length of the grating. Subject to a limit defined by internal loss [4] and non-linear refractive index changes, reflection sensitivity and laser noise performance are expected to improve with host gratings of increasing κL value [5]. However with high κL gratings, all longitudinal modes have reduced gain thresholds, and hence higher order longitudinal modes may be close to threshold. Further, for practical gratings it is expected that grating phase imperfections manifest in a reduced threshold margin between the fundamental and higher order modes. Therefore, improving threshold margin is an important consideration for high-κL DFB-FL designs. In this paper, we present a new technique for sidemode suppression based on apodizing the effective signal gain over the length of the grating in the DFB-FL. We demonstrate for the first time a method of achieving selective gain tuning based on CO2 laser exposure.

[1] This manuscript is submitted to the postdeadline session of *OECC / IOOC 2001 Conference – Incorporating ACOFT,* (Sydney, Australia), July, 2001. Authors: M. A. Englund, S. W. Løvseth, D. Yu. Stepanov, and E. C. Mägi.

5.2 Technique

It is well known that core dopants in germanosilicate fibre diffuse at high temperatures [6]. Diffusion of core dopants alters the refractive index profile of the fibre which correspondingly changes the mode field diameter (MFD). It is also clear that diffusion of the core dopants in erbium fibres during fibre manufacture can lead to changes in the maximum signal gain achievable [7]. Diffusion at raised fibre temperatures alters the overlap between the signal and pump fields and the erbium distribution. The magnitude and sign of the resulting gain change is dependent on the dopant concentration profiles. Therefore, the local signal gain in a section of erbium doped fibre may be tuned by exposure to an appropriate heat source. Extending this notion to a length of erbium doped fibre provides a means of imposing a longitudinal signal-gain profile. In the context of a DFB-FL, this provides a means for discriminating against higher order modes of the cavity.

To appreciate how this process can be used for higher order mode suppression we consider the spatial distribution of the longitudinal mode intensities in a DFB-FL cavity, as depicted in Fig. 1(A). The power distribution of the fundamental mode in high κL lasers is tightly confined around the phase shift in the grating. In contrast, the ±1 and ±2 higher order mode power distribution is less concentrated and have peak intensities towards the outer regions of the grating structure. By decreasing the relative signal-gain available in these outer regions an increase in the threshold of the higher order modes is induced relative to the fundamental mode. In addition, by not apodizing the grating strength in these regions, a higher κL value is maintained for the fundamental mode and all the aforementioned performance advantages.

5.3 Modelling Results

To examine the effect of apodizing the signal gain across a DFB-FL cavity, a modified version of the transfer matrix method used in [8] was developed. We configured the model for a 10 cm long grating structure with a κ of 167.5 m^{-1}, and gain parameters multiplied by a factor of two compared to [8]. We have assumed that the thermal diffusion process is able to reduce the signal gain by a maximum of 50%.

A series of apodization functions, $G(z)$, of the form,

$$G(z) = 0.5(1 + \exp(-\left(\frac{z}{w}\right)^6))$$

of varying width w were applied to the signal and pump absorption and gain coefficients. z is the position relative to the centre of the grating. The model calculates the steady state output power of the lasing modes of the structure as a function of window width. A plot of the results appears in Fig. 1(B), where the

output power of the fundamental mode and the total output power of the side modes are plotted as a function of *w*. It is clear that the window has minimal effect on any of the modes until the width of the window decreases to 6 cm. From this point, there is a rapid decrease in the power of the side modes until, at *w* = 4.2 cm, the side modes are below the lasing thresholds. The power of the fundamental mode is largely unaffected, and does not significantly decrease until *w* is less than 2 cm. The threshold grating coupling coefficients for the higher order modes were also calculated for a window width of 2 cm and then compared to a uniform gain DFB-FL that otherwise had the same characteristics. The grating strength required for the gain-apodised laser to reach higher order mode threshold was 213.5 m^{-1} and for the uniform-gain laser it was significantly lower at 162 m^{-1}. It should also be noted that the thresholds of the higher order modes were particularly sensitive to changes in gain parameters. Overall these results suggest there is a significant advantage in reducing the available signal gain on the wings of the grating structure. This increased threshold margin provides the potential to fabricate DFB-FLs with very high grating strength without the onset of higher order modes. For sensor applications where it is not always possible to isolate the laser from perturbations, this increased threshold margin is particularly important.

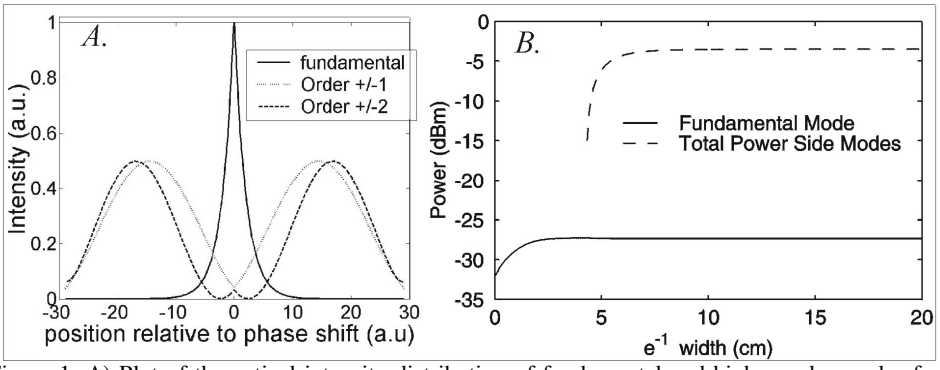

Figure 1: A) Plot of theoretical intensity distribution of fundamental and higher order modes for typical DFB-FL. B) Plot of power distribution between modes as a function of apodization length.

5.4 Experimental Results

To verify the proposed technique a CO2 laser was set up to repeatedly scan a length of Er fibre as depicted in the schematic of Figure 2.

The Er fibre used in this experiment had a small signal absorption of 17 dB/m at 1530 nm. A series of CO2 scans were done across an 80 mm section of the 100.mm Er fibre sample. The induced fibre temperature was estimated to be in the range of 1400-1700 C. At the conclusion of each scan, the small signal absorption and the background loss were both characterised. The former was measured at 980 and 1530 nm and the latter at 1300 nm, these results are plotted

in Figure 3. The absorption peaks at 980 nm and 1550 nm were observed to decrease monotonically, whereas the background loss was seen to slightly increase but remain relatively stable. It should be noted that the signal level at the absorption peaks moved in the opposite direction to the signal level at

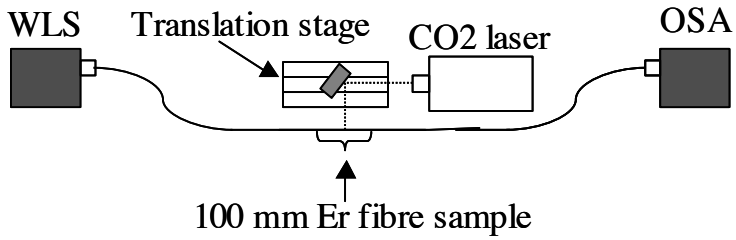

Figure 2: Experimental setup for CO2 processing of Er fibre. OSA: optical spectrum analyser, WLS: white light source.

1300 nm and increased. These results firmly suggest that the CO2 exposure has decreased the overlap between the MFD of the pump and signal and the Er distribution. Therefore, we have correspondingly reduced the small signal gain in the fibre. During the exposure intervals the cut-off wavelength was seen to remain within a few nanometres of the original value of 970 nm, suggesting the normalised frequency remained approximately invariant. The magnitude of the absorption change achieved at 980 nm and 1530 nm was ~1.25 and ~2 dB/m respectively. To achieve a spatial profile in gain the CO2 exposure time and/or induced fibre temperature can be profiled during the CO2 exposure.

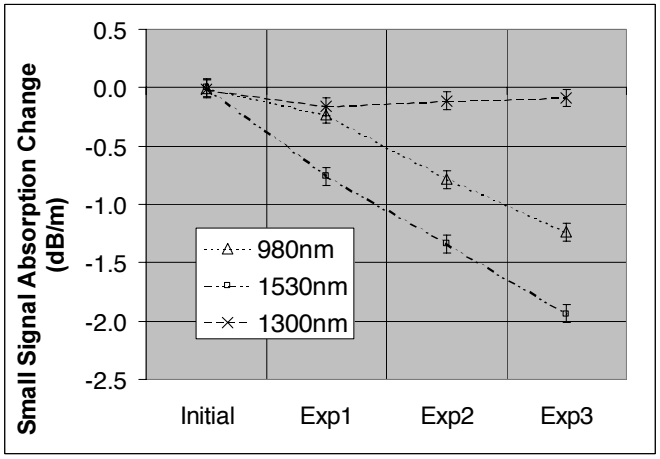

Figure 3: Small signal absorption change at 980 and 1530 nm plotted with signal level change at 1300 nm.

5.5 Conclusions

We have proposed a new technique for achieving high κL DFB-FLs with high side mode suppression. A numerical model has been developed to investigate the quantitative implications of modifying the local gain. The numerical results indicate a significant improvement in the threshold margin of the side modes in a DFB-FL. We have demonstrated for the first time the use of a CO2 laser for selective gain tuning along a length of Er fibre. Tailoring the spatial distribution of signal gain is expected to have wider applications to other optical waveguide devices, this may include multimode (transverse modes) waveguides and optical amplifiers.

We acknowledge P. Blazkiewicz, J. Canning, J. Chow and G. Town for assistance in the experimental work. S. W. Løvseth acknowledges support from the Norwegian Research Council.

References

[1] J. T. Kringlebotn, et al., *Opt. Lett.*, vol.19, no.24, p.2101, 1994.
[2] E. Rønnekleiv, et al., *Opt. Lett.*, vol.24, no.9, p.617, 1999.
[3] E. Rønnekleiv, Dr.ing. thesis, Norwegian Univ. of Sci. and Tech. NTNU, 1999.
[4] V. C. Lauridsen, et al., *Electron. Lett.*, vol.35, no.4, p.300 1999.
[5] E. Rønnekleiv, et al., *Appl. Opt.*, vol.38, no.21, p.4558, 1999.
[6] K. Shiraishi, et al., *J. Lightwave Technol.*, vol.8, no.8, p.1151, 1990.
[7] S. Tammela, et al., *Fiber Laser Sources and Amplifiers II, vol.1373 SPIE*, p.103, 1994.
[8] E. Rønnekleiv, et al., *IEEE J. Quantum. Electron.*, Vol. 36, No. 6, p. 656, 2000.

Chapter 6

Analysis of Multiple Wavelength DFB Fiber Lasers

Authors: Sigurd Weidemann Løvseth and Dmitrii Yu. Stepanov.

Published in *IEEE Journal of Quantum Electronics*, vol. 37, pp. 770–780, June 2001.

Analysis of Multiple Wavelength DFB Fiber Lasers

Sigurd Weidemann Løvseth and Dmitrii Yu Stepanov

***Abstract*—The behavior of multiwavelength distributed feedback fiber lasers is simulated in a comprehensive numerical model. Multiple fundamental modes can coexist, even though the coupling coefficients of their respective refractive index gratings are not equal, due to induced dynamic gain gratings. We have investigated the effect on the lasing state of variations in coupling strengths, gain parameters, grating Bragg frequency separation, relative phase between the gratings, length of the structure relative to the beat lengths between the gratings, grating center phase-shift errors, and saturation level of the UV-induced refractive index change.**

***Index Terms*—Distributed feedback lasers, erbium, optical fiber Bragg gratings, optical fiber lasers, optical hole burning, sampled optical fiber Bragg gratings.**

I. Introduction

MULTIPLE wavelength, distributed feedback (DFB) fiber lasers [1], [2] are attractive for a range of applications in optical communications, including soliton and microwave generation. In conventional DFB fiber lasers, comprising a UV-induced Bragg grating fabricated in a rare-earth-doped fiber, two fundamental polarization modes can coexist, and such lasers are analyzed in [3]–[5]. However, in conventional doped single-mode fibers, the frequency spacing between the two polarization modes is a function of both intrinsic and UV-induced birefringence and, as such, is difficult to control and limited to a few gigahertz. In this work, we will consider erbium-doped DFB fiber lasers where the grating structures are superpositions of several individual Bragg gratings with different Bragg frequencies, and each laser operates with two or more lasing modes sharing the same gain medium. These grating structures can also be viewed as sampled gratings, and offer predictable and flexible frequency separation. Although such lasers have been demonstrated experimentally [2], there has been little work in the literature regarding the understanding of multiple wavelength DFB lasers. In this paper, we argue that the coexistence of two or more fundamental modes of the same polarization can be attributed to the effect of dynamic gain gratings set up by the intra-cavity standing waves of different laser modes. As discussed in [6], a gain grating is in anti-phase with the standing-wave pattern that created it, and, therefore, its presence is destructive for the corresponding laser mode. On the other hand, its interaction with other laser modes is small because of the frequency mismatch. Thus, the effect of the gain gratings is a reduction of the power of the dominant mode and an increase of the available gain for the other modes, resulting in stable multiple wavelength operation of the laser. This type of spatial hole burning has been well understood since the 1960s [7], [8] and was early identified as the reason for multiple longitudinal mode lasing in other types of erbium-doped fiber lasers [9]. However, because of carrier diffusion, dynamic gain gratings are usually not an issue for semiconductor lasers [10], and similar semiconductor DFB lasers would, therefore, probably show a lot of mode partition noise or be single mode.

By combining the theory given in [6] with the conventional coupled-mode formalism, we have constructed a numerical model that calculates the power and detuning of an arbitrary number of modes for an arbitrary complex index coupling function. We have simulated multiwavelength phase-shifted DFB fiber lasers as a function of gain parameters, coupling strengths, laser frequency separations, grating phase-shifts, relative phases between the superimposed gratings, structure length relative to the beat length and the degree of saturation of the UV-induced refractive index change during writing of the grating.

II. Multiple Λ DFB Grating Structures

In this work, we consider multiple number of Bragg gratings with different periodicity Λ_i superimposed in a single rare earth-doped fiber, as illustrated in Fig. 1(a). For the remainder of the paper, the individual superimposed Bragg gratings and the resulting grating structures will be referred to as subgratings and multiple Λ DFB structures, respectively. Dual Λ gratings are also known as a Moiré-gratings, and if the two subgratings have equal coupling strength, a dual Λ structure will be a Bragg grating without chirp and with a sinusoidally modulated coupling coefficient κ, as illustrated at the bottom half of Fig. 1(a). With the sinusoidal modulation function, a π phase shift has to be introduced at each zero of κ, and the beat length of the modulation is inversely proportional to the Bragg frequency mismatch $\Delta\nu$ between the subgratings. If the subgratings do not have equal strength, the periodic amplitude modulation of κ will no longer be purely sinusoidal, and the discrete phase shifts will be replaced with a continuous chirp.

For a larger number of subgratings, the multiple Λ structure will become more complex, but the chirp and amplitude modulation will be periodic if the Bragg frequency separation between the subgratings are multiples of each other. Multiple Λ structures are, therefore, often called sampled gratings and viewed as a sampling of a uniform Bragg grating with a generally complex sampling function.

Manuscript received September 6, 2000; revised February 22, 2001. The work of S. W. Løvseth was supported by the Norwegian Research Council.

S. W. Løvseth was with the Australian Photonics CRC, Optical Fibre Technology Centre (OFTC), University of Sydney, Australia. He is now with the Department of Physical Electronics, Norwegian University of Science and Technology, N-7491 Trondheim, Norway, and also with Optoplan AS, N-7448 Trondheim, Norway.

D. Y. Stepanov was with the Australian Photonics CRC, Optical Fibre Technology Centre (OFTC), University of Sydney, Australia. He is now with Redfern Optical Components Pty. Ltd., Australian Technology Park, Eveleigh, NSW 1430, Australia.

Publisher Item Identifier S 0018-9197(01)04299-3.

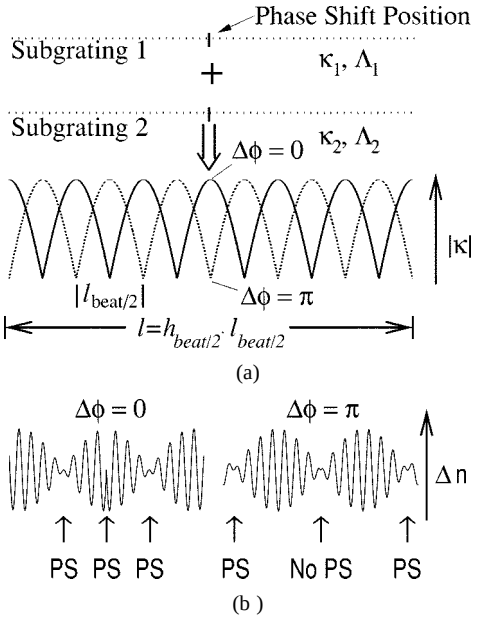

Fig. 1. (a) Dual Λ DFB grating structure. (b) Index profile around the center phase shift of a dual Λ DFB grating structure with $\Delta\phi = 0$ and $\Delta\phi = \pi$. The π phase shifts (PS) of the index modulation are indicated.

Just as in conventional semiconductor DFB lasers, we introduce an additional phase shift of π in the center of the grating to facilitate single-mode lasing in the transmission stopband corresponding to each subgrating. These modes, which will have their power distribution concentrated around the center phase shift, we call fundamental. This is in line with the terminology used in other papers on DFB lasers, but note that there may be several such fundamental modes for a multiple Λ DFB structure, one for each subgrating. With large gain or grating strength, higher order modes, with frequency outside the stopbands and with a wider spatial distribution, may also reach threshold.

A superposition of Bragg gratings will not lead to a superposition of their reflection spectra, because the resulting spectrum is dependent on the phase relation between the subgratings. This is particularly important in center phase-shifted, multiple Λ DFB structures, because most of the power is concentrated in a small region around the phase shift. Depending on the phase relation between the subgratings, the local superstructure around the phase shift will be very different, leading to different values for the detuning of the laser modes from the subgrating Bragg frequencies. In the case of a dual Λ structure, the two extreme cases are if the subgratings are in phase ($\Delta\phi = 0$) and anti-phase ($\Delta\phi = \pi$) at the center. This means that the phase shift is located at a node and anti-node, respectively, of the beat pattern of the structure, as illustrated in Fig. 1(b). For dual Λ structures where the two subgratings have equal strength, the case $\Delta\phi = \pi$ corresponds to a removal of the sign shift of one of the beat pattern nodes.

Apart from the detuning, $\Delta\phi$ could affect the effective reflectivity of the two half sections of the grating at each side of the center phase shift. If we again consider dual Λ structures, the integrated values of $|\kappa|$ of the two half sections, and thus the cavity finesse seen by the two modes, are dependent on $\Delta\phi$ if the total laser length l is not equal to an integral number of half-beat lengths $l_{\mathrm{beat}/2}$. If, in addition, $\Delta\phi$ is not equal to π or 0, the reflectivity of the two halves of the grating will be different even though they have the same length, leading to an asymmetric power output.

The influence of $\Delta\phi$ on detuning, cavity finesse, and power output decreases with larger Bragg frequency separation between the subgratings and smaller coupling strength. The reason is that the coupling strength integrated over a sampling period then will be smaller, or, as seen in the frequency domain, that the overlap between the reflection spectra of the different subgratings becomes smaller.

III. Numerical Model

A. Coupled-Mode Analysis

We have constructed a numerical model that calculates the steady state of all the modes of a general, single polarization, multiple Λ DFB fiber laser. We describe the spatial distribution of the laser modes by slowly varying complex amplitudes, A_m and B_m for the right and left propagating mode number m, respectively. In this notation, the total local field of the mode becomes

$$E_m(z, t) = A_m(z)e^{j(\omega_m t - \overline{\beta} z)} + B_m(z)e^{j(\omega_m t + \overline{\beta} z)}. \quad (1)$$

Here, $\overline{\beta}$ is the average Bragg wavenumber of the subgratings, which will be used as a reference for the detuning, and ω_m is the angular frequency of mode m. In order to calculate the spatial field distribution of the modes, we use a coupled-mode formalism [11] with a spatially varying complex coupling coefficient κ, given by

$$\kappa = \sum_{i=1}^{N_g} \kappa_i e^{-j[2(K_i - \overline{\beta})z + \phi_i]}. \quad (2)$$

Here, κ_i, $K_i = \pi/\Lambda_i$, Λ_i and ϕ_i are the coupling strength, the Bragg wavenumber, the period, and a generally z-dependent phase term, respectively, of subgrating number i. N_g is the total number of subgratings.

Including the effect of dynamically induced gain gratings [6], [12], the relevant coupled-mode equations become

$$\begin{aligned} \frac{\partial A_m}{\partial z} &= d_m A_m + (j\kappa + g_2^*) B_m \\ -\frac{\partial B_m}{\partial z} &= d_m B_m + (j\kappa^* + g_2) A_m \end{aligned} \quad (3)$$

where

$$d_m = g_0 - a_0 - j\delta_m.$$

Here, δ_m is the detuning of the mode from the average Bragg wavenumber $\overline{\beta}$, g_0 and g_2 are the average gain and gain grating coefficients, respectively, to be discussed and properly defined in Section III-B, and a_0 is the unbleachable losses of the fiber.

Since the laser modes have different frequencies, there is no direct coupling between them. However, the modes influence each other through the gain parameters g_0 and g_2.

Equations (3) have to be modified in order to describe the interaction between laser modes in different polarizations, and an

in-depth analysis of dual-polarization DFB fiber lasers was performed in [3]–[5]. Here, we assume that all modes are operating in the same polarization. Permanent single-polarization DFB fiber lasers have been fabricated by writing a polarization-dependent grating [13] or adding a polarization-dependent phase shift during post processing [14], [15].

B. Gain Model

We assume that homogeneously broadened Er-doped media can be described by two-level rate equations [16], which is a good approximation for Er-doped silica fibers, even when pumped with a 980-nm source [17]. It is further assumed that the erbium doping radius is small compared to the mode field radius of the fiber, so that the radial variation of the Er^{3+} inversion can be neglected [18]. Using the formalism developed in [5], we divide the erbium ions into sub-media to allow for UV-induced lifetime quenching for a certain fraction of the ions. By performing a Fourier integral, the zeroth-order $g_{k,0}$ and second-order Fourier component $g_{k,2}$ with respect to $\overline{\beta}$ of the total spatially varying, but locally pseudo-periodic, gain function [6], [12], [19] for each gain medium k can be found [5]

$$g_{\mathrm{unsat},k} = \xi_k \left(\frac{a_p r_{\mathrm{wl}} P_p}{P_{\mathrm{sat},k}} - a_s \right) \tag{4a}$$

$$g_{k,0} = g_{\mathrm{unsat},k} \Big/ \sqrt{a^2 - |b|^2} \tag{4b}$$

$$g_{k,2} = g^*_{k,-2} = g_{k,0} \frac{\sqrt{a^2 - |b|^2} - a}{b} \tag{4c}$$

where

$$P_{\mathrm{sat},k} = \left((a_p + g_p) r_{\mathrm{wl}} P_p + \frac{\zeta_k}{2} P_{\mathrm{sp}} \right) \Big/ (a_s + g_s)$$

$$a = 1 + P_{\mathrm{tot}}/P_{\mathrm{sat},k}, \qquad b = 2P_c/P_{\mathrm{sat},k}$$

$$P_{\mathrm{tot}} = \sum_m^{N_m} |A_m|^2 + |B_m|^2, \qquad P_c = \sum_m^{N_m} A_m B_m^*.$$

$g_{k,0}$ and $g_{k,2}$ are called the *mean gain* and *gain grating* coefficients, respectively. In (4), medium k consists of a fraction ξ_k of the total number of erbium ions, that have their spontaneous emission lifetime quenched by a factor of ζ_k. P_p is the pump power, r_{wl} is the ratio between the pump and signal wavelengths, P_{sp} is the spontaneous emission power per unit length before the onset of UV quenching, and g_s, g_p, a_s, and a_p are the signal and pump gain at full inversion and signal and pump absorption at zero inversion, respectively. Furthermore, N_m is the total number of modes, and the superscript "$*$" denotes complex conjugation.

The total gain parameters used in the coupled-mode equations (3) are found by summing the contributions from the different gain media [5]; thus

$$g_{2r} = \sum_{k=1}^{N_{\mathrm{gm}}} g_{k,2r}, \qquad r = 0, 1. \tag{5}$$

Here, N_{gm} is the total number of gain media.

From (4) and (5), it can be deduced that the presence of a standing wave pattern ($P_c \neq 0$) increases the average gain (g_0) compared to the case where all waves are incoherent. If one mode locally has a higher power than the other modes, g_2 will couple the forward and backward propagating waves of that particular mode in a destructive manner, since the phase of g_2 is determined by the phase of P_c, which is again largely dependent on the field of the high power mode. However, the other modes will be almost unaffected by g_2 because of the spatial frequency mismatch, and only benefit from the increase of g_0 [6]. If all modes have approximately equal amplitudes, g_2 will provide negative and equal feedback for all modes. Thus, the presence of gain gratings will reduce any threshold differences between laser modes, and enable multiple modes to simultaneously coexist in the laser. The negative feedback from the gain grating will decrease for each mode with an increasing number of modes. Therefore, the stabilizing effect of the gain gratings is strongest for lasers with relatively few modes.

Gain diffusion, i.e., nonradiative migration of electronic excitation of Er^{3+}, is ignored in the model used in this work. We do not believe gain diffusion is important for the Er^{3+} concentrations typically found in DFB fiber lasers, but if diffusion played a role, the higher harmonics of the gain function would attain smaller values [10]. We have also assumed that no clustering is present in the gain medium. Apart from increasing the lasing threshold and inducing self-oscillations, such clustering will reduce the mean lifetime of the erbium ions, thus lowering the strength of the gain grating.

C. Numerical Implementation

The DFB fiber structure was divided into several sections, and in each section the coupled-mode equations were solved using a transfer matrix approach [20]. Thus, we calculated the complex amplitudes of mode m at the right end of section q from the field of the sections to the left

$$\begin{bmatrix} A_{m,q} \\ B_{m,q} \end{bmatrix} = T_m^{q,q-1} \begin{bmatrix} A_{m,q-1} \\ B_{m,q-1} \end{bmatrix} = T_m^{q,0} \begin{bmatrix} A_{m,0} \\ B_{m,0} \end{bmatrix}$$
$$= T_m^{q,q-1} T_m^{q-1,q-2} T_m^{q-2,q-3} \cdots T_m^{1,0} \begin{bmatrix} A_{m,0} \\ B_{m,0} \end{bmatrix} \tag{6a}$$

with

$$T_m^{q,q-1} = \begin{bmatrix} r_m + d_m s_m, & (g_2^* + j\kappa) s_m \\ -(g_2 + j\kappa) s_m, & r_m - d_m s_m \end{bmatrix}$$

$$r_m = \cosh \gamma_m \Delta z_q, \qquad s_m = \frac{\sinh \gamma_m \Delta z_q}{\gamma_m}$$

$$\gamma_m = \sqrt{d_m^2 - (j\kappa + g_2^*)(j\kappa^* + g_2)}. \tag{6b}$$

Here, Δz_q is the length of section q, and in expressions (6b), all quantities are to be evaluated in the center of segment q. The section numbers are assigned in increasing order from left to right. In order to get accurate results, the length of each section Δz_q needs to be short enough to resolve the spatial variation of the modes and κ in the structure, i.e., in a multiple Λ structure Δz_q needs to be considerably shorter than the shortest beat length between the individual subgratings. The lasing condition

TABLE I
LASER PARAMETERS USED IN THE CALCULATIONS
(SYMBOLS ARE DEFINED IN THE TEXT)

Parameter	Value
g_s	15.9 dB/m
a_s	11.7 dB/m
g_p	3.0 dB/m
a_p	8.9 dB/m
a_0	0.24 dB/m
P_{sp}	4.1 mW/m
P_p	140 mW
N_{gm}	2
$\xi_2 = 1 - \xi_1$	0.38
$[\zeta_1, \quad \zeta_2]$	[1, 26]
r_{wl}	1480/1550=0.955

is fulfilled when the transmissivity of the structure is infinite for all modes [20], or

$$(T_m^{N_s,0})_{2,2} = 0, \qquad m = 1 \ldots N_m. \tag{7}$$

Here N_s is the total number of segments. It can be shown that this condition is mathematically identical to the round-trip condition used in [3].

Equation (7) is solved by iteration, where the detuning and the left output power of the modes are varied. The gain parameters g_0 and g_2 are found as a function of the local signal and pump fields from (4) to (5). The pump absorption a_{pump} and, thus, the local pump power P_p is found from g_0 through the following relation [3]:

$$a_{\text{pump}} = a_p + a_0 - \frac{g_p + a_p}{g_s + a_s}(g_0 + a_s). \tag{8}$$

IV. SIMULATION RESULTS

Using the algorithm outlined in Section III, we investigated the laser performance as a function of a range of different variables, including coupling strengths, Bragg frequency separation, grating phase shift, erbium concentration, degree of UV saturation during fabrication of gratings, phase relationship between the subgratings, and laser length. Although the numerical model can handle an arbitrary number of subgratings, we have for simplicity restricted the analysis in this work to dual Λ structures. In all calculations, we assumed a laser grating structure that was $l \approx$10-cm long. Except when considering saturation effects, each subgrating i also had a uniform coupling strength κ_i, and had a phase shift in the center $z = 0$. Except when the effect of varying this phase shift was investigated, its value was π, corresponding to a quarter of the Bragg wavelength of the subgrating. All other laser parameters common for the simulations are given in Table I, where the gain parameters are taken from one of the DFB fiber lasers characterized in [5]. That laser had a length of only $l = 4$ cm, but we have chosen longer structures in our examples since the photo-sensitivity has to be shared between two subgratings in a dual Λ structure.

A. Spatial Field and Gain Distributions

In order to understand the mechanism behind multimodal operation of DFB fiber lasers, we have found it useful to plot the spatial distribution of g_0, g_2, and the power of the laser modes. Not only the amplitude, but also the phase of g_2 is important. In order to understand the significance of the phase of g_2, we define for mode m

$$F_m = g_2 \frac{A_m}{B_m}. \tag{9}$$

It can be deduced from (3) that if the phase of this feedback parameter $\angle F_m$ averages around $\pm\pi$, the coupling due to the gain grating provides destructive interference for mode m. On the other hand, if $\angle F_m$ fluctuates quickly, the reflections from different sections of the gain grating will not be in phase and the gain grating will not affect the power of the mode.

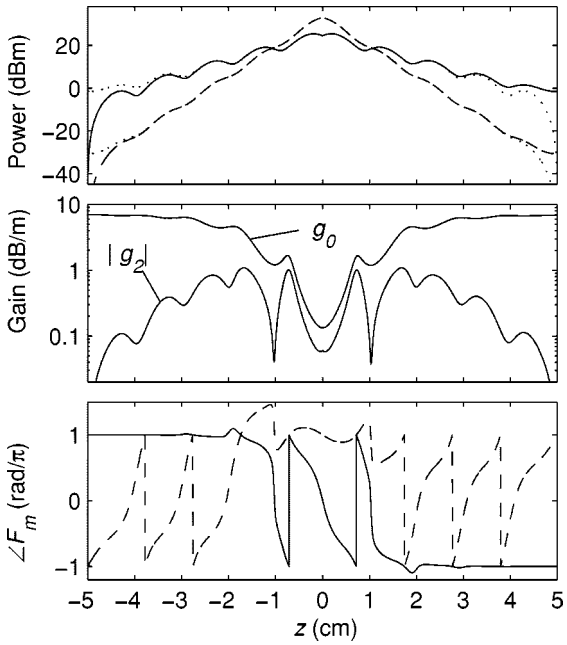

Fig. 2. Spatial distribution of gain parameters and the power of the two modes of a dual Λ DFB fiber laser with $\Delta\nu = 10$ GHz, $\Delta\phi = \pi$, and $l = 10$ cm. The stopbands of the two subgratings with coupling coefficients of $\kappa_1 = 73.5$ m^{-1} and $\kappa_2 = 160$ m^{-1} support one mode each, plotted with solid and dashed curves, respectively. Top: Local power of A_m, with B_m plotted with a dotted curve. Middle: g_0 and $|g_2|$. Bottom: $\angle F_m$.

In Figs. 2 and 3, we have plotted the power distribution of the lasing modes g_0, g_2, and $\angle F_m$ for two lasers with dual Λ gratings. We have chosen a relatively small separation between the Bragg frequencies of $\Delta\nu = 10$ GHz, so that the beat lengths are long enough to be clearly seen in the plots. The fundamental modes of single Λ DFB lasers have a close to exponential growth of the fields on both sides of the phase shift. In the top graph of both Figs. 2 and 3, we see that these profiles are perturbed by ripples. This will generally be the case for multiple Λ gratings, because the local degree of coupling between the forward and backward traveling waves is dependent on the absolute value of the total complex coupling function κ, and the phase relation between the grating and the standing wave pattern of the mode, both of which are varying in a periodic manner. The resulting ripples in gain and mode field power distribution will have an increase in frequency and decrease in amplitude with larger Bragg frequency separation between the subgratings.

In Fig. 2, the DFB laser structure has $\kappa_1 = 73.5$ m^{-1}, $\kappa_2 = 160$ m^{-1}, $\Delta\phi = \phi_2 - \phi_1 = \pi$, and $l = 10$ cm. The structure

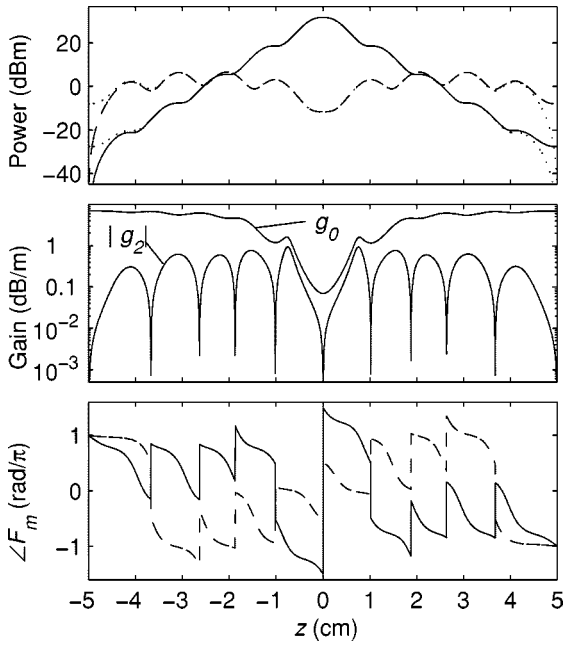

Fig. 3. Same as Fig. 2, but here $\kappa_1 = \kappa_2 = 150\ \mathrm{m}^{-1}$. The two fundamental modes (solid curve) and higher order modes (dashed curve) are plotted. Only $\angle F_m$ for one of the fundamental modes and higher order modes are plotted; for the other fundamental mode and higher order mode, the sign is opposite.

is lasing in two fundamental modes, operating in the stopband of the subgratings that will be denoted grating 1 and grating 2, respectively. Since grating 2 is much stronger than grating 1, the corresponding laser mode 2 has a lower lasing threshold. However, as discussed in [21], if κl of a DFB fiber laser becomes large enough, the maximum power of its fundamental mode around the phase shift will be clamped due to the intrinsic, unbleachable losses a_0 of the fiber. Once the maximum power of the mode is clamped, the output power will decrease when the coupling strength is increased as the mode becomes more confined to the area around the phase shift. Thus, more gain is left for other modes, and mode 1 has, in fact, larger output power than mode 2. As predicted by (4), the profiles of g_0 and especially g_2 do not depend only on the total average power P_{tot}, but also on the standing wave phasor P_c of the fields. For instance, the small values of g_2 around $z \approx \pm 1$ cm indicate that P_c is close to zero in these areas, and the local maxima and minima of g_0 do not correspond to the local minima and maxima, respectively, of the sum of the power of the modes. In regions where mode 1 has much larger power than mode 2, $\angle F_1 \approx \pm\pi$, whereas the phase of F_1 is oscillating rapidly in regions where mode 2 is larger, and vice versa for $\angle F_2$. Thus, the gain grating locally suppresses the dominating mode. If the subgratings had approximately the same coupling coefficients, the fundamental modes would have approximately the same spatial field distribution, and if one mode grew much larger than the other, it would experience negative feedback in the whole laser structure. Thus, the gain gratings always try to equalize the powers of the modes.

In Fig. 3, $\kappa_1 = \kappa_2 = 150\ \mathrm{m}^{-1}$, $\Delta\phi = \pi$, and $l = 10$ cm. Since the coupling coefficients of the two subgratings are equal, the spatial distribution of their corresponding fundamental modes are also identical. Again, since the coupling coefficients of the two subgratings are rather large, the fundamental modes are only able to saturate the gain around the phase shift of the laser, and enough gain is left for two higher order modes to reach threshold. Because of the symmetry in the dual Λ DFB structure, also the frequencies of the higher order modes are detuned in a symmetrical manner from the two subgrating Bragg frequencies, and thus also the two higher order modes have identical power distribution. Although the total stored energy of the higher order modes is smaller, and they have a higher threshold, their output power is larger than that of the fundamental modes, and their frequencies are located between the two grating stopbands. In most applications, such higher order modes are not wanted because they are less stable and more susceptible to back reflections into the cavity. Because of the symmetry of the frequencies and amplitudes of the modes, g_2 now has zeros. One of the zeros is at the phase shift, which is as expected since $\Delta\phi = \pi$.

B. Laser Operation as a Function of Coupling Strengths, Laser Length, and $\Delta\phi$

Prior to the fabrication of DFB fiber laser, it is useful to know what grating strength is needed to reach lasing threshold and maximum output power [21]. In many applications also, the threshold of higher order modes is of interest. In Fig. 4, the total left output power of the fundamental and higher order modes of dual Λ DFB lasers are plotted as functions of the integrated coupling coefficient $\kappa_1 l = \kappa_2 l$ for different structure lengths l and the two extreme values of $\Delta\phi$, $\Delta\phi = 0$ and $\Delta\phi = \pi$. The power is plotted for lasers with $\Delta\nu = 10$ GHz, and with lengths equal to $h_{\mathrm{beat}/2} = l/h_{\mathrm{beat}/2} = l(K_2 - K_1)/\pi = 9, 9.5, 10$, and 10.5 half-beat lengths of the grating amplitude modulation function. For comparison, the power of single Λ lasers with identical grating lengths are shown in the same plots.

As mentioned in Section II, the reflectivity of the grating will change with $\Delta\phi$ if $h_{\mathrm{beat}/2}$ is not an integer, leading to a $\Delta\phi$-dependent threshold when $h_{\mathrm{beat}/2} = 10 \pm 0.5$ in Fig. 4. For $h_{\mathrm{beat}/2} = 9.5$, the reflectivity is larger for the case $\Delta\phi = \pi$ than for $\Delta\phi = 0$, resulting in a lower threshold in the former than for the latter and single Λ case. As can be deduced from Fig. 1(a), this will generally be the case when the integral part of $h_{\mathrm{beat}/2}$ is an odd number. However, when the integral part of $h_{\mathrm{beat}/2}$ is an even number, the case $\Delta\phi = 0$ has a higher reflectivity, and thus has the lowest threshold. When $h_{\mathrm{beat}/2}$ is an integer, the reflectivities of the two dual Λ cases and the single Λ case are similar at the lasing wavelength, and no significant difference in threshold κ_1 has been found. For larger values of κ_1, where the output power drops, the case $\Delta\phi = 0$ has the highest power regardless of the length of the structure. As mentioned in Subsection IV-A, the internal loss determines the output power in this regime. For the case $\Delta\phi = \pi$, the coupling coefficient in the middle of the laser is zero. Thus, the central peak where the gain medium is bleached the most is broader than in the single Λ case, and the fundamental mode will, therefore, experience larger loss. The case $\Delta\phi = 0$, on the other hand, has a maximum of the coupling coefficient at the phase shift, and thus has the largest output power.

For some applications, back reflection into the cavity is not avoidable, but the detrimental effect on laser performance can be reduced if the reflectivity of the cavity mirrors are increased

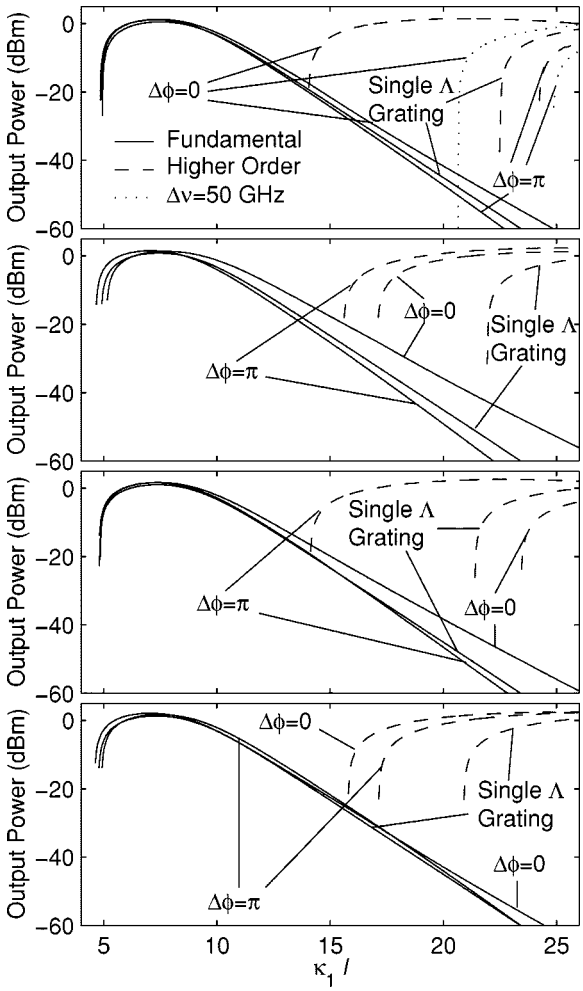

Fig. 4. Calculated total left output power of the fundamental (solid curve) and higher order (dashed curve) modes of dual Λ DFB fiber lasers with $\Delta\nu = 10$ GHz and different $\Delta\phi$ and l as functions of integrated coupling strength $\kappa_1 l$. The corresponding curves of single Λ DFB lasers are also plotted. Top: $l = 9.22$ cm equal to $h_{\mathrm{beat}/2} = 9$ half-beat lengths. Also shown is the higher order modes of structures with $\Delta\nu = 50$ GHz and the same $l = 9.22$ cm and $h_{\mathrm{beat}/2} = 45$. Upper middle: $l = 9.73$ cm and $h_{\mathrm{beat}/2} = 9.5$. Lower middle: $l = 10.24$ cm and $h_{\mathrm{beat}/2} = 10$. Bottom: $l = 10.75$ cm and $h_{\mathrm{beat}/2} = 10.5$.

[22]. Unfortunately, as discussed in Section IV-A, high values of κ enable higher order modes to lase. The thresholds of these modes are, therefore, of interest, even though these thresholds can be increased somewhat by removing the sharp outer edges of the grating through apodization [23]. By comparing the different curves of Fig. 4, it is evident that the onset of higher order modes for the dual Λ lasers is highly dependent on $\Delta\phi$, especially when $h_{\mathrm{beat}/2}$ is an integer. Usually, the thresholds of higher order mode operation are lower than in the single Λ case, because the higher order modes with lowest threshold will operate between the stopbands of the subgratings, and, therefore, their detuning will be smaller. However, higher order modes in the single Λ case will see a bit higher gain, since the two fundamental modes of a dual Λ structure saturate gain to a larger degree than a single mode because of the gain gratings. The lasing higher order modes of a dual Λ structure in the case of $\Delta\nu = 10$ GHz are close in frequency to the Bragg frequency of the compound grating. Thus, around each phase shift of the dual Λ DFB structure there will be a DFB-like subcavity for these modes,

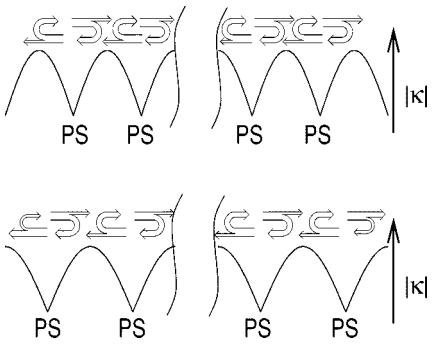

Fig. 5. Illustration of subcavities formed for higher order modes around each π phase shift of dual Λ DFB structures. Top: The subcavities at the grating ends are symmetric, corresponding to $\Delta\phi = 0$ and odd integer $h_{\mathrm{beat}/2}$ or $\Delta\phi = \pi$ and even integer $h_{\mathrm{beat}/2}$. Bottom: The subcavities at the grating ends are not symmetric, leading to higher mirror losses.

as illustrated in Fig. 5. If all subcavities are symmetric, as will be the case for $\Delta\phi = 0$, $h_{\mathrm{beat}/2} = 9$ and $\Delta\phi = \pi$, $h_{\mathrm{beat}/2} = 10$, the thresholds for these modes are significantly lowered compared to the single Λ case. However, if the outermost phase shifts of the dual Λ structure are closer to the edge of the grating, the cavity at the ends of the fiber will not be balanced. Such unbalance causes an increase of cavity loss and, thus, higher threshold for higher order mode operation. Keeping $\Delta\phi$ and $h_{\mathrm{beat}/2} = 9$ constant, the $\kappa_1 l$-threshold for higher order modes will decrease slightly with increasing cavity length, as it does for the single Λ cases plotted in Fig. 4. Although the lowest threshold we simulated for the dual Λ lasers was as high as $\kappa_1 l = 14$, it is important to bear in mind that this threshold is strongly dependent on the unbleachable losses, and could go as low as $\kappa_1 l = 12$ for larger values of a_0. If the center phase shift is not optimal, if there are phase errors in the gratings, or if the gain is higher, the higher order modes could be further enhanced. In Fig. 4, also the higher order modes for $\Delta\nu = 50$ GHz are shown for the two cases of $\Delta\phi$ for $h_{\mathrm{beat}/2} = 45$. As expected, the separation between $\Delta\phi = 0$ and $\Delta\phi = \pi$ is smaller than in the case $\Delta\nu = 10$ GHz, $h_{\mathrm{beat}/2} = 9$, which has the same physical length.

C. Unbalanced Coupling Strengths

In the previous section, we assumed that the coupling coefficients of the subgratings were equal. In practice, however, the effective coupling coefficients often will be different either purposely, due to imperfections of the grating fabrication setup, or, as discussed in Section IV-E, due to saturation of the UV sensitivity of the fiber. At the top of Fig. 6, the powers of the two fundamental modes of dual Λ DFB fiber lasers are plotted as functions of κ_1 for $\Delta\phi = \pi$ and $\Delta\phi = 0$. There is a detuning of $\Delta\nu = 10$ GHz between the subgratings, and the structure length is $h_{\mathrm{beat}/2} = 9.5$. κ_2 is kept constant at $\kappa_2 = 72.5$ m^{-1} and $\kappa_2 = 80$ m^{-1}, respectively. When $\kappa_1 = \kappa_2$, this corresponds to the maxima of the output powers plotted in Fig. 4. Mode 1 has the higher frequency of the modes, but for the output power it does not matter which mode has the lowest frequency, since we have assumed that the gain is equal for the two modes. For a fairly large range of values of κ_1 around κ_2, the two fundamental modes are lasing with comparable output powers. In the same graph we have also plotted the power of the modes

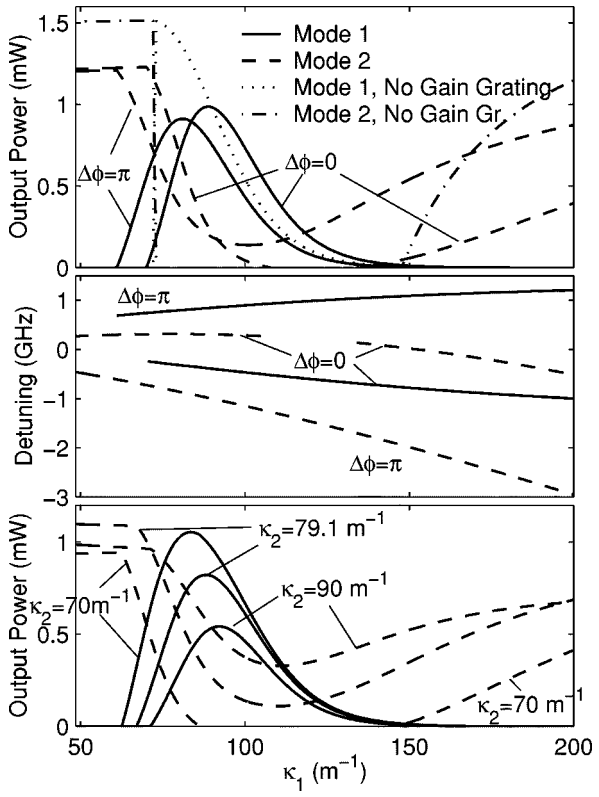

Fig. 6. Calculated left output power and detuning of the laser modes of dual Λ DFB fiber lasers as a function of κ_1. The frequency of mode 1 and mode 2 are in the stopband of the subgratings with coupling coefficients κ_1 and κ_2, respectively. For all calculations, $\Delta\nu = 10$ GHz and $h_{\mathrm{beat}/2} = 9.5$. Top: Power of modes, $\kappa_2 = 72.5$ m^{-1} and $\Delta\phi = \pi$, and $\kappa_2 = 80$ m^{-1} and $\Delta\phi = 0$, respectively. For $\Delta\Phi = \pi$, also the case with the gain gratings ignored is included. Middle: Detuning of the modes in the top plot. Bottom: Power of modes with κ_2 as a parameter, $\Delta\phi = \pi$ and $h_{\mathrm{beat}/2} = 9$.

when the gain gratings are ignored by setting $P_c = 0$ in the gain model. In this case, the two modes cannot coexist, unless the difference in coupling coefficient between the two subgratings is very large and we have global spatial hole burning of the type shown in Fig. 2. Thus, the gain gratings enable multiple fundamental modes in a DFB fiber laser. For different values of $h_{\mathrm{beat}/2}$, keeping κ_2 at the overall power maximum, the plots are similar around $\kappa_1 \approx \kappa_2$, but generally the slopes are smaller in the case $\Delta\phi = \pi$ than $\Delta\phi = 0$, since the latter has a larger output power for higher coupling coefficients, as discussed in Section IV-B. For most grating fabrication setups, it is probably also easier to fabricate good gratings with $\Delta\phi = \pi$, so that is perhaps the preferred choice of $\Delta\phi$ for most applications. Note that for $\Delta\phi = \pi$ at the top of Fig. 6, both modes are lasing for all values of κ_1 above the threshold of Mode 1. This will also be the case for many values of $h_{\mathrm{beat}/2}$ when $\Delta\phi = 0$, although it is not the case for $h_{\mathrm{beat}/2} = 9.5$. The difference between the extreme cases of $\Delta\phi$ decreases with increasing frequency separation, since the amplitude and period of the ripples in the spatial power distributions become smaller.

The middle graph in Fig. 6 shows the detuning of the modes plotted in the top graph. The detuning is referenced relative to the closest Bragg frequency of the subgratings. Mode 1 still has the highest frequency of the two modes; if it had the lowest frequency, all the detuning values would shift sign because of the symmetry of the problem. For the case $\Delta\phi = 0$, the modes are detuned toward each other, whereas in the case $\Delta\phi = \pi$, the modes are repelled from each other. This will be the case for all values of $\Delta\nu$, $h_{\mathrm{beat}/2}$, κ_1, and κ_2 for a dual Λ structure with a center phase shift value of π, and could be understood by extending the discussion of Section II. A fundamental lasing condition is that the round-trip phase should be zero, which for a symmetric cavity means that each grating half needs to have a real reflectivity. For a π phase-shifted single Λ DFB fiber laser, this condition will be met at the Bragg frequency, when reflections from all parts of the grating mirrors will be added in phase. For a dual Λ DFB fiber laser, reflections from different parts of the grating will not be added in phase because of the phase shifts or chirp of the grating, and the two modes will be at frequencies where the imaginary contributions cancel each other. For a weak grating or large $\Delta\nu$, these two laser frequencies will be close to the Bragg frequency of the subgratings. However, for stronger gratings and smaller $\Delta\nu$, the cancellation will not be exact at the subgrating Bragg frequencies because of the quasiexponential decline of the modal power with increasing distance from the phase shift. This has to be compensated by a detuning of the modes, whose sign depends on $\Delta\phi$, i.e., the location of the sign shift in the beat pattern.

We also investigated the effect of varying κ_1 for higher and lower values of κ_2, and an example is shown in the lower part of Fig. 6 for $h_{\mathrm{beat}/2} = 9$ and $\Delta\phi = \pi$. The maximum output power of the laser in this case is at $\kappa_2 = \kappa_1 = 79.1$ m^{-1}. When increasing κ_2 to 90 m^{-1}, the slopes of the curves become lower around $\kappa_2 \approx \kappa_1$, but this decrease in fabrication tolerance comes at the expense of lower output power. For values of κ_2 lower than 79.1 m^{-1}, the output power also decreases but, at the same time, the power dependence of the modes on κ_1 around $\kappa_2 \approx \kappa_1$ increases, because the fundamental modes are closer to the lasing threshold. We have also investigated the effect of increasing or decreasing the gain parameters, and found that an increase in gain increases both the robustness of the dual mode lasing and the output power, but in fiber fabrication higher gain often comes at the cost of lower photo-sensitivity and/or Er^{3+} clustering.

D. Dependence on the Value of the Center Phase Shift

If the discrete center phase shift of an ordinary single Λ DFB fiber laser deviates from the optimal value of π, the frequency of the fundamental mode will gradually be moved away from the Bragg center frequency. Also the fundamental mode frequencies of a multiple Λ laser will move, but the individual modes will be affected differently. In the dual Λ case with equal subgrating strength, the detuning of the two modes from $\overline{\beta}$ will no longer have the same absolute value. This asymmetry in detuning leads to an asymmetry in the mirror reflectivity, because the real, constructively interfering, contributions to the reflectivity for the two modes will come from different regions of the amplitude modulated grating mirrors. In Fig. 7, this effect has been illustrated by plotting the output power of various dual Λ lasers as a function of the center phase-shift value. We have assumed that the deviation from the optimal phase-shift value is the same for

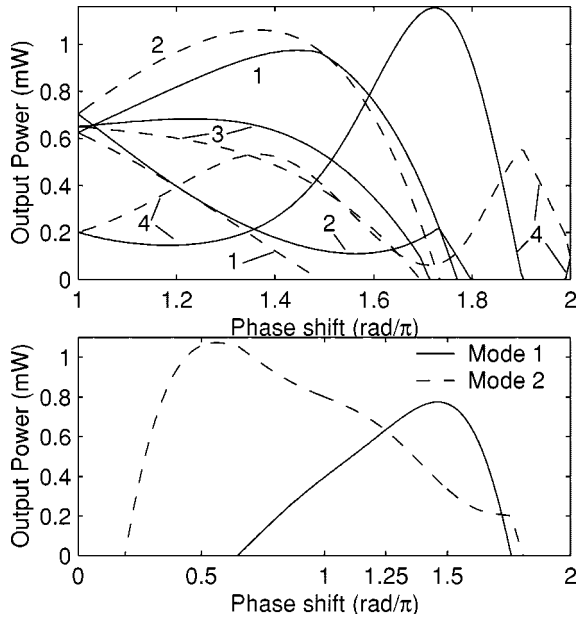

Fig. 7. Left output power of all modes for various dual Λ DFB fiber lasers as a function of center phase shift. Mode 1 (solid curve) has higher frequency than mode 2 (dashed curve), and $l = 9.22$ cm corresponding to an odd integer value of $h_{\mathrm{beat}/2}$ for all structures. 1: $\Delta\nu = 10$ GHz, $\Delta\phi = \pi$, $\kappa_1 = \kappa_2 = 79.1$ m^{-1}. 2: $\Delta\nu = 10$ GHz, $\Delta\phi = 0$, $\kappa_1 = \kappa_2 = 80.4$ m^{-1}. 3: $\Delta\nu = 90$ GHz, $\Delta\phi = \pi$, $\kappa_1 = \kappa_2 = 80.7$ m^{-1}. 4: $\Delta\nu = 10$ GHz, $\Delta\phi = \pi$, $\kappa_1 = \kappa_2 = 110$ m^{-1}. Bottom: $\Delta\nu = 10$ GHz, $\Delta\phi = \pi$, $\kappa_1 = 85$ m^{-1}, $\kappa_2 = 79.1$ m^{-1}.

both subgratings in the DFB structures. Both subgratings of the structures plotted in the top plot of Fig. 7 have equal strength, and the curves are, therefore, antisymmetric around the center phase-shift value of π.

For $\Delta\phi = \pi$, the mode lasing in the stopband with the lowest frequency will move further away from the closest subgrating Bragg frequency when the value of the phase shift gets larger than π, and, thus, the effective finesse of the cavity decreases. For the case $\kappa_1 = \kappa_2 = 79.1$ m^{-1}, which for a phase-shift value of π yields maximum output power, the power of the mode will then decrease with increasing phase shift. However, for higher coupling coefficients, the output power will initially increase for reasons discussed in Section IV-B. The other mode, however, will initially get closer to its Bragg frequency and its output power will thus increase for lower coupling coefficients and decrease for higher coupling coefficients. When the phase shift is around 1.23π for the case $\kappa_1 = \kappa_2 = 79.1$ m^{-1}, the high-frequency mode is lasing at the subgrating Bragg frequency, but continues to gain power as the power of the other mode decreases, and it ceases to lase only for a phase-shift value around 1.77π with a negative detuning of -1.93 GHz, not far from the edge of the stopband. For $\Delta\phi = 0$, we see roughly the same trends with opposite signs for the two modes. Again, in this case the curves are slightly steeper than in the case $\Delta\phi = \pi$. When the frequency separation between the two modes is larger, it is expected that the modes respond to changes in the phase shift in a more uniform manner. However, the power difference between the two modes in the case of $\Delta\nu = 90$ GHz is still considerable, with a maximum power difference of 0.15 mW, or about 30% relative to the mode with the highest power. It is interesting to note that at quite high, but obtainable, values of the coupling coefficient and rather low frequency separations, the DFB structure will never cease to lase with at least one mode, regardless of the value of the phase shift, as shown by Curve 4 in Fig. 7.

Since a change in the value of the phase shift leads to a change of the power difference between the modes, it should be possible to equalize the power of the two modes by tuning the phase shift. This is exemplified in the lower part of Fig. 7, where the response of the modal output powers to the tuning of the phase shift for a dual Λ structure with $\kappa_1 = 79.1$ m^{-1}, $\kappa_2 = 85$ m^{-1}, $\Delta\nu = 10$ GHz, and $\Delta\phi = \pi$ is plotted. In spite of the difference in the subgrating coupling coefficients, the output powers of the two modes are equalized at a phase-shift value of 1.25π radians.

E. Errors in Chirp and Grating Amplitude Modulation Due to UV Saturation

Except for variations in the value of the center phase shift, we have so far assumed that the gratings are perfect. However, in a typical grating writing setup, the quality of the grating could be limited by factors such as unintended quadratic and linear chirp, finite UV beam size, and, finally, saturation of the UV-induced refractive index change of the fiber. Quadratic and linear chirp may affect the quality of a multiple Λ DFB fiber laser, but can in theory be measured and corrected for during fabrication. Since the UV beam size is finite in any setup, the spatial resolution is limited, and it may, therefore, be difficult to write several superimposed Bragg gratings with large frequency separation in one single scan. However, the problem can be eliminated by using multiple scans.

For a specified subgrating strength, the maximum absolute value of the intended total multiple Λ coupling function increases with the number of subgratings. Thus, saturation of the UV-induced refractive index change of the fiber is more likely to cause problems in multiple Λ gratings than in single Λ gratings. Such saturation generally limits the maximum achievable grating strength, but in the multiple Λ case it also leads to periodic errors in the absolute value of κ and, more seriously, periodic chirp. In order to evaluate these effects, we chose an exponential response of the refractive index change as a function of the UV fluence:

$$\Delta n_{\mathrm{loc}}(z) = \Delta n_{\mathrm{sat}}\left[1 - \exp\left(-\frac{\Delta n_{\mathrm{unsat}}(z)}{\Delta n_{\mathrm{sat}}}\right)\right] \triangleq n_{\mathrm{sat}}\left(1 - e^{-\alpha(z)}\right). \tag{10}$$

Here, $\Delta n_{\mathrm{unsat}}(z)$ is the intended local index change assuming a linear response to the UV fluence, Δn_{sat} is the saturation level of the index change, and Δn_{loc} is the actual local index change. In the following, it is assumed that the total fluence averaged over a period of the grating is constant along the DFB structure

$$\alpha(z) = \alpha_0 + \alpha_1(z)\cos\left(2\overline{\beta}z + \Phi_0(z)\right). \tag{11}$$

Here, $\alpha_0 \geq \alpha_1$ is constant, whereas $\alpha_1(z)$ is proportional to the intended local amplitude of the complex coupling function κ,

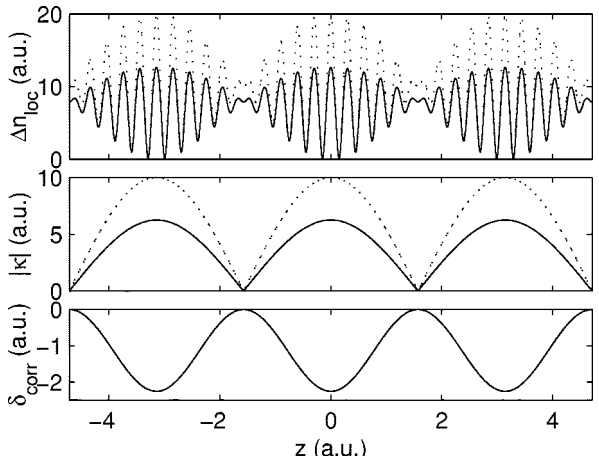

Fig. 8. Saturation of the UV-induced refractive index change in a dual Λ grating structure. The intended (dotted curve) and actual (solid curve) of Δn and $|\kappa|$ are shown in the top and middle graph, respectively. The saturation level is $\kappa_{\rm sat} = \Delta n_{\rm sat} = 20$. The bottom graph shows the resulting variation in detuning, $\delta_{\rm corr}$.

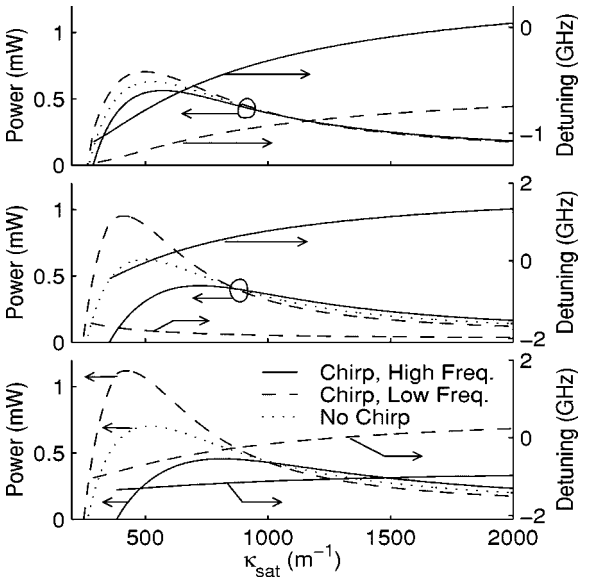

Fig. 9. Left output power and detuning of modes as a function of saturation level for a dual Λ laser where both subgratings have an unsaturated coupling strength of 130 $\rm m^{-1}$ over a length $l = 9.22$ cm. Both the cases with and without chirp induced by UV saturation are plotted, but the detuning for the unchirped case is omitted. Top: $\Delta\nu = 50$ GHz, $\Delta\Phi = \pi$. Middle: $\Delta\nu = 10$ GHz, $\Delta\Phi = \pi$. Bottom: $\Delta\nu = 10$ GHz, $\Delta\Phi = 0$.

and $\Phi_0(z)$ is its intended phase. By assuming that α_1 and the derivative of Φ_0 are slowly varying, we can calculate the zeroth- and second-order Fourier component of $\Delta n_{\rm loc}$ from (10) and (11). The zeroth-order Fourier component corresponds to the mean local refractive index, whereas the second-order Fourier component corresponds to the local grating strength. Performing these Fourier integrals leads to the following expressions for the additional detuning $\delta_{\rm corr}$ and absolute value of the complex coupling coefficient κ

$$\delta_{\rm corr} = 2n\kappa_{\rm sat} e^{-\alpha_0}[1 - I_0(\alpha_1)] \tag{12}$$

$$|\kappa| = 2\kappa_{\rm sat} e^{-\alpha_0} I_1(\alpha_1). \tag{13}$$

Here, we have defined $\kappa_{\rm sat} = \kappa_{\rm unsat}/\alpha_1$, where $\kappa_{\rm unsat}$ is the coupling coefficient expected from a linear response, and the relationship between refractive index modulation and the coupling coefficient provided by [11] has been used. $I_i(\alpha_1)$ is the modified Bessel function of the first kind and order i, and n is the refractive index. The effect of saturation of the UV induced refractive index shift on $\Delta n_{\rm loc}$, $|\kappa|$ and $\delta_{\rm corr}$ is illustrated in Fig. 8. The average shift $\Delta n_{\rm sat}(1 - e^{-\alpha_0})$ is ignored in equation (12), and, thus, $\delta_{\rm corr} = 0$ when $\alpha_1 = 0$ and $\delta_{\rm corr} < 0$, otherwise. The reason that we get a negative shift of $\delta_{\rm corr}$ for larger values of $\kappa_{\rm unsat}$, is that there is larger saturation for higher values of $\Delta n_{\rm loc}$. Thus, at average there will be more saturation in regions of the fiber with larger index modulation, even though the mean UV fluence, quantified by α_0, is constant along the fiber axis. From (12) and (13), the coupling function corrected for UV saturation effects becomes

$$\kappa = |\kappa| e^{j(\Phi_0(z) + \Phi_{\rm corr})} \text{ where } \Phi_{\rm corr} = -2\int_{-L/2}^{z} \delta_{\rm corr}\, dz. \tag{14}$$

In the integral of (14), it is, as before, assumed that the grating center is located at $z = 0$.

In Fig. 9, we have plotted the power and detuning of the two modes of a dual Λ DFB with $\kappa_{\rm unsat} = 130\ \rm m^{-1}$ as a function of saturation level $\kappa_{\rm sat}$ for various laser structures, with the modified coupling function κ given in equation (14). In addition, we have plotted the power of the modes for the same structures, but with no chirp induced by saturation of the UV-induced refractive index change, or $\delta_{\rm corr} = 0$. The figure shows that the saturation seriously affects the output power of the lasers. Firstly, the deviation from the correct values of κ leads to a lower reflectivity in the two stopbands of the gratings. In addition, there will be several weaker stopbands in the reflection spectrum of the grating, since the deviation from the correct profile represents an introduction of higher order harmonics in the amplitude modulation function. However, the two fundamental modes are affected in a symmetrical manner, and in the absence of any extra chirp, their powers remain equal to each other. On the other hand, the introduction of $\delta_{\rm corr}$ leads to a split of the output power levels and breaks the symmetry of the detuning of the modes. Since $\delta_{\rm corr}$ decreases with increasing $|\kappa|$, the low-frequency mode will be less detuned from the grating in regions with large values of $|\kappa|$ than in regions where $|\kappa|$ is smaller, while the opposite will be true for the high-frequency mode. Therefore, the effective mirror reflectivity will be larger for the low-frequency mode than the high-frequency mode. Again, the effect seems to be larger for $\Delta\phi = 0$ and for smaller $\Delta\nu$, in the latter case because $\delta_{\rm corr}$ becomes larger relative to the total detuning δ_m between the grating and the laser modes.

V. Conclusion

We have analyzed multiple wavelength DFB fiber lasers using a comprehensive numerical model. Such lasers consist of several superimposed phase-shifted Bragg gratings, and modes can lase in or at the edge of the stopbands of the individual

gratings, sharing the same gain medium. We have studied the effect of variations of grating coupling strengths, phase relationship between the superimposed gratings, structure length, gain parameters, grating Bragg frequency separations, grating phase-shifts, and saturation level of the UV-induced refractive index variation, on the number of lasing modes and their respective powers and frequencies.

We have found that several fundamental modes with similar spatial field distribution can lase simultaneously with identical polarization in the same gain medium, although the modes have slightly different thresholds. The simultaneous lasing of multiple modes is attributed to the dynamically induced gain gratings, which cause destructive feedback for the modes with the highest power. Without this effect, the mode with lowest threshold would clamp the gain to its threshold value, and two or more modes would not coexist.

A structure with two superimposed Bragg gratings sharing the same gain medium can support two fundamental modes with comparable output powers, even though the difference between the coupling strengths of the two gratings is quite large. If the two gratings are in anti-phase around the phase shift, we have found that the difference in lasing powers usually is less sensitive to changes in coupling strength than if the two superimposed gratings are in phase. The location of the phase shift in the former case also puts fewer demands on the spatial resolution of the grating writing process, since the phase shift would be located at a minimum of the grating superstructure, and is, thus, probably the preferred choice in most applications. The importance of the phase relationship between the two gratings decreases with increasing frequency separation. We have also found that an increase in the available gain leads to more stable dual-mode operation, as well as higher output power.

The thresholds for both the fundamental and higher order modes are dependent on the phase relationship between the superimposed gratings and the length of the structure relative to the beat lengths between the superimposed gratings. For a structure with two superimposed gratings of equal strength, the threshold for higher order mode operation is highest if the gratings are either in phase at the center phase-shift position and an even number of half-beat-lengths long, or in anti-phase at the center phase-shift position and an odd number of half-beat-lengths long.

Deviation from the ideal phase-shift value of π between the two halves of the gratings leads to changes in the difference between the output powers of the lasing modes. These changes in the output powers are caused by detuning of the resonant frequencies of the superimposed gratings. Even if the phase shift is correct, the resonances are detuned from the center frequencies of their respective solitary Bragg gratings because their reflection spectra interact in the superimposed structure. For a dual wavelength DFB fiber laser, where the modes initially do not have equal output powers, it is in many cases possible to compensate for the imbalance by tuning the phase shift.

Saturation of the UV-induced refractive index change has been identified as a possible limitation for the fabrication of multiwavelength DFB lasers. This saturation puts a limit on the maximum grating strength, and it could make it impossible to obtain the relative large coupling coefficients needed for multiple mode lasing. In addition, such saturation leads to periodic chirp in a structure with multiple superimposed Bragg gratings, favoring the mode with lowest frequency. However, if using a fiber with sufficiently high photo-sensitivity and compensation for any periodic chirp, saturation of the UV-induced refractive index does not need to be a problem. The periodic chirp can be compensated for by either using a spatially periodic UV fluence during grating writing, writing one of the gratings stronger than the other one, or deviating the phase-shift value from π radians.

ACKNOWLEDGMENT

The authors would like to thank K. Bløtekjær for his guidance during the work and E. Rønnekleiv for useful advice.

REFERENCES

[1] J. T. Kringlebotn, J. Archambault, L. Reekie, and D. N. Payne, "$Er^{3+}:Yb^{3+}$-codoped fiber distributed feedback laser," *Opt. Lett.*, vol. 19, pp. 2101–2103, Dec. 1994.

[2] M. Ibsen, E. Rønnekleiv, O. Hadeler, G. J. Cowle, M. N. Zervas, and R. I. Laming, "Stable multiple wavelength generation in all-fiber DFB lasers," in *Proc. BGPP—Topical Meeting on Bragg Gratings, Photosensitivity, and Poling in Glass Waveguides*, ser. 1999 OSA Tech. Dig. Stuart, FL, Sept. 1999, pp. 149–154.

[3] E. Rønnekleiv, M. N. Zervas, and J. T. Kringlebotn, "Modeling of polarization-mode competition in fiber DFB lasers," *IEEE J. Quantum Electron.*, vol. QE-34, pp. 1559–1568, Sept. 1998.

[4] ——, "Corrections to 'Modeling of polarization-mode competition in fiber DFB lasers'," *IEEE J. Quantum Electron.*, vol. 35, pp. 1097–1100, July 1999.

[5] E. Rønnekleiv, M. Ibsen, and G. J. Cowle, "Polarization characteristics of fiber DFB lasers related to sensing applications," *IEEE J. Quantum Electron.*, vol. 6, pp. 656–664, June 2000.

[6] M. Horowitz, R. Daisy, B. Fischer, and J. L. Zyskind, "Linewidth-narrowing mechanism in lasers by nonlinear wave mixing," *Opt. Lett.*, vol. 19, no. 18, pp. 1406–1408, 1994.

[7] M. Sargent III, M. O. Scully, and W. E. Lamb Jr., *Laser Physics*. Reading, MA: Addison-Wesley, 1974.

[8] C. L. Tang, H. Statz, and G. deMars, "Spectral output and spiking behavior of solid-state lasers," *J. Appl. Phys.*, vol. 34, pp. 2289–2295, Aug. 1963.

[9] P. R. Morkel, G. J. Cowle, and D. N. Payne, "Traveling-wave erbium fiber ring laser with 60 kHz linewidth," *Electron. Lett.*, vol. 26, pp. 632–634, May 1990.

[10] B. Jaskorzynska, E. Vanin, and S. Helmfrid, "Gain-saturation gratings with an arbitrary diffusion rate of excited states," *J. Opt. Soc. Amer. B*, vol. 15, pp. 945–950, Mar. 1998.

[11] H. Kogelnik and C. V. Shank, "Coupled-wave theory of distributed feedback lasers," *J. Appl. Phys.*, vol. 43, pp. 2327–2335, May 1972.

[12] W. S. Rabinovich and B. J. Feldman, "Spatial hole burning effects in distributed feedback lasers," *IEEE J. Quantum Electron.*, vol. 25, pp. 20–29, Jan. 1989.

[13] M. Ibsen, E. Rønnekleiv, G. J. Cowle, M. O. Berendt, O. Hadeler, M. N. Zervas, and R. I. Laming, "Robust high-power (>20 mW) all-fiber DFB lasers with unidirectional and truly single polarization outputs," in *Proc. Conf. Lasers and Electro-Optics (CLEO) 1999*, Baltimore, MD, 1999, pp. 245–246.

[14] H. Storøy, B. Sahlgren, and R. Stubbe, "Single polarization fiber DFB laser," *Electron. Lett.*, vol. 33, pp. 56–58, Jan. 1997.

[15] J. I. Philipsen, M. O. Berendt, P. Varming, V. C. Lauridsen, J. H. Povlsen, J. Hübner, M. Kristensen, and B. Pálsdóttir, "Polarization control of DFB fiber laser using UV-induced birefringent phase-shift," *Electron. Lett.*, vol. 34, pp. 678–679, Apr. 1998.

[16] C. R. Giles and E. Desurvire, "Modeling erbium-doped fiber amplifiers," *J. Lightwave Technol.*, vol. 9, pp. 271–283, Feb. 1991.

[17] E. Desurvire, "Erbium-doped fiber amplifiers: Basic physics and characteristics," in *Optical Engineering*, M. J. F. Digonnet, Ed. New York: Marcel Dekker, 1993, vol. 37, ch. 10.

[18] V. C. Lauridsen, T. Søndergaard, P. Varming, and J. H. Povlsen, "Design of distributed feedback fiber lasers," in *Proc. 23rd Eur. Conf. Optical Communications IOOC-ECOC 97 (Conf. Publ. no. 448)*, vol. 3, London, UK, 1997, pp. 39–42.

[19] G. P. Agrawal and M. Lax, "Effects of interference on gain saturation in laser resonators," *J. Opt. Soc. Amer.*, vol. 69, pp. 1717–1719, Dec. 1979.
[20] G. Björk and O. Nilson, "A new exact and efficient numerical matrix theory of complicated laser structures: Properties of asymmetric phase-shifted DFB lasers," *J. Lightwave Technol.*, vol. LT-5, pp. 140–146, Jan. 1987.
[21] V. C. Lauridsen, J. H. Povlsen, and P. Varming, "Optimising erbium-doped DFB fiber laser length with respect to maximum output power," *Electron. Lett.*, vol. 35, pp. 300–302, Feb. 1999.
[22] E. Rønnekleiv and S. W. Løvseth, "Stability of distributed feedback fiber lasers with optical feedback," in *Proc. 13th Int. Conf. Optical Fiber Sensors*, vol. 3746, B. Y. Kim and K. Hotate, Eds..
[23] D. Y. Stepanov, J. Canning, L. Poladian, R. Wyatt, G. Maxwell, R. Smith, and R. Kashyap, "Apodized distributed-feedback fiber laser," *Opt. Fiber Technol.*, vol. 5, pp. 209–214, 1999.

Sigurd Weidemann Løvseth received the Siv.Ing. degree in physics in 1996 from the Norwegian Institute of Technology, University of Trondheim, Trondheim, Norway. He is currently working toward the Dr. Ing. degree in fiber optics at the Norwegian University of Science and Technology, Trondheim, Norway.

Since 1997, he has been with the Department of Physical Electronics, Norwegian University of Science and Technology, Trondheim, Norway, and since March 2001, also with Optoplan AS, Trondheim, Norway. Prior to this, he was with the European Laboratory for Particle Physics (CERN), Geneva), Switzerland, in 1994, the Norwegian Defence Research Establishment in 1996, the Department of Electrical Engineering, University of Minnesota, Minneapolis, during 1995–1996, the Royal Norwegian Air Force Academy during 1996–1997, and the Australian Photonics CRC, Optical Fibre Technology Centre (OFTC), The University of Sydney, Sydney, Australia, during 1999–2000. He has studied semiconductor directional couplers, but his current research interest is in the understanding and applications of advanced active and passive fiber Bragg grating structures, in particular distributed feedback fiber lasers.

Dmitrii Yu Stepanov was born in Moscow, Russia. He received the M.S. degree in physics from Moscow State University, Moscow, Russia, in 1983, and the Ph.D. degree in laser physics from General Physics Institute, Russian Academy of Sciences, Moscow, Russia, in 1992.

He is currently with Redfern Optical Components (ROC), Eveleigh, NSW, Australia, where he is the inventor of ROC's core grating writing technology and is Chief Technical Officer, leading the company's R&D and contributing to the development of the company strategy. His responsibilities include overall scientific direction and technical supervision of the R&D projects, direct technical contributions with strong focus on the core grating writing technology, and technology transfer to the manufacturing environment. He has previously conducted research with the General Physics Institute in the areas of photo-induced phenomena in optical fibers and glasses, nonlinear optics, and nonlinear guided wave optics. In 1994, he joined Australian Photonics CRC, Optical Fibre Technology Centre (OFTC), The University of Sydney, Sydney, Australia, where he was a Senior Research Fellow and Key Researcher, working on various aspects of grating technology and its applications in fiber devices for telecommunications and sensors. He has published over 80 papers and is a co-inventor in over 10 patent applications.

Chapter 7

Dynamic analysis of multiple wavelength DFB fiber lasers

Authors: Lovseth, S.W.; Stepanov, D.Yu.;

Published in IEEE journal of quantum electronics

Dynamic Analysis of Multiple Wavelength DFB Fiber Lasers

Sigurd Weidemann Løvseth and Dmitrii Yu Stepanov

***Abstract*—The behavior of multi- and single-wavelength distributed feedback fiber lasers is simulated in a comprehensive dynamic model. The evolution of the spatial distribution of gain, saturation-induced gain gratings, and spontaneous emission is taken into account. Stability and relative intensity noise (RIN) of the different laser types and laser modes are compared, and the effect of varying degree of pump RIN and quenching of spontaneous emission lifetimes is analyzed.**

***Index Terms*—Distributed feedback lasers, erbium, laser modes, laser noise, laser stability, optical fiber Bragg gratings, optical fiber lasers, optical hole burning.**

I. Introduction

MULTIPLE wavelength distributed feedback fiber lasers (DFB-FL) [1], [2] are attractive for a range of applications in optical communications, including soliton and microwave generation. In [3] we performed a static analysis of such lasers. However, probably more interesting is the dynamic behavior of multi-wavelength DFB-FLs. The fluctuations of the optical roundtrip path length due to fundamental thermal noise [4] and environmental acoustic and thermal perturbations [5] are thought to be dominating sources of frequency noise outside the relaxation oscillation peak [6] for a laser that is shielded against optical feedback [7]. Thus, the frequency noise of multiple wavelength DFB-FLs will be close to that of single wavelength lasers with similar gain and grating parameters, since there will be large overlap between their modal field distributions. Using the same logic, we also note that there will be a high degree of temporal correlation between the frequency noise of the modes of a multiple wavelength DFB-FL. Thus, an optically isolated multi-wavelength DFB-FL would provide a very stable beat frequency.

Such a stable beat frequency would, however, be of little use if the laser had excess intensity noise. As argued in [6], the frequency noise has little effect on the intensity noise of the laser. In this work, we will therefore analyze the dynamics of both single-mode and multiple-wavelength DFB-FLs, ignoring the frequency noise. Other dynamic models for DFB-FLs that have been published [8]–[11] treat only the single-mode case and ignore gain gratings, which is very important in order to understand the operation of multiple wavelength lasers. References [10], [11] in addition ignore variations in the spatial distribution of the laser, and the former also assumes low saturation, which is clearly wrong in the case of the high-finesse DFB-FLs.

Manuscript received March 21, 2001; revised July 2, 2001. This work was supported by the Norwegian Research Council.

S. W. Løvseth was with the Australian Photonics CRC, Optical FibreTechnology Centre, The University of Sydney, Australia. He is now with the Department of Physical Electronics, Norwegian University of Science and Technology, N-7491 Trondheim, Norway, and also with Optoplan AS, N-7448 Trondheim, Norway.

D. Yu. Stepanov is with Redfern Optical Components Pty. Ltd., Australian Technology Park, Eveleigh, NSW 1430, Australia.

Publisher Item Identifier S 0018-9197(01)08335-X.

II. Numerical Model

A. Dynamic and Static-Coupled Mode Analysis

We have constructed a numerical model that calculates the dynamic evolution of all the modes of a general, single-polarization, multiple-wavelength DFB-FL. We describe the spatial distribution of the different laser modes by slowly varying complex amplitudes A_m and B_m for the right and left propagating mode number m, respectively. In this notation, the total local field of the mode becomes

$$E_m(z,\,t) = A_m(z,\,t)e^{j(\omega_m t-\overline{\beta}z)} + B_m(z,\,t)e^{j(\omega_m t+\overline{\beta}z)}. \quad (1)$$

Here, $\overline{\beta}$ is the average Bragg wavenumber of the gratings, which will be used as a reference for the detuning, and ω_m is the angular frequency of mode m.

In [12] and [13], a large-signal dynamic model for DFB semiconductor lasers was proposed. We use a similar time-dependent coupled-mode [14] formulation with some notable alterations.

Firstly, in order to correctly account for the interaction between several superimposed gratings, a complex index-coupling function κ is defined

$$\kappa = \sum_{i=1}^{N_g} \kappa_i e^{-j2(K_{B,\,i}-\overline{\beta})z+j\phi_i}. \quad (2)$$

Here, κ_i, $K_{B,\,i} = \pi/\Lambda_i$, Λ_i, and ϕ_i are the coupling strength, the Bragg wavenumber, the period, and a generally z-dependent phase term, respectively, of grating number i. N_g is the total number of gratings. A laser with several superimposed Bragg gratings with different Bragg wavelengths will be referred to as multiple Λ DFB-FLs for the remainder of the paper.

Secondly, we have to add saturation induced gain gratings [3], [15]–[17] to the formalism of [12] and [13], and we then get the following dynamic coupled-mode equations [14] for mode number m of the laser

$$\begin{aligned}\frac{\partial A_m}{\partial z} &= \left(d_m - \mu_m^+\right) A_m + \left(j\kappa + g_2^*\right) B_m + i_{f,\,m} \\ -\frac{\partial B_m}{\partial z} &= \left(d_m - \mu_m^-\right) B_m + \left(j\kappa^* + g_2\right) A_m + i_{b,m} \end{aligned} \quad (3a)$$

where

$$\begin{aligned}\mu_m^+ &= \frac{1}{A_m C_g}\frac{\partial A_m}{\partial t}, \qquad \mu_m^- = \frac{1}{B_m C_g}\frac{\partial B_m}{\partial t} \\ d_m &= g_0 - a_0 - j\delta_m. \end{aligned} \quad (3b)$$

Here C_g is the group velocity of light in the fiber, δ_m is the detuning of the mode from the average Bragg wavenumber. $\overline{\beta}$, g_0 and g_2 are the mean gain and gain grating coefficients to be discussed in Section II-B, a_0 is the unbleachable loss of the fiber, and the superscript "*" denotes complex conjugation. $i_{f,m}$ and $i_{b,m}$ represent the spontaneous emission into the forward and backward traveling mode, respectively, which will be discussed in Section II–C.

B. Gain Model

We have assumed the same nature of the gain medium as in our previous work [3]. Following the ideas of [18], the erbium ions are divided into different sub-media to allow for UV-induced lifetime quenching. Starting with the two-level rate equations, the time evolution of the gain medium consisting of a fraction ξ_k of the total number of ions and having a quenching of the spontaneous emission lifetime by a factor ζ_k may be written

$$\frac{\partial}{\partial t} g_{\mathrm{loc},k} = \frac{2\xi_k}{\tau P_{\mathrm{sp}}} (g_s + a_s) \cdot \left[(a_p r_{\mathrm{wl}} P_p + a_s P_s) - \left(\frac{g_{\mathrm{loc},k}}{\xi_k} + a_s \right) \cdot (P_{\mathrm{sat},k} + P_s) \right] \tag{4a}$$

$$P_{\mathrm{sat},k} = \left((a_p + g_p) r_{\mathrm{wl}} P_p + \frac{\zeta_k}{2} P_{\mathrm{sp}} \right) \Big/ (a_s + g_s)$$

$$P_s = \sum_m^{N_m} |A_m|^2 + |B_m|^2 + 2\,\mathrm{Re}\left(A_m B_m^* e^{-2j\overline{\beta}z} \right). \tag{4b}$$

Here, $g_{\mathrm{loc},k}$ is the local amplitude gain of medium k, τ is the unquenched spontaneous emission lifetime, P_{sp} is the spontaneous emission power per unit length before the onset of quenching, and g_s, g_p, a_s, and a_p are the signal and pump gain at full inversion and signal and pump absorption at zero inversion, respectively. P_s and P_p are the local signal and pump power, respectively. Furthermore, r_{wl} is the ratio between the pump and signal wavelengths and N_m is the total number of modes. Although we can set the quenching factor arbitrarily large in this formalism, we cannot model saturable absorber states induced by clustering properly, since such clusters have to be modeled as systems with three or more excitation levels [19].

From (4a), we find the following coupled equations for $g_{2n,k}$, the $2n$th-order spatial Fourier components of the medium k gain with respect to $\overline{\beta}$:

$$\frac{\partial}{\partial t} g_{0,k} = F_{0,k} - [F_1^* g_{-2,k} + F_{2,k}(g_{0,k} + \xi_k a_s) F_1 g_{2,k}] \tag{5a}$$

$$\frac{\partial}{\partial t} g_{2n,k}\bigg|_{n\neq 0} = -\left(F_1^* g_{2n-2,k} + F_{2,k} g_{2n,k} + F_1 g_{2n+2,k} \right) \tag{5b}$$

with

$$g_{\mathrm{loc},k} = \sum_{n=-\infty}^{\infty} g_{2n,k} e^{2zn\overline{\beta}}$$

$$F_{0,k} = \frac{2\xi_k(g_s + a_s)}{\tau P_{\mathrm{sp}}} (a_p r_{\mathrm{wl}} P_p + a_s P_{\mathrm{tot}})$$

$$F_1 = \frac{2(g_s + a_s)}{\tau P_{\mathrm{sp}}} P_c$$

$$F_{2,k} = \frac{2(g_s + a_s)}{\tau P_{\mathrm{sp}}} (P_{\mathrm{sat},k} + P_{\mathrm{tot}})$$

$$P_{\mathrm{tot}} = \sum_m^{N_m} |A_m|^2 + |B_m|^2$$

$$P_c = \sum_m^{N_m} A_m B_m^*. \tag{5c}$$

By setting $\partial g_{\mathrm{loc},k}/\partial t = 0$, (4a) reduces to the steady-state solution known from previous work [16], [20], [21]

$$g_{\mathrm{loc,ss},k} = \frac{g_{\mathrm{unsat},k}}{1 + P_s/P_{\mathrm{sat},k}} \tag{6a}$$

$$g_{\mathrm{unsat},k} = \xi_k \left(\frac{a_p r_{\mathrm{wl}} P_p}{P_{\mathrm{sat},k}} - a_s \right). \tag{6b}$$

The Fourier components at steady-state $g_{\mathrm{ss},2n,k}$ can be found by performing Fourier integrals on $g_{\mathrm{loc,ss},k}$ given in (6a) [16], [17], [22]. Alternatively, we can set the derivative in (5b) to zero, and find a simple expression for the higher order Fourier components

$$g_{0,\mathrm{ss},k} = g_{\mathrm{unsat},k} \Big/ \sqrt{a^2 - |b|^2} \tag{7a}$$

$$g_{2,\mathrm{ss},k} = g_{-2,\mathrm{ss},k}^* = g_{0,\mathrm{ss},k} \frac{\sqrt{a^2 - |b|^2} - a}{b} \tag{7b}$$

$$g_{2n,\mathrm{ss},k}\big|_{n\geq 0} = g_{-2n,\mathrm{ss},k}^* = g_{0,\mathrm{ss},k} \left(\frac{g_{2,\mathrm{ss},k}}{g_{0,\mathrm{ss},k}} \right)^n \tag{7c}$$

with

$$a = 1 + P_{\mathrm{tot}}/P_{\mathrm{sat},k}, \qquad b = 2P_c/P_{\mathrm{sat},k}. \tag{7d}$$

The total gain is found by summing the contributions from the different gain media [18], thus

$$g_{\mathrm{loc}} = \sum_{k=1}^{N_{\mathrm{gm}}} g_{\mathrm{loc},k}, \qquad g_{2n} = \sum_{k=1}^{N_{\mathrm{gm}}} g_{2n,k}. \tag{8}$$

Here, N_{gm} is the total number of gain media.

Gain diffusion, i.e., nonradiative migration of electronic excitation of Er^{3+}, is ignored in this work. We do not think gain diffusion is important for the Er^{3+} concentrations typically found in DFB-FLs. If diffusion played a role, the higher harmonics of the gain function would attain a smaller value [23]. We have also ignored shot noise of P_{sp}, P_p, and P_{tot} in (5). This is an approximation that yielded good agreement with experiments in [6].

C. Spontaneous Emission

The spontaneous emission is essential in the model because it provides the seeding for the laser. Since we have assumed no optical external feedback into the laser, spontaneous emission is also the most important source of relative intensity noise (RIN), possibly in addition to pump noise, but it is thought to play a small role for the frequency noise of DFB-FLs [6]. The spontaneous emission is a white noise process both in time and space. However, in order to integrate (3) numerically, $i_{f,m}$ and $i_{b,m}$ have to be kept constant in finite spatial and temporal steps. A generalization of the discrete time step formalism of [24] yields

$$i_{s,m} = \sqrt{\frac{R}{2\Delta t \Delta z}}\,(x_{s,1} + jx_{s,2}) \tag{9}$$

where $x_{s,1}$ and $x_{s,2}$ are Gaussian variables with $\langle x_{s,1}^2\rangle + \langle x_{s,2}^2\rangle = 1$ that are independent for any integration time slot of length Δt, mode m, and section of length Δz in the forward ($s = f$) and backward ($s = b$) case. R is the spontaneous emission energy injected into the modes per length. Note that the spectral power density of $i_{s,m}$ as given in (9) approaches white noise for $\Delta t \to 0$, but the power spectrum has its first zero at a frequency $1/\Delta t$, and thus $1/\Delta t$ should be much larger than the relaxation oscillation frequency [24].

The spontaneous emission power is proportional to the inversion. It follows from general laser theory that, when the gain medium is fully inverted, the spontaneous photon emission rate into a mode is equal to the power gain. Thus

$$R = 2\hbar\omega g_s I = 2\hbar\omega g_s \frac{g_0 + a_s}{g_s + a_s} \tag{10}$$

where $\hbar$ is Planck's constant divided by 2π and I is the inversion.

D. Numerical Implementation

The DFB fiber structure was divided into several sections, and in each section the coupled-mode equations were solved using a transfer matrix approach [25] modified to include spontaneous emission [12]. Thus, we calculated the complex amplitudes of mode m at the right end of section q by multiplying the fields at the left end of the section with the transfer matrix and perturb the result with the spontaneous emission

$$\begin{bmatrix} A_{m,q} \\ B_{m,q} \end{bmatrix} = T_m^{q,q-1} \begin{bmatrix} A_{m,q-1} \\ B_{m,q-1} \end{bmatrix} + \Delta z_q \begin{bmatrix} i_{f,m,q} \\ -i_{b,m,q} \end{bmatrix} \tag{11a}$$

with

$$T_m^{q,q-1} = e^{-(\mu_m^+ - \mu_m^-/2)\Delta z_q} \begin{bmatrix} r_m + f_m s_m, & (g_2^* + j\kappa)s_m \\ -(g_2 + j\kappa^*)s_m, & r_m - f_m s_m \end{bmatrix}$$

$$r_m = \cosh\gamma_m \Delta z_q, \quad f_m = d_m - \frac{\mu_m^+ + \mu_m^-}{2}$$

$$s_m = \frac{\sinh\gamma_m \Delta z_q}{\gamma_m}$$

$$\gamma_m = \sqrt{f_m^2 - (j\kappa + g_2^*)(j\kappa^* + g_2)}. \tag{11b}$$

In (10) and (11b), all quantities are to be evaluated in the center of section q, except $A_{m,q}$, $B_{m,q}$, and $\mu_m^\pm$, which are evaluated at the end of the section. The section numbers q are assigned in increasing order from left to right. Expression (11a) can be cascaded, so that fields at the right end of section q can be found from the amplitudes $A_{m,0}$ and $B_{m,0}$ to the left of the structure and the random spontaneous emission in sections $1 \cdots q$. In order to get accurate results, the length of each section Δz_q needs to be short enough to resolve the spatial variation of the modes and κ in the structure, i.e., in a multiple Λ structure Δz_q needs to be considerably shorter than the shortest spatial beat period between the individual subgratings.

The dynamic lasing condition is fulfilled when we have infinite transmission through the structure for all lasing modes, or

$$B_{m,N_s}\big|_{A_{m,0}=0,\, B_{m,0}\neq 0} = 0, \qquad m = 1 \cdots N_m. \tag{12}$$

Here, N_s is the number of segments, and N_m is the number of modes. Equation (12) is valid also when the system is out of equlibrium because the time derivatives μ_m^+ and μ_m^- are included in the transfer matrix formalism.

The set of equations (12) is simultaneously solved by iteration in each time step, where the detuning δ_m and left output power $B_{m,0}$ of all modes m are optimized. The gain parameters are taken from the previous time step, and μ_m^+ and μ_m^- are estimated from the local fields of the previous time step and current trial solution

$$\mu_{m,q}^+(t) = \frac{A_{m,q-1,\,\mathrm{trial}}(t) - A_{m,q-1}(t-\Delta t)}{A_{m,q-1,\,\mathrm{trial}}(t) C_g \Delta t}$$

$$\mu_{m,q}^-(t) = \frac{B_{m,q-1,\,\mathrm{trial}}(t) - B_{m,q-1}(t-\Delta t)}{B_{m,q-1,\,\mathrm{trial}}(t) C_g \Delta t}. \tag{13}$$

The pump absorption a_{pump} and thus local pump power P_p is found from g_0 through the following relation [21]:

$$a_{\mathrm{pump}} = a_p + a_0 - \frac{g_p + a_p}{g_s + a_s}(g_0 + a_s). \tag{14}$$

When a solution is found, the gain is updated through the coupled equations (5). Note that, in principle, we need to keep track of an infinite number of Fourier components in order to calculate the time-dependent g_0 and g_2. In practice, however, the higher order Fourier components are small, and inspired by the steady-state solution (7c), we terminate the sequence of Fourier components $g_{2n,k}$ with

$$g_{2N_{\mathrm{last}},k}(t+\Delta t) = g_{2N_{\mathrm{last}}-2,k}^2(t+\Delta t)/g_{2N_{\mathrm{last}}-4,k}(t+\Delta t). \tag{15}$$

We found no significant change in the simulation results if we increased N_{last} above 3.

III. Simulation Results

Using the algorithm outlined in the previous section, the dynamic evolution starting from any physical initial condition of a range of single polarization grating fiber lasers could be calculated. Except for the simulations in Section III-C, where ξ_2 and ζ_2 are varied, the fiber and laser parameters summarized in Table I have been used for all calculations in this work. Except for τ, they are identical to the ones used in [3] and are taken from one of the DFB-FLs characterized in [18]. Fig. 1 shows the simulated startup of a dual Λ DFB-FL, where the two

TABLE I
LASER PARAMETERS USED IN THE CALCULATIONS. EXCEPT THE EFFECTIVE REFRACTIVE INDEX n_{eff}, ALL SYMBOLS ARE DEFINED IN THE TEXT

Parameter	Value
g_s	15.9 dB/m
a_s	11.7 dB/m
g_p	3.0 dB/m
a_p	8.9 dB/m
a_0	0.24 dB/m
P_{sp}	4.1 mW/m
P_p	140 mW
N_{gm}	2
$\xi_2 = 1 - \xi_1$	0.38
$[\zeta_1, \quad \zeta_2]$	[1, 26]
r_{wl}	1480/1550=0.955
τ	10 ms
n_{eff}	1.465

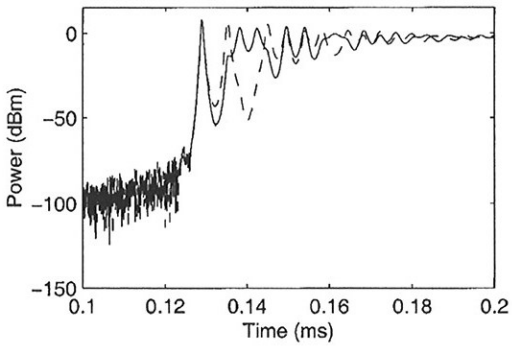

Fig. 1. Simulation of startup of a dual Λ DFB-FL with $\kappa_1 = \kappa_2 = 79.1$ m^{-1}, a structure length of $l = 9.21$ cm, and a center phase shift of π. The two superimposed subgratings have a Bragg frequency separation of $\Delta\nu = 10$ GHz, and the relative phase between the subgratings at the center phase shift [3] is $\Delta\phi = \pi$.

sub-gratings have equal grating strength. The pump is switched on with a constant pump power of 140 mW at the time $t = 0$, and we assume zero inversion of the gain medium for $t < 0$. The threshold for both modes are reached after roughly 126 μs, and both modes are self-pulsing with an amplitude that is damped with a time constant of roughly 20 μs. Since the spontaneous emission processes of the two modes are not correlated, the oscillations of the two modes are not in phase. After the intensity oscillations have relaxed, the time-averaged output power of the two modes are equal to the powers calculated in the static model of [3].

A. RIN Spectra of Multiple Λ DFB-FLs

By initiating the simulations with the steady-state solution and letting the simulation run for a long time, we can find the

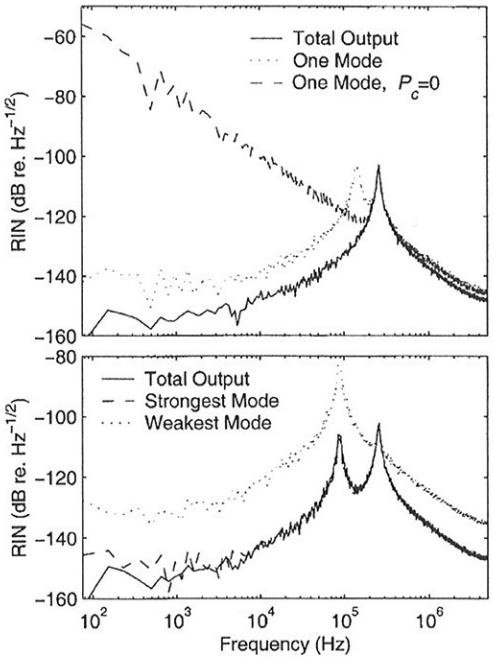

Fig. 2. Calculated RIN spectra of total output and single modes of dual Λ DFB-FLs. Top: Laser parameters as in Fig. 1. Single-mode RIN when the gain gratings are ignored ($P_c = 0$) is also shown. Bottom: $\kappa_1 = 79.1$ m^{-1}, $\kappa_2 = 70$ m^{-1}. Laser parameters are otherwise as in Fig. 1.

RIN spectra of the laser by performing a discrete Fourier transform on the time dependent laser output powers. For the symmetric dual Λ structure discussed above, a calculated RIN spectrum of the total output and of one of the modes are shown on top of Fig. 2. The simulation was performed with time steps of $\Delta t = 0.1$ μs over a period of 13 ms, corresponding to a sampling frequency of 10 MHz and a frequency resolution of 77 Hz, respectively. The spectra in the plot are smoothed with progressively larger resolution bandwidth with increasing frequencies in order to damp the random ripple caused by the spontaneous emission.

The RIN of the total intensity shows a relaxation oscillation peak of $f_R = 257$ kHz, which is a typical number for single-mode DFB-FLs we have characterized in our laboratory. In fact, this spectrum is not distinguishable from the spectrum calculated for a single-mode DFB-FL in the same fiber with similar grating parameters. The noise of the individual modes exceeds the noise of the total output by approximately 11 dB at low frequencies, and has a second noise peak at $f_L = 138$ kHz. The excess noise seen in the spectrum of the individual mode compared with the spectrum of the total output is called the mode partition noise. Since the second noise peak is not visible in the RIN spectrum of the total output, it means that the two modes oscillate in anti-phase at this frequency. Such behavior was theoretically predicted for two-mode lasers with spatial hole burning already in the 1960s [15], but has attracted considerable attention recently [26]–[31]. In [31], an analytical expression for the ratio between phase and anti-phase relaxation oscillation peak frequencies (f_L/f_R) as a function of cross saturation was found. f_L will always be smaller than f_R

because the feedback loop for the total intensity, characterized by the transfer function between the relative intensity and g_0, has a cutoff frequency proportional to $P_{\text{sat}} + P_{\text{tot}}$ [6], whereas the mode selective feedback, given by the transfer function between the relative intensity and g_2 has a cutoff frequency proportional to only P_{tot}. Similar arguments can also be made for other types of hole burning mechanisms. Anti-phase states have been experimentally observed for Nd : YAG lasers [26], $LiNdP_4O_{12}$ lasers [27]–[29], and Nd^{3+}-doped [27] and Er^{3+}-doped [30], [31] fiber lasers.

It is important to note that semiconductor DFB lasers do not have strong gain gratings because of carrier diffusion, and, therefore, cannot lase stably in multiple longitudinal modes [32]. To illustrate this fundamental difference, a plot of the RIN of a single mode of the same dual Λ laser with the gain gratings omitted from the simulations ($P_c = 0$) is also given on top of Fig. 2. This spectrum is very similar to what is reported for semiconductor lasers, with RIN in excess of -56 dB ($\text{Hz}^{-1/2}$) at low frequencies.

As mentioned above, the mode partition noise peak of the two modes cancel each other at the top of Fig. 2, and it is not visible in the RIN spectrum of the total laser output. If the grating strengths of the two modes are not equal, the differences in photon lifetime and spatial-mode distribution between the two modes [3] will break the reciprocity in the gain cross saturation, and a second noise peak can be seen also for the RIN of the total output power. An example of such a laser is shown at the bottom of Fig. 2, where we have plotted the RIN of a dual Λ DFB-FL with $\kappa_1 = 79.1\ \text{m}^{-1}$ and $\kappa_2 = 70.1\ \text{m}^{-1}$. Similar effects have been observed experimentally between transverse modes of a $LiNdP_4O_{12}$ micro-chip solid state laser [29]. The degree of anti-phase behavior will decrease with decreasing spatial overlap and increasing difference in cavity photon life time and, when we have fundamental and higher order longitudinal modes lasing simultaneously in the same DFB structure [3], the noise spectra of the modes are almost independent of each other.

For all types of cross saturation, like spatial, frequency, or polarization hole burning, there will also be anti-phase dynamics for lasers with more than two modes. In theory [26], [28], the number of resonance frequencies for each individual mode equal the total number of modes, and if the modes have identical photon lifetimes, the noise spectra of the total output power will display only the relaxation oscillation noise peak with the highest frequency. In Fig. 3, we have plotted the RIN spectra of multiple Λ DFB-FLs with three, four, and five superimposed subgratings, with nearest neighbor separation between the subgrating Bragg frequencies of $\Delta\nu = 10$ GHz. Even with all the subgratings having an equal coupling coefficient $\kappa_i = 90\ \text{m}^{-1}$, the cavity finesse seen by each laser mode and their spatial distribution will be different due to interference between the reflection spectra of the subgratings [3]. With many modes, smaller threshold differences are tolerated, and although the phases between the subgratings of the lasers plotted in Fig. 3 are optimized with respect to equal modal output powers, the output power of and cavity finesse seen by the different modes for each DFB-FL is not equal. Thus, just like for the laser plotted in the bottom graph of Fig. 2, the reciprocity in the cross saturation is broken and the RIN curves

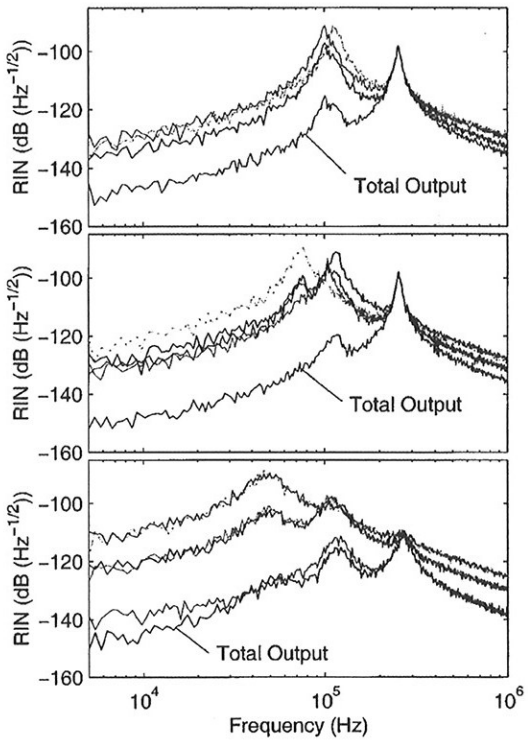

Fig. 3. RIN of the total output and the individual modes of a multiple Λ DFB-FL with three modes (top), four modes (middle), and five modes (bottom). The grating length is $l = 8.2$ cm and each superimposed subgrating i has a strength of $\kappa_i = 90\ \text{m}^{-1}$. The Bragg frequencies of the subgratings of each structure are in an equidistant sequence with a nearest neighbor separation of $\Delta\nu = 10$ GHz.

of the total output have multiple resonance peaks. So far, RIN seeded by the pump has been ignored. It is, however, often of interest to know how stable the pump source needs to be in order to get minimum DFB-FL RIN. In Figs. 4 and 6, the RIN of various DFB-FLs are plotted as a function of pump RIN, RIN_p. It is assumed that the pump RIN is white, which is a good approximation except for very low frequencies. Note that noise can be induced by the pump not only due to its RIN, but also from fluctuations in its polarization state and frequency due to, for instance, pump-mode partition noise, since the effective a_p will vary with these parameters. Such fluctuations can, however, be considered as an addition to RIN_p and will not be treated separately here. In addition, there will also be shot noise in the absorption of the pump by the laser gain medium [6], effectively limiting the lowest possible pump RIN.

Although the multiple Λ DFB-FL RIN spectra are quite complex, some general trends can be extracted from Fig. 3. The RIN of the individual modes increases with the number of modes, especially at lower frequencies. The reason is that the gain grating amplitude has to be shared between the modes, and the negative feedback of each mode thus become less effective. An exception to this trend is the low noise mode of the five-mode laser in the bottom plot of the figure, because this mode is responsible for more than half of the output power of the laser and, thus, induces most of the gain grating amplitude. We also see that the number of resonance peaks increases with an increasing number

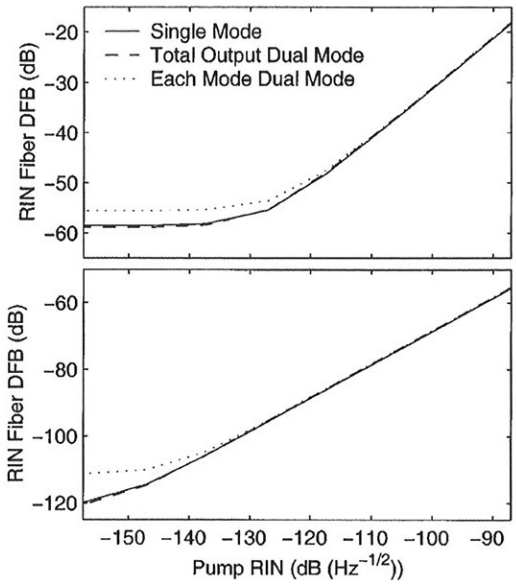

Fig. 4. RIN as a function of RIN_p for a DFB-FL with parameters as in Fig. 1 together with a single Λ structure with $\kappa = 81.3\ \mathrm{m}^{-1}$. Top: RIN integrated over all frequencies. Bottom: RIN integrated up to 1 kHz.

of modes, while the resonance Q values decrease, which is particularly true for the main relaxation oscillation resonance of the cavity. This blurring of the spectrum can also be attributed to the decreasing reciprocy in the gain cross saturation, i.e., to the differences in cavity finesse between the modes.

B. Pump-Induced RIN

The top graph of Fig. 4 shows the total frequency integrated RIN of the symmetric dual Λ structure analyzed in Fig. 1 and the top of Fig. 2. In the same plot, the RIN of a single Λ structure with a coupling coefficient that gives a similar effective cavity finesse [3] is given. The noise is relatively unaffected for $\mathrm{RIN}_p \lessapprox -140$ dB (Hz$^{-1/2}$), but for $\mathrm{RIN}_p \gtrapprox -130$ dB (Hz$^{-1/2}$), the RIN of DFB-FLs increases with a rate that approaches proportionality with RIN_p. The RIN of the total output of the dual Λ laser shows a similar dependence on RIN_p as the single Λ structure. The RIN of each individual mode is a bit higher because of the mode partition noise, but since we have ignored polarization effects and have assumed identical gain parameters for the two modes, the mode partition noise does not increase with RIN_p. For many applications, and in particular sensing, the high-frequency noise is not a major concern, as it can be filtered out. Thus, in the lower half of Fig. 4, we have plotted the RIN below a noise frequency of 1 kHz. For the total intensity and single Λ case, the shot noise limit of the pump absorption is estimated to be $\mathrm{RIN}_p \approx -156$ dB (Hz$^{-1/2}$), whereas it is approximately $\mathrm{RIN}_p \approx -153$ dB (Hz$^{-1/2}$) for the individual modes. In contrast to the total RIN, the RIN below 1 kHz increases with RIN_p for all values above the shot noise limits.

In Fig. 5, the RIN spectra is plotted for the dual-mode structures with $\mathrm{RIN}_p = -147$ dB (Hz$^{-1/2}$) and $\mathrm{RIN}_p = -87$ dB (Hz$^{-1/2}$). For $\mathrm{RIN}_p = -147$ dB (Hz$^{-1/2}$), there is no significant difference from the case $\mathrm{RIN}_p = 0$ plotted on top of Fig. 2

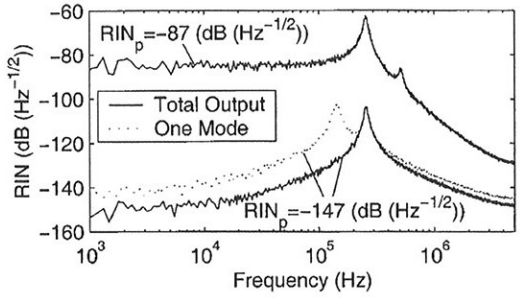

Fig. 5. RIN spectra of a dual Λ DFB-FL with a pump RIN of $\mathrm{RIN}_p = -87$ dB (Hz$^{-1/2}$) and $\mathrm{RIN}_p = -147$ dB (Hz$^{-1/2}$). Laser parameters otherwise as in Fig. 1.

except for the increase in low frequency RIN. However, when $\mathrm{RIN}_p = -87$ dB (Hz$^{-1/2}$), the anti-phase resonance has disappeared and the modes are oscillating in phase. A second harmonic of the relaxation oscillation peak has appeared, which is a first sign that the laser is approaching a pulsed state.

In Fig. 6, we have plotted the total RIN and the RIN below 1 kHz of a dual Λ laser with $\kappa_1 = \kappa_2 = 160\ \mathrm{m}^{-1}$, which corresponds to a rather large integrated coupling strength of $\kappa_{1,2} l = 14.7$. From [3], we know that this laser operates with two higher order modes, in addition to the two fundamental modes. The side modes, which have much higher output power than the fundamental modes, have significantly higher noise floor induced by spontaneous emission. This is expected, since the side modes have shorter photon lifetime, and thus a higher spontaneous emission rate. In addition, because of the high intra-cavity power of the fundamental mode compared with the higher order mode, the latter has a much stronger partition noise resonance. The difference between the total RIN of the fundamental modes and side modes is 33 dB in the low RIN_p limit; however, as RIN_p increases, this difference is reduced to 8 dB. The pump-induced RIN for a mode increases with the relaxation oscillation center frequency, its resonance Q-value, and the change in round-trip gain g_{rt} as a function of relative pump power change [6]

$$k_{\mathrm{sat},p} = P_p \frac{\partial g_{\mathrm{rt}}}{\partial P_p}. \tag{16}$$

$k_{\mathrm{sat},p}$ is larger for the higher order modes, since its effective gain is not as saturated. Closer studies of the spectra reveals that the higher order modes also have much higher relaxation oscillation Q values, but they have lower relaxation oscillation frequencies. When calculating the low-frequency RIN, the relaxation oscillation resonances are filtered out, and the differences between the higher order modes and the fundamental modes are smaller than the differences in total RIN, especially in the high RIN_p limit. Note that even if the difference in RIN between the fundamental and higher order modes is reduced in the high RIN_p regime, it is expected that the higher order mode will tolerate much less optical feedback and will also be affected much more by twisting and bending of the fiber.

In Fig. 6, we have also plotted the RIN of a dual Λ grating where the two subgratings have slightly different coupling coefficients, $\kappa_1 = 79.1\ \mathrm{m}^{-1}$ and $\kappa_2 = 70\ \mathrm{m}^{-1}$, i.e., the structure that had its RIN spectrum drawn at the bottom of Fig. 2.

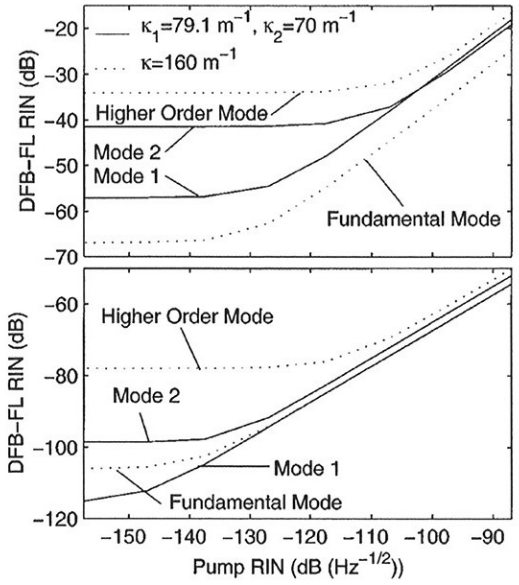

Fig. 6. RIN as a function of RIN_p of a fundamental and a higher order mode of a dual Λ laser with $\kappa = \kappa_1 = \kappa_2 = 160\ \mathrm{m}^{-1}$ and of the modes of a dual Λ laser with $\kappa_1 = 79.1\ \mathrm{m}^{-1}$ and $\kappa_2 = 70\ \mathrm{m}^{-1}$. Both structures are 9.21-cm long, and have a relative phase between the subgratings at the center phase shift [3] of $\Delta\phi = \pi$. Top: RIN integrated over all frequencies. Bottom: RIN integrated up to 1 kHz.

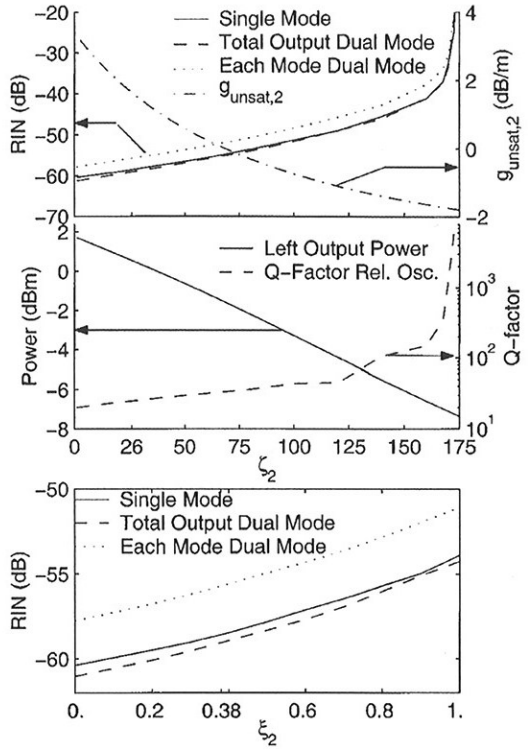

Fig. 7. Spontaneous lifetime quenching and DFB-FL stability. Laser parameters as in Fig. 4. Top: RIN of single and dual Λ DFB-FLs and $g_{\mathrm{unsat},2}$ as a function of the quenching factor ζ_2, with $\xi_2 = 0.38$. Middle: Left output power and relaxation oscillation Q factor as a function of ζ_2, with $\xi_2 = 0.38$. Bottom: RIN as a function of quenching fraction ξ_2, with $\zeta_2 = 26$.

Although the difference in mirror transmissivity is only about 4 dB, the weaker mode has more than 18-dB larger total spontaneous emission induced RIN than the other mode. However, the weaker mode has a lower relaxation oscillation frequency and, therefore, it in fact has a lower RIN than the more powerful mode when the performance is limited by the pump. Because of internal unbleachable loss, the stronger mode in this DFB-FL also has higher intracavity intensity than the fundamental modes of the laser with $\kappa = 160\ \mathrm{m}^{-1}$, leading to a lower low-frequency RIN.

C. Spontaneous Emission Lifetime Quenching

UV-induced spontaneous emission lifetime quenching is experimentally observed [33], [34], but although it has been shown by the use of Kramers–Kronig relations that UV-transitions of erbium gain media are important for its interaction with infrared light [35], no clear physical explanation of the quenching has been reported so far. This type of lifetime shortening is orders of magnitudes smaller than what is seen due to Er^{3+} clustering, but still, UV quenching leads to a significant decrease of the output power of DFB-FLs and an increase of laser threshold, and perhaps more seriously, it leads to a reduction in the stability phase margin of the lasers [6]. Thus, although the relation between UV exposure and spontaneous lifetime quenching is poorly understood, it is of great interest to know its effect on the noise properties of DFB-FLs.

On top of Fig. 7, the RIN of dual and single Λ lasers is plotted as a function of the quenching factor ζ_2, keeping $\xi_2 = 0.38$. Starting from $\zeta_2 = 0$, the RIN of both the single and dual Λ DFB-FLs increases slightly more than exponential, before reaching a critical value around $\zeta_2 \approx 170$, where both the single and dual Λ DFB-FL start to self-pulsate (RIN $\gtrsim 1$). In order to understand this behavior, the unsaturated gain of the quenched medium $g_{\mathrm{unsat},2}$, the left output power, and the relaxation oscillation quality (Q) factor of the single-mode laser is plotted in the same figure. The Q factor is defined as the ratio of the relaxation oscillation peak frequency f_R to the 3-dB bandwidth of the resonance and is estimated from the RIN spectra. $g_{\mathrm{unsat},2}$ decreases monotonically from its unquenched value of 3.4 dB/m down to -1.8 dB/m at $\zeta_2 = 175$. As long as $g_{\mathrm{unsat},2}$ is positive, the stability phase margin of the DFB-FL decreases with decreasing laser power, but will increase with decreasing spontaneous emission lifetime [6]. Accordingly, we see that the Q factor, which is approximately inversely proportional to the phase margin, does not increase much for low values of ζ_2. However, when $g_{\mathrm{unsat},2}$ turns negative, the quenched ions act as saturable absorbers that provide positive feedback to the relaxation oscillation. With growing values of ζ_2, the strength of these absorbers increases, due to a smaller $g_{\mathrm{unsat},2}$ and a weaker bleaching by the close to exponential falling power level of the mode. In addition, they relax faster, and thus give a more effective positive feedback to the relaxation oscillation. At $\zeta_2 \approx 170$, corresponding to a spontaneous emission rate of 15% of f_R, the DFB-FL becomes unstable. Clustered Er^{3+} ions, on the other hand, have a spontaneous emission rate that is many times larger than f_R, and DFB-FLs are expected to self-pulsate with a fraction of clustered ions of only a few percent [19].

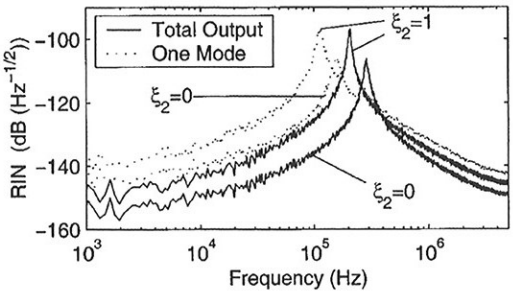

Fig. 8. RIN spectra of a dual Λ DFB-FL with $\xi_2 = 0$ and $\xi_2 = 1$. Laser parameters otherwise as in Fig. 1.

At the bottom of Fig. 7, we have plotted dual and single Λ DFB-FL RIN as a function of the fraction of quenched ions ξ_2 with $\zeta_2 = 26$. The increase in RIN from $\xi_2 = 0$ to $\xi_2 = 1$ is 6.4 dB in the single-mode case and 6.6 dB in the dual Λ case. The laser power drops by approximately 4 dB in the same interval, indicating that most of the increase in RIN comes from an increase in the ratio between the spontaneous emission and the laser mode powers, and not from a decrease in the stability phase margin of the laser.

In Fig. 8, RIN spectra are given for two dual Λ DFB-FLs. One of the lasers is without quenching ($\xi_2 = 0$), whereas all the erbium ions of the other laser are quenched by a factor 26 ($\xi_2 = 1$ and $\zeta_2 = 26$). For DFB-FLs, the peak frequency of the relaxation oscillation resonance decreases with its Q factor [6]. Similar arguments can be made for the anti-phase resonance, and thus, both resonance peaks have shifted to lower frequencies for the case $\xi_2 = 1$. There will be similar shifts for larger values of ζ_2 with $\xi_2 = 0.38$, but when the laser approaches self pulsation, the anti-phase behavior partly breaks down, and higher order harmonics appear in the spectra.

IV. Conclusion

A comprehensive numerical model has been presented that calculates the dynamic operation of multi-moded DFB-FLs. The model gives realistic predictions for the temporal evolution of the modal output powers for any physical initial condition. Effects like spontaneous emission and dynamically varying pump levels are included. The model may easily be extended to include optical feedback or modes in different polarizations [7], [18], [21], [36].

The operation of single-mode DFB-FLs has been compared with DFB-FLs that are lasing in multiple fundamental modes [3]. When the cavity finesse seen by the mode in the single-mode case and both modes in the dual-mode case is similar, it has been found that the RIN spectra of the total output power in the two laser structures are approximately equal. Saturation-induced gain gratings provide negative feedback for the mode partition noise process, and thus the RIN of the individual-modes in the dual-mode case is only a few decibels larger than the RIN of the single-mode laser. However, the gain grating feedback provides an additional noise resonance in the noise spectra of the individual modes, and this will limit the resolution of, for instance, acoustical sensing at frequencies around the noise peak. For lasers with more than two fundamental modes, the mode partition noise generally increases as a function of the number of modes. Most of the increase is, however, below the main relaxation oscillation peak, and the total integrated modal RIN levels are far from the pulsing regime even for a MW-DFB-FL with five modes. Thus, the individual modes of such a laser are expected to have only negligible larger linewidths than a comparable single-mode DFB-FL [6]. In a MW-DFB-FL, modes that see a lower finesse in the structure generally displays larger RIN in the low pump RIN limit, but this is not necessarily the case if the pump is the most important source of RIN for the DFB-FL.

High mirror reflectivities are often of interest in order to reduce the effect of optical feedback in sensing applications. However, as reported in [7], the laser may operate with higher order modes with high output powers if the grating strength is too large [3]. The dynamical model presented here predicts that the side modes have very large RIN compared with the fundamental modes, and they are in addition more susceptible to optical feedback, and should thus be avoided at all costs.

UV-induced spontaneous lifetime quenching potentially can degrade the stability and RIN performance of a DFB-FL. Our results indicate that the quenching factor is more important than the ratio between the quenched and unquenched erbium ions.

Acknowledgment

The authors thank K. Bløtekjær for his guidance during the work and E. Rønnekleiv for helpful suggestions.

References

[1] J. T. Kringlebotn, J. Archambault, L. Reekie, and D. N. Payne, "Er^{3+} : Yb^{3+}-codoped fiber distributed feedback laser," *Opt. Lett.*, vol. 19, pp. 2101–2103, Dec. 1994.

[2] M. Ibsen, E. Rønnekleiv, G. J. Cowle, M. N. Zervas, and R. I. Laming, "Multiple wavelength all-fiber DFB lasers," *Electron. Lett.*, vol. 36, pp. 143–144, Jan. 2000.

[3] S. W. Løvseth and D. Y. Stepanov, "Analysis of multiple wavelength DFB fiber lasers," *IEEE J. Quantum Electron.*, vol. 37, pp. 770–780, June 2001.

[4] K. H. Wanser, "Fundamental phase noise limit in optical fibers due to temperature fluctuations," *Electron. Lett.*, vol. 28, pp. 53–54, Jan. 1992.

[5] S. W. Løvseth, E. Rønnekleiv, J. T. Kringlebotn, and K. Bløtekjær, "Fiber distributed-feedback lasers used as acoustic sensors in air," *Appl. Opt.*, vol. 38, pp. 4821–4830, Aug. 1999.

[6] E. Rønnekleiv, "Frequency and intensity noise of single frequency fiber Bragg grating lasers," *Opt. Fiber Technol.*, vol. 7, pp. 206–235, July 2001.

[7] E. Rønnekleiv and S. W. Løvseth, "Stability of distributed feedback fiber lasers with optical feedback," in *Proc. SPIE—13th Int. Conf. Optical Fiber Sensors*, vol. 3746, B. Y. Kim and K. Hotate, Eds., 1999, pp. 466–469.

[8] Y.-H. Liao and H. G. Winful, "Gigaherz self-sustained pulsations in chirped distributed feedback fiber lasers," in *OSA Conf. Optical Fiber Communications, Tech. Dig.*, vol. 6, Washington, DC, 1997, pp. 164–165.

[9] ——, "Dynamics of distributed-feedback fiber lasers: Effect of nonlinear refraction," *Opt. Lett.*, vol. 21, pp. 471–473, Apr. 1996.

[10] Q. Yujun, P. Varming, J. H. Povlsen, and V. C. Lauridsen, "Dynamic response analysis of DFB fiber lasers," in *Proc. ECOC'98-24th European Conf. Optical Communication*, vol. 1, Madrid, Spain, Sept. 1998, pp. 147–148.

[11] Y. Qian, P. Varming, J. H. Povlsen, and V. C. Lauridsen, "Dynamic noise responses of DFB fiber lasers in presence of pump power fluctuations," *Electron. Lett.*, vol. 35, pp. 299–300, Feb. 1999.

[12] L. M. Zhang and J. E. Carrol, "Large-signal dynamic model of the DFB laser," *IEEE J. Quantum Electron.*, vol. 28, pp. 604–611, Mar. 1992.

[13] J. E. Whiteaway, A. P. Wright, B. Garret, G. H. B. Thompson, J. E. Carrol, L. M. Zhang, C. F. Tsang, I. H. White, and K. A. Williams, "Detailed large-signal dynamic modeling of DFB laser structures and comparison with experiment," *Opt. Quantum Electron.*, vol. 26, pp. S817–S842, 1994.
[14] H. Kogelnik and C. V. Shank, "Coupled-wave theory of distributed feedback lasers," *J. Appl. Phys.*, vol. 43, pp. 2327–2335, May 1972.
[15] C. L. Tang, H. Statz, and G. deMars, "Spectral output and spiking behavior of solid-state lasers," *J. Appl. Phys.*, vol. 34, pp. 2289–2295, Aug. 1963.
[16] W. S. Rabinovich and B. J. Feldman, "Spatial hole burning effects in distributed feedback lasers," *IEEE J. Quantum Electron.*, vol. 25, pp. 20–29, Jan. 1989.
[17] M. Horowitz, R. Daisy, B. Fischer, and J. L. Zyskind, "Linewidth-narrowing mechanism in lasers by nonlinear wave mixing," *Opt. Lett.*, vol. 19, no. 18, pp. 1406–1408, 1994.
[18] E. Rønnekleiv, M. Ibsen, and G. J. Cowle, "Polarization characteristics of fiber DFB lasers related to sensing applications," *IEEE J. Quantum Electron.*, vol. 36, pp. 656–664, June 2000.
[19] F. Sanchez, P. Le Boudec, P.-L. François, and G. Stephan, "Effects of ion pairs on the dynamics of erbium-doped fiber lasers," *Phys. Rev. A*, vol. 48, pp. 2220–2228, Sept. 1993.
[20] M. Sargent, III, W. H. Swanter, and J. D. Thomas, "Theory of distributed feedback laser," *IEEE J. Quantum Electron.*, vol. 16, pp. 465–472, Apr. 1980.
[21] E. Rønnekleiv, M. N. Zervas, and J. T. Kringlebotn, "Modeling of polarization-mode competition in fiber DFB lasers," *IEEE J. Quantum Electron.*, vol. 34, pp. 1559–1568, Sept. 1998.
[22] G. P. Agrawal and M. Lax, "Effects of interference on gain saturation in laser resonators," *J. Opt. Soc. Amer.*, vol. 69, pp. 1717–1719, Dec. 1979.
[23] B. Jaskorzynska, E. Vanin, and S. Helmfrid, "Gain-saturation gratings with an arbitrary diffusion rate of excited states," *J. Opt. Soc. Amer. B*, vol. 15, pp. 945–950, Mar. 1998.
[24] N. Schunk and K. Petermann, "Noise analysis of injection-locked semiconductor injection lasers," *IEEE J. Quantum Electron.*, vol. QE-22, pp. 642–650, May 1986.
[25] G. Björk and O. Nilson, "A new exact and efficient numerical matrix theory of complicated laser structures: Properties of asymmetric phase-shifted DFB lasers," *J. Lightwave Technol.*, vol. LT-5, pp. 140–146, Jan. 1987.
[26] K. Wiesenfeld, C. Bracikowski, G. James, and R. Roy, "Observation of antiphase states in a multimode laser," *Phys. Rev. Lett.*, vol. 65, pp. 1749–1742, Oct. 1990.
[27] K. Otsuka, P. Mandel, S. Bielawski, D. Derozier, and P. Glorieux, "Alternate time scale in multimode lasers," *Phys. Rev. A*, vol. 46, pp. 1692–1695, Aug. 1992.
[28] K. Otsuka, M. Georgiou, and P. Mandel, "Intensity fluctuations in multimode lasers with spatial hole burning," *Jpn. J. Appl. Phys.*, vol. 31, pp. L1250–L1252, Sept. 1992.
[29] K. Otsuka, "Transverse effects on antiphase laser dynamics," *Jpn. J. Appl. Phys.*, vol. 32, pp. L1414–L1417, Oct. 1993.
[30] P. Le Boudec, C. Jaouen, P. L. François, J.-F. Bayon, F. Sanchez, P. Besnard, and G. Stéphan, "Antiphase dynamics and chaos in self-pulsing erbium-doped fiber lasers," *Opt. Lett.*, vol. 18, pp. 1890–1892, Nov. 1993.
[31] E. Lacot, F. Stoeckel, and M. Chenevier, "Dynamics of an erbium-doped fiber laser," *Phys. Rev. A*, vol. 49, pp. 3997–4008, May 1994.
[32] K. Petermann, "Laser diode modulation and noise," in *Advances in Optoelectronics (ADOP)*. Dordrecht, The Netherlands: Kluwer , 1988, vol. 3, ch. 7.
[33] J. Hübner, T. Feuchter, C. V. Poulsen, and M. Kristensen, "Directly UV-written erbium doped waveguides," in *Photosensitivity and Quadratic Nonlinearity in Glass Waveguides: Fundamentals and Applications*, ser. OSA Tech. Dig., 1995, vol. 22.
[34] E. Rønnekleiv, O. Hadeler, and G. Vienne, "Stability of an Er–Yb-doped fiber distributed-feedback laser with external reflections," *Opt. Lett.*, vol. 24, pp. 617–619, May 1999.
[35] M. J. F. Digonnet, R. W. Sadowski, H. J. Shaw, and R. H. Pantell, "Experimental evidence for strong UV transition contribution in the resonant nonlinearity of doped fibers," *J. Lightwave Technol.*, vol. 15, pp. 299–303, Feb. 1997.
[36] E. Rønnekleiv, M. N. Zervas, and J. T. Kringlebotn, "Corrections to 'Modeling of polarization-mode competition in fiber DFB lasers'," *IEEE J. Quantum Electron.*, vol. 35, pp. 1097–1100, July 1999.

Sigurd Weidemann Løvseth received the Siv.Ing. degree in physics in 1996 from the Norwegian Instute of Technology, University of Trondheim, Trondheim, Norway, and the Dr.Ing. degree in fiber optics from the Norwegian University of Science and Technology, Trondheim, Norway, in 2001.

Since 1997, he has been with the Department of Physical Electronics, Norwegian University of Science and Technology, and also with Optoplan AS, Trondheim, Norway, since March 2001. Prior to this, he was with the Department of Electrical Engineering, University of Minnesota, Minneapolis, during 1995–1996, the Royal Norwegian Air Force Academy, Trondheim, Norway, during 1996–1997, and the Optical Fibre Technology Centre (OFTC), The University of Sydney, Sydney, Australia, during 1999–2000. He has studied semiconductor directional couplers, and his current research interest is in the understanding and applications of advanced active and passive fiber Bragg grating structures, in particular distributed feedback fiber lasers.

Dmitrii Yu. Stepanov was born in Moscow, Russia. He received the M.S. degree in physics from Moscow State University in 1983 and the Ph.D. degree in laser physics from the General Physics Institute of Russian Academy of Sciences in 1992.

In 1983, he joined the General Physics Institute, Russian Academy of Sciences, where he conducted research in the areas of photo-induced phenomena in optical fibers and glasses, nonlinear optics, and nonlinear guided wave optics. In 1994, he joined the Australian Photonics Cooperative Research Centre, where he was Senior Research Fellow and Key Researcher, and worked on various aspects of grating technology and its applications in fiber devices for telecommunications and sensors. He is currently with Redfern Optical Components (ROC), as the inventor of ROC's core grating writing technology. As Chief Technical Officer of ROC, he is leading the company R&D and contributing to the development of the company strategy. His responsibilities include overall scientific direction and technical supervision of the R&D projects, direct technical contributions with strong focus on the core grating writing technology, and technology transfer to the manufacturing environment. He has published over 80 papers and is a co-inventor in over ten patent applications.

Chapter 8

Intra-Grating Quasi-Distributed Sensing using Active and Passive Phase-Shifted Multi-Wavelength Fiber Bragg Structures [1]

Abstract

We present a novel active and passive multiple wavelength Bragg grating sensor. The basic structure consists of several superimposed quarter-wavelength-shifted Bragg gratings with different periodicity. The center phase shifts will lead to one notch per grating in the reflection spectrum in the passive case, or one laser mode per grating in the active case. The center frequencies of these notches or laser modes are very sensitive to local perturbations around the corresponding phase shifts. Because of the narrow bandwidth of the notches and laser modes, a sensor with high spatial resolution in the range 0.1 - 5 mm can be made by separating the phase shifts. High finesse phase-shifted FBG sensors also provide ultra-high measurand resolution. With two superimposed Bragg gratings, the device may be used as an accurate gradient sensor.

8.1 Introduction

There has been a lot of interest in fiber distributed sensors during the last decades. Almost all techniques utilize a physical backscattering, loss, or

[1] This chapter is based on Norwegian patent application no. 2001.2593 authored by Sigurd Weidemann Løvseth and Jon Thomas Kringlebotn

gain mechanism, for instance Rayleigh or Raman scattering, spontaneous or stimulated Brillouin scattering, or rare earth gain [1,2]. The general sensor principle is that the strength and/or characteristic optical frequencies of these effects are dependent on physical parameters like temperature and strain. The distribution of the measurand is typically found by using some kind of optical frequency (OFDR), time (OTDR), or coherence (OCDR) domain reflectometry. Distributed sensing of time-varying perturbations has also been demonstrated using a Sagnac interferometer in combination with a Mach-Zehnder interferometer [3] or a dual loop Sagnac interferometer [4,5]. Recently a distributed pressure sensor was demonstrated by determination of the free-spectral range shift induced by mode coupling in a mode locked fiber ring laser [6].

A different approach is to multiplex several fiber Bragg grating (FBG) sensors along the same fiber [7]. The center frequency ν_{B_i} of the main peak, also known as the stop band, in the reflection spectrum of a FBG for light in polarization i is given by:

$$\nu_{B_i} = \frac{c}{\lambda_{B_i}} = \frac{c}{2n_i\Lambda} \tag{8.1}$$

ν_{B_i} is also known as the center Bragg frequency, and λ_{B_i} is the Bragg wavelength. c is the speed of light, n_i is the generally polarization dependent refractive index, and Λ is the periodicity of the grating. Thus, a perturbation of n_i or Λ by a measurand will be detected as a shift in the Bragg frequency ν_{B_i}.

When the FBG sensors are multiplexed, the localization of a perturbation can be determined by using different periodicity for each grating. Similar quasi-distributed sensing can be achieved with Bragg grating based fiber lasers in rare earth doped fibers [8–10].

A common problem with most of the aforementioned techniques is that their highest spatial resolution is in the order of meters. However, Bragg gratings can be made quite short, with the minimum length limited by the UV beam size during the grating inscription. Alternatively, intra-grating perturbations of a Bragg structure can be measured by simultaneously measuring the group delay and power of the reflection spectrum [11–14]. Unfortunately, when using conventional FBGs, an enhancement in spatial resolution better than 10 cm inevitably will lead to a lower resolution in the measurand.

It is well known that by introducing a phase shift in an otherwise uniform Bragg grating, the two gratings at each side of the phase shift will act as the mirrors of an optical resonator, and there will be a notch in the peak of the grating reflection spectrum [15–19]. When the phase shifts equal π, the notch center frequency will equal the Bragg frequency. The notch is very narrow (typically less than one pm) compared with the stop band of the grating, and, therefore, much smaller perturbations can be measured

than for conventional FBGs. The narrow notch will also be split by the birefringence $B = n_x - n_y$ [20] caused by the fiber itself or a birefringent Bragg grating. Since shifts in different measurands perturb the birefringence to varying degrees, simultaneous measurements of two measurands can be achieved by tracking the notches of both polarizations [21].

As discussed in Chapter 1, distributed feedback fiber lasers (DFB-FL) with stable single longitudinal mode operation can be made by writing a phase-shifted FBG in a rare earth doped fiber [15, 22]. Single polarization operation can be obtained for instance by using polarization dependent gratings [23]. The laser frequency will equal the notch frequency in the grating stop band of the grating in the laser mode polarization. The linewidth of the laser modes are typically $\sim 1 - 10$ kHz, which means that DFB-FL sensors have much higher resolution in the measurand than corresponding passive phase shifted FBGs. Another advantage with DFB-FL sensors compared with the passive alternative is that no complex opto-electronics is needed to interrogate the sensor. DFB-FLs have been demonstrated for a number of sensor applications, some of which are listed in Chapter 1. Like phase-shifted FBGs, dual polarization DFB-FL can be used to simultaneously measure two measurands [24].

Both in passive and active phase-shifted FBG sensors, the resonant field at the reflection spectrum notch frequency falls off in an exponential manner from the phase shift. The effective cavity length is approximately inversely proportional to the grating strength. Thus, the effective sensing length is far shorter than the length of the grating [25], meaning that perturbations far away from the phase shift do not significantly affect the resonance frequency.

FBGs with periodic superstructures are often called sampled gratings or multiple wavelength fiber Bragg gratings (MW-FBG). A simple sinusoidal sampling function corresponds to a superposition of two uniform Bragg gratings with different ν_B. The reflection spectra of such gratings will have two reflection peaks slightly detuned from the stop bands of the two superimposed Bragg gratings. By using more complex sampling functions, or superimposing more gratings with different periodicity Λ, gratings with several reflection peaks with similar shapes and widths can be made [26]. However, since there is a limit to the refractive index contrast that can be achieved in a fiber grating, the maximum achievable reflection strength will decrease with increasing number of superimposed Bragg gratings.

Recently, a dual wavelength DFB-FL was reported, using dual wavelength FBGs with a center phase shift [27]. Such lasers do not have a semiconductor equivalent, since semiconductor lasers do not have the spatial hole burning mechanism required for stable multimode operation [28]. Because the two modes have almost overlapping mode profiles, these lasers will have a very stable beat frequency, which can be utilized in microwave [29] and soliton generation. A DFB-FL of this kind operating with four modes distributed in two polarizations and two stop bands, has also been used for

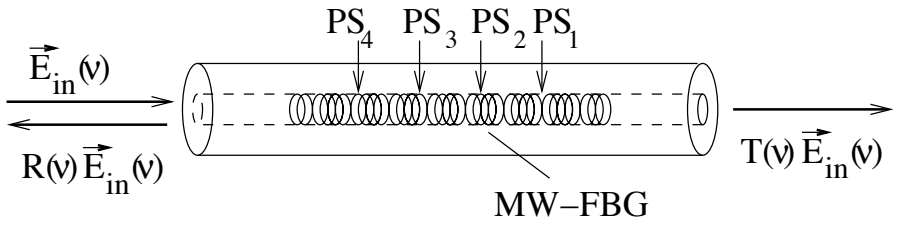

(a)

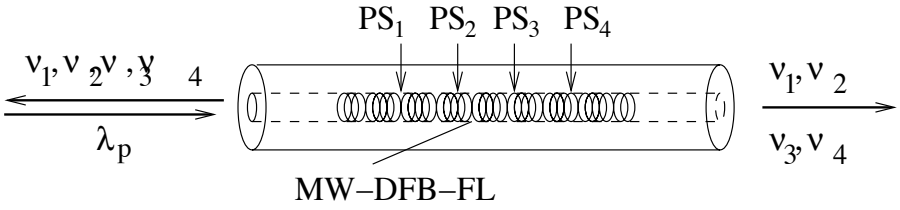

(b)

Figure 8.1: Illustration of MW-FBG (a) and MW-DFB-FL (b) distributed sensors.

simultaneous strain and temperature measurements [30]. It is possible to make DFB-FLs with more modes, but the maximum number of modes is limited by the available refrative index contrast of the fiber. We call such lasers multiple wavelength DFB-FLs (MW-DFB-FLs).

In this chapter, we will show that it is possible to use a combination of multiple phase-shifted FBGs to make active and passive sensors with high resolution in space and the measurand, utilizing that phase-shifted FBG and DFB-FL sensors are most sensitive to perturbations around their phase shifts.

8.2 Technique

The proposed intra-cavity distributed sensor consists of several superimposed or partly overlapping phase-shifted FBGs with different ν_B. In Figure 8.1(a) an example with $N_g = 4$ superimposed gratings, which we will call subgratings in the following, is shown. The subgratings $q = 1...N_g$ have individual phase shifts, PS_q, separated from each other along the fiber axis. The frequencies of the narrow reflection spectrum notches corresponding to the different subgratings will then be most sensitive to perturbations in

different spatial regions of the structure. The spatial distribution of a perturbation can be measured by tracking each notch frequency in the transmission $T(\nu)$ or reflection $R(\nu)$ spectrum of the MW-FBG structure. The notch frequencies can for instance be measured by use of a tunable laser with interferometric control [31].

By using rare earth doped fibers with gain, such structures may also be used as MW-DFB-FLs, as illustrated in Figure 8.1(b), where a DFB-FL is pumped by a source with wavelength λ_p. Provided the structure has large enough gain and subgrating strengths, it can start to lase in the stop band of all N_g subgratings, with frequencies ν_q, $q = 1..N_g$. The same spatial resolution can be achieved with even higher resolution in the measurand than for the passive structure. Sensors based on MW-DFB-FLs can be pumped from one or both ends and interrogated from either end. For gradient and higher order differential measurements only the beat frequencies between the modes need to be measured. If also the absolute value of the measurand is needed, at least one laser frequency has to be measured using for instance interferometric techniques. Alternatively, all laser frequencies can be measured directly.

As with phase-shifted FBGs sensors and dual polarization DFB-FLs, the ratio of change in birefringence to change in Bragg grating frequency as a result of a perturbation differs between measurands. Thus, the proposed distributed MW-FBG sensor can simultaneously measure two measurands by detecting both the frequency shift and the polarization frequency splitting of the reflection spectrum notches of each subcavity. In a dual polarization implementation of the proposed MW-DFB-FL sensor, the two measurands can be separated by simultaneously measuring the polarization beat frequency and one or both of the laser frequencies of each subgrating.

As with all FBG devices, MW-FBG and MW-DFB-FL sensors can be wavelength multiplexed serially or in parallel. Thus, it is for instance possible to measure the spatial distribution of a measurand gradient.

In Figures 8.2 the sensor principle is illustrated in more detail. The power distributions P_q, $q = 1...N_g$, resulting from incoming optical waves $\vec{E}$ with frequencies ν_q in a MW-FBG like the one shown in Figure 8.1(a) are sketched. As above, ν_q is equal to the notch frequency of subgrating q. At each ν_q, the optical wave will resonate around the phase shift of the corresponding subgrating. The power will drop sharply in a close to exponential manner as a function of $\kappa_q|z - z_q|$, i.e. the product of distance from phase shift q and the subgrating strength. In cases where κ_q is varying along the fiber axis, $\kappa_q|z - z_q|$ should be substituted with the integral of κ_q with respect to $|z - z_q|$. The modes of a MW-DFB-FL, like the one shown in Figure 8.1(b), will have a similar modal spatial power distribution. In Figure 8.2, we have also plotted a spatial distribution of a measurand M along the fiber axis. The measurand can for instance be temperature, strain, static or acoustic pressure, force, or any other physical quantity that can perturb the

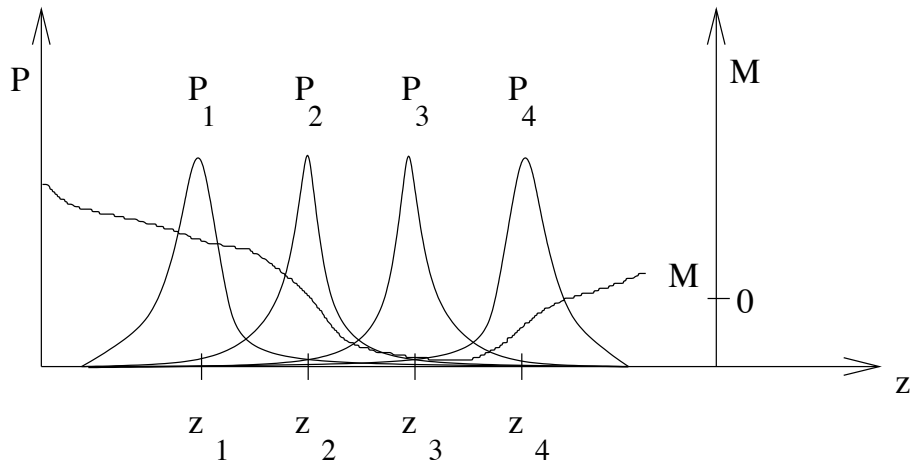

Figure 8.2: Sketch of power distributions at the resonances of the proposed MW-FBG or MW-DFB-FL distributed sensor. The spatial distribution of a measurand M is also plotted.

effective refractive index, n_x or n_y, periodicity Λ of the grating structure, or the birefringence $B = n_x - n_y$ of the fiber. Since there is little overlap between the spatial power distributions, and thus sensing lengths [25], of the different modes, they will have different response to M, and the notch frequency shifts of mode 1 and 2 will be of opposite sign compared with the frequency shifts of mode 3 and 4.

8.3 Design and Fabrication Considerations

The strength or number of subgratings that can be superimposed in a given fiber is limited by the maximum UV-induced refractive index change of the fiber. For both MW-FBG and MW-DFB-FL distributed sensors that means there is a limit on the achievable spatial resolution for a given grating length. For the MW-DFB-FL, the number of lasers that can be superimposed will be limited since the mirror reflectivity has to be above threshold in all subgratings. For a passive MW-FBG, there is no fundamental lower limit on the subgrating strength. However, as the subgrating strength becomes lower, the power distribution becomes wider at each resonance, effectively broadening the sensitive length of each subgrating. At the same time the spectral width of the reflection spectrum notch will be larger, leading to lower resolution in the measurand. However, how effectively the available refractive index contrast can be utilized is largely a question of clever design and fabrication techniques, and in this section we will discuss the feasibility of different approaches.

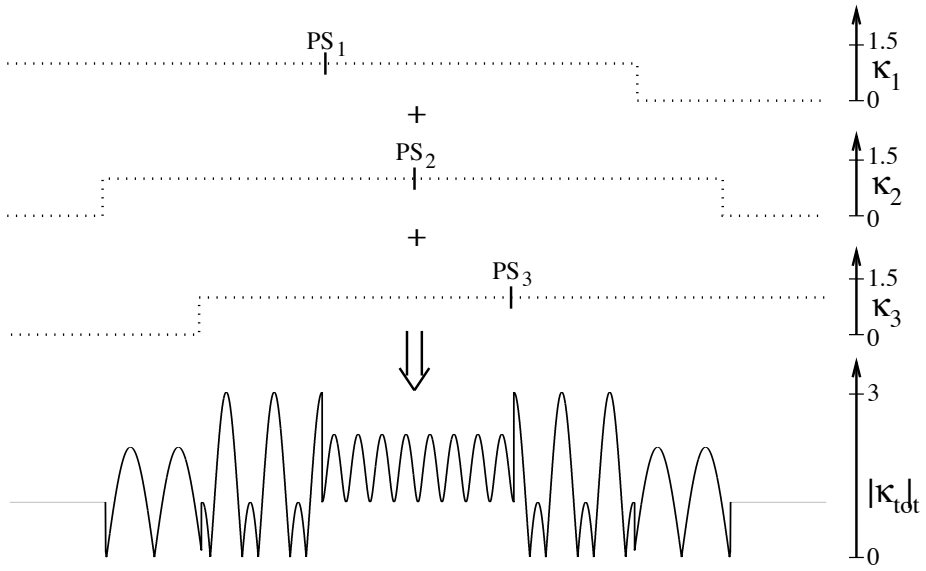

Figure 8.3: Illustration of a MW-FBG sensor structure produced by superimposing three phase-shifted uniform subgratings with different periodicities Λ. The coupling coefficients κ_q, $q = 1...3$ and κ_{tot} are in arbitrary units.

Figure 8.3 illustrates a superposition of three uniform subgratings with equal coupling coefficients $\kappa_1 = \kappa_2 = \kappa_3$, that all have a phase shift PS_q of π in the middle. The gratings, including their phase shifts, are spatially shifted from each other, leading to a grating structure similar to the ones shown in Figure 8.1. The subgratings are only partially overlapping, and the phase relation between the subgratings changes at each subgrating phase shift. This results in a total coupling coefficient $|\kappa_{\mathrm{tot}}(z)|$ where both the beat amplitude and DC level vary significantly along the grating axis. $|\kappa_{\mathrm{tot}}|$ is proportional to the required refractive index contrast, and if the sections with high peak values of $|\kappa_{\mathrm{tot}}|$ are to have the correct profile, the potential refractive index contrast in other sections of the grating will be poorly utilized.

In Figure 8.4 another MW-FBG with three phase-shifted subgratings is illustrated. The distances between the π phase shifts PS_q of the different subgratings $q = 1...3$ are the same as in Figure 8.3. Also here the reflectivity of the subgrating mirrors are equal to each other, but the subgrating strengths are varied along the fiber axis in such a way that the ripple peak values of $|\kappa_{\mathrm{tot}}|$ is the same in all sections of the grating. Compared with the previous example shown in Figure 8.3, this leads to a relaxed refractive index contrast or structure length requirement for a given subgrating reflectivity level. Furthermore, in order to increase the spatial resolution of

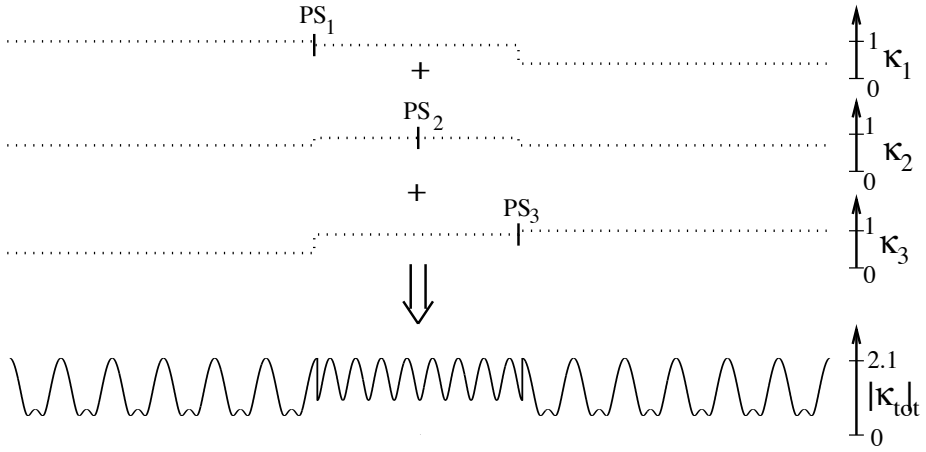

Figure 8.4: Illustration of a MW-FBG sensor structure produced by superimposing three phase-shifted subgratings with different periodicity, spatially separated phase shifts, and phases and local coupling coefficients optimized for efficient use of the refractive index contrast. The coupling coefficients are in arbitrary units.

the sensor, the resonant mode field distributions should have as little overlap as possible. This overlap decreases with increasing subgrating strength between the phase shifts. Thus the relative phase differences between the subgratings are optimized between the phase shifts in order to maximize the subgrating strength for a given refractive index contrast, i.e. maximum κ_{tot}. In short, it is ensured that the three subgratings are never in phase. This optimization technique will discussed in further detail in Appendix 8.A.

The third example shown in Figure 8.5, is also a structure consisting of three superimposed phase-shifted Bragg gratings, with the same phase shift separations as in Figures 8.3-8.4. Here the subgratings are not overlapping between the phase shifts. Instead, the overlap between the resonances is minimized by assigning each subgrating all available index contrast around its phase shift. Otherwise the structure is similar to the one shown in Figure 8.4, in that the required refractive index contrast everywhere is the same, but since there is no grating superposition between the phase shifts, the inter-subgrating phase can in this case be optimized at the edges of the grating.

8.4 Analysis

In the upper half of Figure 8.6, the calculated modal field distributions of a MW-DFB-FL of the design type illustrated in Figure 8.4 is plotted. The modes are found using a coupled mode transfer matrix method [28]. The

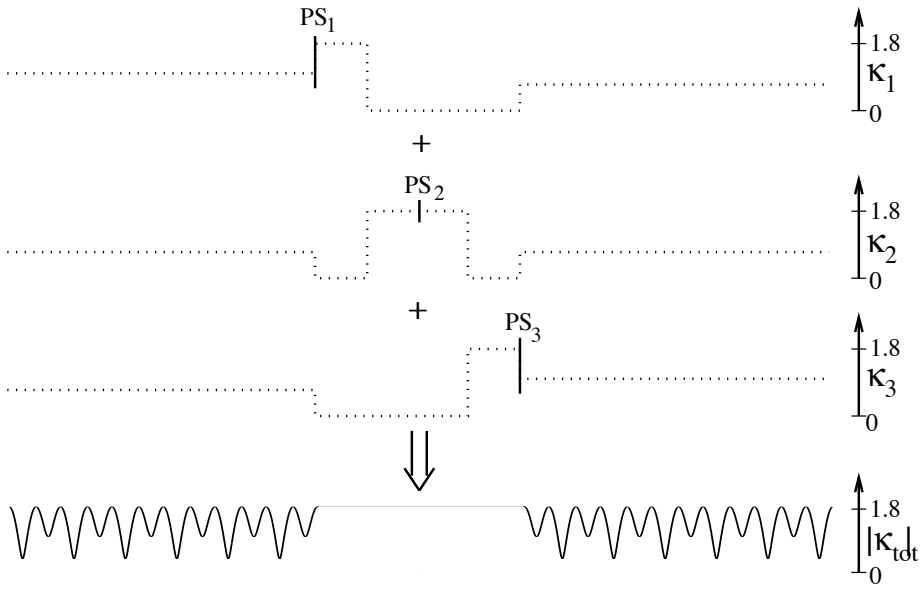

Figure 8.5: Illustration of an alternative way of implementing a MW-FBG sensor with high utilization of the refractive index contrast. The coupling coefficients are in arbitrary units.

grating structure consists of 3 superimposed subgratings, and the subgrating phase shifts and Bragg frequencies are spaced 2.5 cm and 10 GHz apart, respectively. The total grating length is 12.3 cm, and the maximum total grating strength $|\kappa_{\text{tot}}|$ is 200 m^{-1} corresponding to a refractive index modulation amplitude of approximately $\Delta n = 10^{-4}$. With the optimized relative phase in the length of fiber between the phase shifts, this corresponds to a subgrating strength of 89 m^{-1}.

The power difference between the most powerful and next most powerful mode at the phase shifts is 20 dB at the center phase shift and 22 dB at the outer phase shifts. The spatial power distribution of the field at the different spectral notches with an identical passive structure will be similar, as illustrated in the lower half of Figure 8.6. This indicates that the maximum resolution for a passive system can be much higher than 2.5 cm as in this example. In fact, for strong gratings it can be shown that the cavity length for each resonance q is approximately $1/\kappa_q(z_q)$, where $\kappa_q(z_q)$ is the coupling coefficient of subgrating q around its phase shift. Thus, we can hope for a maximum spatial resolution of the sensor equal to the maximum achievable grating strength, or [32]:

$$\Delta z_{\text{res,max}} \sim \frac{1}{\kappa_{\max}} = \frac{\lambda_B}{\pi \Delta n_{\max}} \tag{8.2}$$

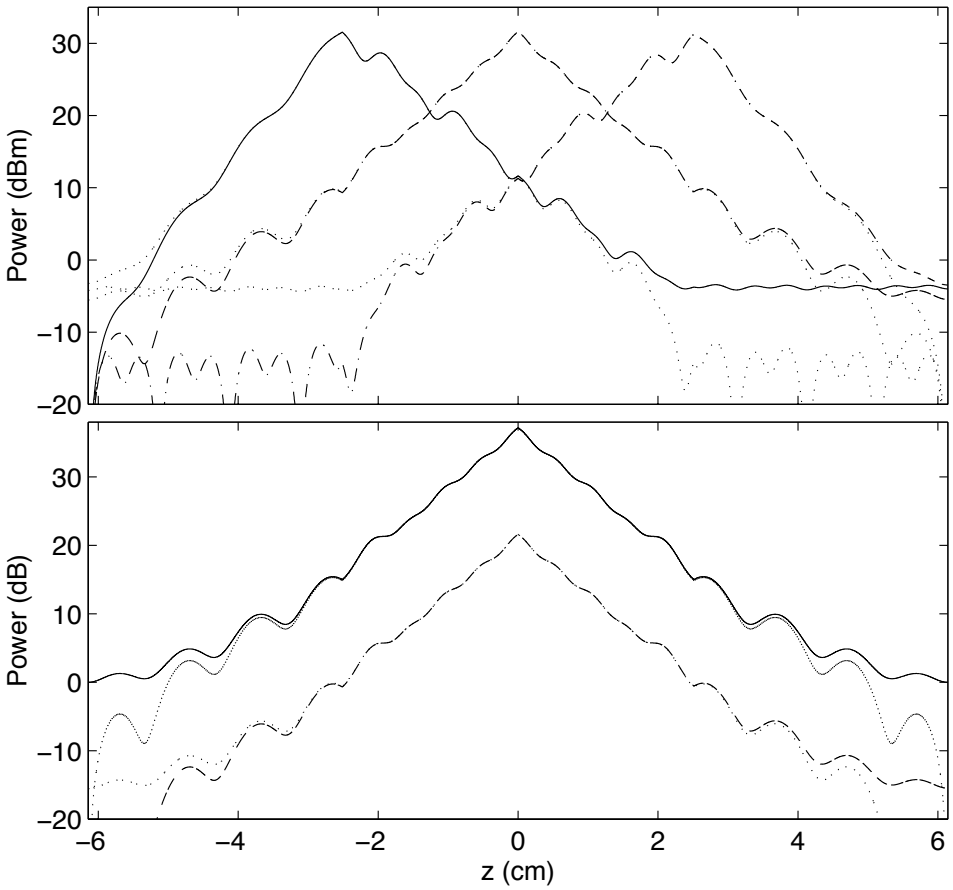

Figure 8.6: Power distributions in passive and active triple-wavelength FBG distributed sensors with identical grating. Top: The modes of a single-polarization MW-DFB-FL. The forward propagating waves are shown with solid, dashed, and dash-dotted curves, whereas the backward propagating waves are shown with dotted curves. Bottom: The power distribution resulting from an incoming wave at the central reflection spectrum notch in a passive MW-FBG. For reference the power distribution of the central laser mode of the MW-DFB-FL is shown in the same plot with dotted lines.

Here $\Delta z_{\mathrm{res,max}}$ is the maximum achievable spatial resolution of the sensor, Δn_{max} is the maximum UV-induced refractive index amplitude, and Λ is the grating periodicity. With hydrogen loading germanium doped fibers $\Delta n_{\mathrm{max}} \gtrsim 5 \cdot 10^{-3}$ can be achieved [33], corresponding to $\Delta z_{\mathrm{res,max}} \approx 0.1$mm at $\lambda_B = 1550$ nm. However, gratings written in non-hydrogenated fibers tend to be more stable and have lower loss, and in non-hydrogenated Ge-doped or co-doped B-Ge silicate fibers the maximum refractive index amplitude is typically $\Delta n_{\mathrm{max}} \approx 2.5 \cdot 10^{-4}$ and $\Delta n_{\mathrm{max}} \approx 4 \cdot 10^{-4}$ [34], corresponding to $\Delta z_{\mathrm{res,max}} \approx 2$ mm and $\Delta z_{\mathrm{res,max}} \approx 1$ mm, respectively. It is more

Table 8.1: Typical maximum achievable index modulation amplitudes, coupling coefficients, and spatial resolutions for various silica fiber types.

Fiber dopant composition	$\Delta n_{\max}$	$\kappa_{\max}$ (mm^{-1})	$\Delta z_{\mathrm{res,max}}$ (mm)
Ge, no H_2	$2.5{\cdot}10^{-4}$	0.5	2
B-Ge, no H_2	$4{\cdot}10^{-4}$	0.8	1
Ge, hydrogenated	$5{\cdot}10^{-3}$	10	0.1
Er-Yb-B-Ge, no D_2	$5{\cdot}10^{-5}$	0.1	10
Er-Yb-B-Ge, D_2-loaded	$1.1{\cdot}10^{-4}$	0.23	4

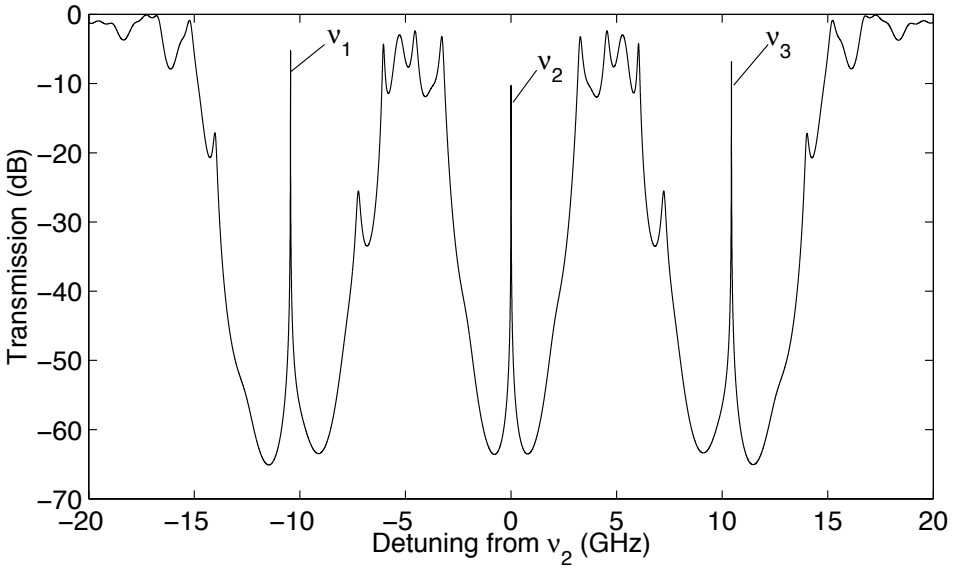

Figure 8.7: Transmission spectrum of a MW-FBG with $\Delta\nu_{1,2} = \Delta\nu_{2,3} = 10$ GHz.

difficult to fabricate non-hydrogenated rare earth doped fibers needed for DFB-FLs with high photosensitivity, but $\Delta n_{\max} \gtrsim 5 \cdot 10^{-5}$, corresponding to $\Delta z_{\mathrm{res,max}} \approx 10$ mm can be achieved using a Ge-B doped photosensitive ring [35], whereas $\Delta n_{\max} \gtrsim 1.1 \cdot 10^{-4}$ corresponding to $\Delta z_{\mathrm{res,max}} \approx 4$ mm has been reported for a deuterium (D_2) loaded fiber of this kind [25]. The maximum refractive index amplitudes and corresponding maximum resolutions for the various fiber types are summarized in Table 8.1.

In Figure 8.7, the calculated transmission spectrum of the grating structure discussed in the previous paragraph is plotted, but this time without gain. Even with this relatively small subgrating Bragg frequency separation, there is only some overlap between the sidebands, and the three stop bands in the spectrum are clearly separated. This eases the interrogation and, as will be discussed below, ensures a relative linear response of the sen-

sor. The stop band notches, which in the transmission spectrum appear as narrow peaks, are too narrow to be completely resolved in the simulations. Closer studies however reveal that the full-width half-maximum (FWHM) of the central stop band notch is approximately 0.6 MHz, corresponding to 0.35 mK in temperature [36] or 4.4 nϵ in strain [37] at a wavelength of 1550 nm. However, as mentioned in Section 8.3, the linewidth depends strongly on the grating length and strength. Following the discussion from the previous paragraph, each subgrating q will have a length of approximately 1 mm= $1/\kappa_q$ in a MW-FBG sensor designed for maximum spatial resolution along the entire grating length written in a non-hydrogenated B-Ge-codoped fiber with many subgratings. Such a short length and high κ_q result in a notch linewidth as broad as 60 GHz, corresponding to 35 K in temperature and 0.4mϵ in strain. Thus, in order to make the resonances sharper and have reasonable resolution in the measurand, the total grating should be made longer than the sensitive length. That is, each subgrating should extend a certain length past the edge of the sensitive subgrating phase shifts region at each side of the MW-FBG structure. In principle, the reflection spectrum notch can be made arbitrarily sharp, a grating with the same strength $\kappa_q = 1$ mm^{-1} of length 3 cm for instance has a transmission notch linewidth of only 8 mHz. Such a narrow notch would of course be extremely difficult to detect. In practice the actual measurand resolution depend on the interrogation technique and can be both higher and lower than what the transmission notch linewidth suggests. In comparison, the resolution of the MW-DFB-FL sensor depends more directly on the laser mode linewidth, although the resolution also here will depend on the interrogation system. For static signals it is in principle possible to average over a long time to achieve high accuracy, whereas for dynamic signals like sound sometimes only a certain frequency band of the noise spectrum is of interest [38]. DFB-FLs with a linewidth of 1 kHz are commercially available, and typical DFB-FLs have a linewidth in the range $\sim 1 - 10$ kHz [39, 40], corresponding to approximately 0.5-5 μK in temperature and 0.1-1 pϵ in strain.

A measurand that varies linearly or quadratically along a fiber grating induces a linear or quadratic chirp, respectively, of the grating period. We therefore investigated the effect of applying a chirp of varying amplitude to the structure plotted in Figure 8.6 consisting of three superimposed subgratings, and the results in the cases of linear and quadratic chirp are shown in Figures 8.8 and 8.9, respectively. In the upper half of the figures the detuning from the 10 GHz Bragg frequency separation between the subgratings are plotted, whereas in the lower half the beat frequencies between the spatially middle mode and the left and right modes are plotted. In the linear chirp case, these two beat frequencies are equal to each other because of the symmetry of the device. The response is reasonably linear, which eases the interrogation of the sensor, with a linear chirp ranging from -20 to

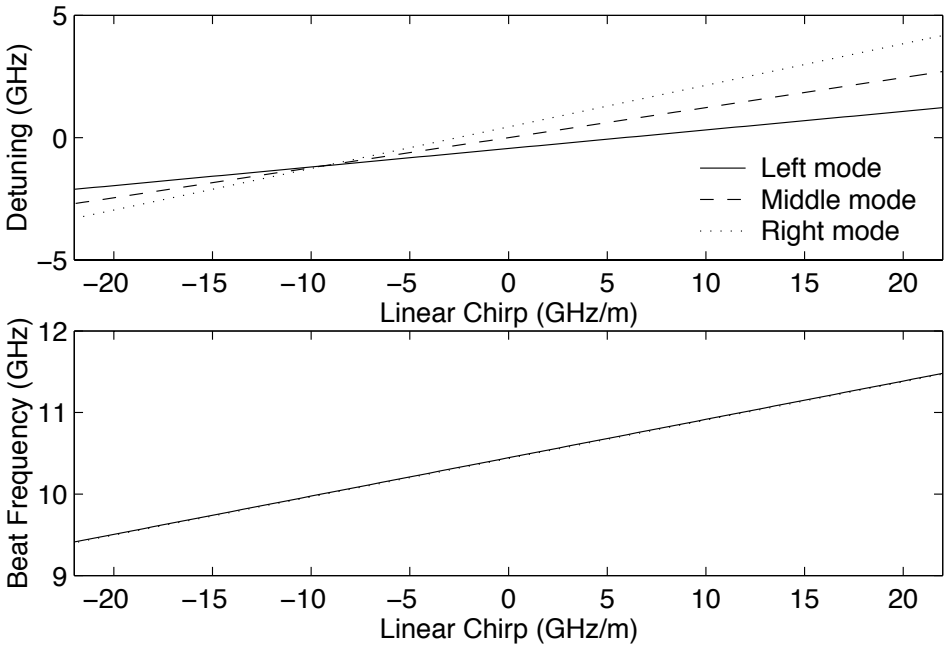

Figure 8.8: The detuning of (top) and the beat frequency between (bottom) the three modes plotted in Figure 8.6 as a function of linear chirp.

20 GHz/m and a quadratic chirp between -550 GHz/m^2 and 550 GHz/m^2. The range in the linear chirp case corresponds to a temperature gradient range of approximately $\pm$12 K/m or strain gradient range of $\pm$146 $\mu\epsilon$/m. The range in the quadratic chirp case corresponds to a second order Taylor coefficient of approximately $\pm$320 K/m^2 in temperature and $\pm$4 mϵ/m^2 in strain.

We have simulated several other structures of all the design types discussed in Section 8.3. By comparing different MW-DFB-FLs of different design with equal cavity finesse it was found that structures of the type illustrated in Figure 8.3 yielded the highest linearity and largest dynamic range in the measurand with all modes operating, whereas the type illustrated in Figure 8.5 had the most nonlinear response and limited dynamic range. However, as discussed in Section 8.3 the former design requires longer gratings and/or higher refractive index contrast, and thus does not give the best response if limitations are imposed on the size of the coupling coefficient or length.

Nonlinearity in the response can be calibrated for in a simple gradient sensor, but this becomes more difficult for a distributed MW-FBG/MW-DFB-FL sensor with many subgratings that are exposed to arbitrary spatial measurand distributions. We believe the relatively small nonlinearities that exist in the response are caused mainly by two mechanisms. Firstly, a

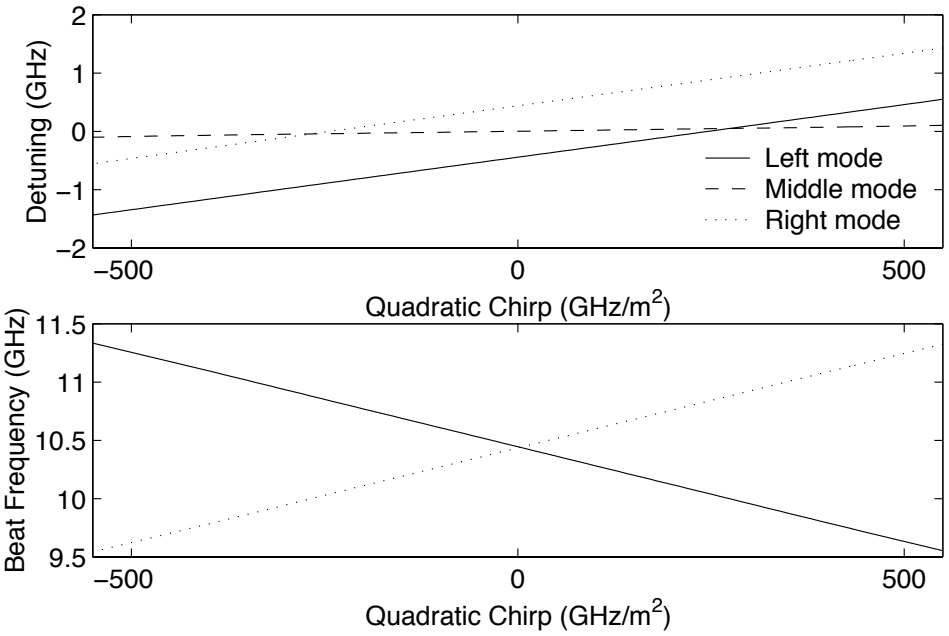

Figure 8.9: The detuning of (top) and the beat frequency between (bottom) the three modes plotted in Figure 8.6 as a function of quadratic chirp.

chirp will detune outer parts of a subgrating from the central part around the phase shift. Thus, for large chirp, the reflectivity of the outer parts will decrease somewhat compared with the central part. When the subgrating is not symmetric around the phase shift, as will be the case for some of the structures discussed in Section 8.3, the notch frequency differences will not scale proportionally to a linear chirp. This will also generally be the case if the chirp is not strictly linear. Secondly, and more important, is the nonlinearity caused by the ripples in the resonance power distributions, as seen in Figure 8.6. These ripples are a consequence of the superstructure of the grating [28], and increase in amplitude and periodicity with decreasing subgrating beat frequency and increasing coupling coefficient. When a notch frequency changes, the ripples of its corresponding power distribution will move relative to the grating structure and the other phase shifts. Thus, some nonlinearity will be induced in the beat frequency response because of changes in the spatial overlap between the resonances, and a large subgrating Bragg frequency separation is needed for high linearity. On the other hand, a distributed MW-DFB-FL sensor with a small inter-modal frequency spacing can be interrogated using a simple beat frequency measurement, and also the passive MW-FBG sensor is easier to interrogate with a small frequency spacing. In addition a small beat frequency means that the sensor can be fabricated with efficient use of the photosensitivity using a single scan of the UV source, as discussed in Appendix 8.A. Thus, in most

cases it will be desirable to have the Bragg frequencies spaced as densely as the linearity requirement for the given application allows.

Apart from nonlinearities, a chirp-induced decrease in effective cavity finesse in the phase shifted MW-FBG sensor will increase the width of the reflection spectrum notch somewhat. In the DFB-FL case, the decrease in cavity finesse changes the output power [28, 41, 42] and noise performance [43]. With certain types of grating perturbations also higher order modes may be induced [44]. However, these unwanted modes, which have their frequencies outside the subgrating stop bands and are less spatially confined than the fundamental modes, are less likely to be induced in a MW-DFB-FL with spatially separated phase shifts than in a conventional MW-DFB-FL with all phase shifts co-located, since the fundamental modes of the former design saturate the gain in a larger fraction of the grating structure length.

8.5 Conclusion

We have presented a new type of active and passive intra-cavity optical fiber Bragg grating sensors. In the new design, the high resolution in the measurand of phase-shifted Bragg grating sensors is combined with high spatial resolution by partly overlapping gratings with different periodicity. Since the fundamental resonance frequency of each superimposed grating is mostly dependent on the periodicity around its phase shift, the spatial distribution of a measurand can be detected by tracking the reflection spectrum notches of the structure, or if the fiber has gain, by measuring the frequency of the laser modes.

The maximum achievable spatial resolution depends on the desired resolution in the measurand, the structure length, and, most importantly, the maximum photoinduced refractive index contrast of the fiber. We found that the maximum spatial resolution for a passive sensor type is in the range 0.1 - 2 mm, depending on the fiber type and degree of hydrogen loading. For a grating written in a rare earth doped fiber applicable for MW-DFB-FLs, a maximum spatial resolution of 5 mm is more realistic. The measurand resolution is dependent on the grating design and interrogation technique in the passive case, whereas a MW-DFB-FL sensor has a potential resolution in temperature and strain in the range of 0.5-5 μK and 0.1-1 pϵ, respectively.

Some refractive index contrast and thus spatial resolution can be gained by optimizing the relative phase between the subgratings and individually varying the strength of each superimposed grating along the fiber axis. In advanced grating writing setups, and if the frequency separation between the superimposed gratings is not too large, limited by the UV spot size, such structures can be fabricated with one single scan by the UV source. By overlaying the individual gratings one by one higher frequency separation between the notch or laser frequencies can be achieved, but if the

relative phase between the gratings is optimized, there will be some cancellations between the gratings everywhere. Thus, in contrast to single scan fabrication some of the available refractive index contrast will be wasted.

We have simulated the response of structures with up to three superimposed gratings with varying degree of linear and quadratic chirp. The frequency shifts of the resonances responded quite linearly with the chirp amplitude. We therefore believe such sensors can be an attractive alternative to measure short distance distributions in for instance temperature or strain. Alternatively, many such structures can be multiplexed in order to measure gradient distributions over larger lengths. In any case, experimental work has to be performed in order to decide the practicality of the proposed devices.

Appendix:

8.A The Optimization of Relative Phase between Subgratings and its Consequences for MW-FBG fabrication

As discussed in Section 8.3, the subgrating strength for a given limit of $|\kappa_{\mathrm{tot}}|$ can be optimized by adjusting the relative phase between the subgratings. Assuming that all subgratings have equal strength κ_1 and that we have equidistant frequency spacing between the subgratings, we have:

$$\begin{aligned} |\kappa_{\mathrm{tot}}| &= \kappa_1 \left| \sum_{q=1}^{N_g} e^{-j(\frac{4\pi q \Delta\nu_B nz}{c} + \phi_q)} \right| = \kappa_1 \left| \sum_{q=1}^{N_g} e^{-j(2q\Delta K z + \phi_q)} \right| \\ &= \kappa_1 \sqrt{N_g + 2 \sum_{q=1}^{N_g-1} \sum_{r=q+1}^{N_g} \cos(2q\Delta K z + \Delta\phi_{r,r-q})} \end{aligned} \tag{8.3}$$

Here, $\Delta\nu_B$ is the nearest-neighbor subgrating Bragg frequency difference, whereas ΔK is the corresponding Bragg wavenumber difference in the fiber. ϕ_q is the phase of grating q, whereas $\Delta\phi_{q,r}$ is the phase difference between grating q and grating r. When all ϕ_q, $q = 1...N_g$ are equal, the maximum value of $|\kappa_{\mathrm{tot}}|$ is $N_g\kappa_1$, which is attained at $z = N\pi/\Delta K$, where N is an integer. However, it is possible to avoid these worst case maxima in $|\kappa_{\mathrm{tot}}|$ and significantly lower the required refractive index contrast by optimizing relative phases between the subgratings. For $N_g = 3$ it is easy to realize that we get the smallest possible ripple in $|\kappa_{\mathrm{tot}}|$ when:

$$\Delta\phi_{21} = \pm\pi + \Delta\phi_{32} \tag{8.4}$$

The maximum value of $|\kappa_{\mathrm{tot}}|$ is then reduced from $3\kappa_1$ to $2.23\kappa_1$. Likewise, it can be shown that the maximum value of $|\kappa_{\mathrm{tot}}|$ can be reduced from $4\kappa_1$

to $2.66\kappa_1$ for $N_g = 4$ provided that:

$$\begin{aligned} \Delta\phi_{41} &= \pm\pi + \Delta\phi_{32} \\ \Delta\phi_{31} &= \pm\pi - \Delta\phi_{42} \end{aligned} \tag{8.5}$$

For $N_g = 5$ the maximum value of $|\kappa_{\mathrm{tot}}|$ can be reduced from $5\kappa_q$ to $2.87\kappa_q$. Finding the optimal phase in an analytical way becomes increasingly difficult with larger N_g. However, it is easy to see that if $\Delta\phi_{q,q-1}$, $q = 2...N_g$ is distributed uniformly in increasing order from 0 to 2π for large N_g, most of the cosine terms in equation (8.1) will cancel each other out, and thus the maximum $|\kappa_{\mathrm{tot}}|$ is reduced to a value close to $\kappa_1\sqrt{N_g}$. In order to find the optimal solution for a given N_g, numerical methods have to be used, and for $N_g = 16$ the maximum value of $|\kappa_{\mathrm{tot}}|$ was found to be $\kappa_1(\sqrt{N_g}+0.75) = 4.75\kappa_1$ [45]. In these highly optimized MW-FBGs, much of the amplitude modulation is in effect transformed to phase modulation. However, it will not be possible to maintain this ideal phase relation everywhere in the MW-FBG/MW-DFB-FL sensors discussed in this chapter, since the subgrating phase shifts are not co-located.

It is important to choose the right method of grating fabrication in order to utilize the full potential of the amplitude modulation cancellations. There are two principal ways of fabricating MW-FBGs. Either the MW-FBGs are produced by overlaying the subgratings one by one, or they are fabricated by writing the MW-FBG in one scan using a complex sampling function with an index profile equal to the sum of the individual subgratings. The advantage of the former method is that, regardless of the Bragg frequency spacing between the subgratings, a high spatial resolution is not required in the grating writing setup. However, it may be difficult to control the relative phases between the subgratings with sufficient accuracy. Anyway, each independently written subgrating will contribute to a shift in the mean refractive index that is independent of its phase [45]. For a perfect subgrating, this shift equals half the peak-to-peak amplitude of the index modulation. Thus, even if the relative phases are ideally optimized, the lower limit of the needed refractive index contrast for the MW-FBG in this case corresponds to a grating of strength $(N_g + \sqrt{N_g})\kappa_m/2$. Writing the subgratings one by one is a good idea if the sensor application requires a large dynamic range or, as discussed in Section 8.A, a high linearity is needed which requires a large frequency spacing between the subgratings. However, if high spatial resolution and thus efficient use of the available refractive index contrast is most important, the MW-FBG grating structures should be written in one scan using a complex sampling function.

References

[1] A. D. Kersey, "A review of recent developments in fiber optic sensor technology," *Opt. Fiber Technol.*, vol. 2, pp. 291–316, July 1996.

[2] K. Hotate, "Fiber sensor technology today," *Opt. Fiber Technol.*, vol. 3, pp. 356–402, Oct. 1997.

[3] J. P. Dakin, D. A. Pearce, A. P. Strong, and C. A. Wade, "A novel distributed optical fiber sensing system enabling location of disturbances in a Sagnac loop interferometer," in *Proc. SPIE*, vol. 838, pp. 325–328, 1987.

[4] E. Udd, "Sagnac distributed sensor systems," *Proc. SPIE*, vol. 1586, pp. 46–52, 1991.

[5] E. Rønnekleiv, K. Bløtekjær, and K. Kråkenes, "Distributed fiber sensor for location of disturbances," in *9th International Conference on Optical Fiber Sensors*, (Florence, Italy), National Research Council of Italy, 1993. Postdeadline paper PD7.

[6] S. Yamashita and K. Hotate, "Distributed pressure sensor with a mode-locked fiber-ring laser," *Opt. Lett.*, vol. 26, pp. 590–592, May 2001.

[7] A. D. Kersey, M. A. Davis, H. J. Patrick, M. L. K. P. Koo, C. G. Askins, M. A. Putnam, and E. J. Friebele, "Fiber grating sensors," *J. Lightwave Technol.*, vol. 15, pp. 1442–1462, Aug. 1997.

[8] K. P. Koo and A. D. Kersey, "Bragg grating-based laser sensors systems with interferometric interrogation and wavelength division multiplexing," *J. Lightwave Technol.*, vol. 13, no. 7, pp. 1243–1249, 1995.

[9] K. P. Koo and A. D. Kersey, "Noise and cross talk of a 4-element serial fiber laser sensor array," in *1996 Conf. on Optical Fiber Communications, Technical Digest*, pp. 266–267, 1996.

[10] J. Hübner, P. Varming, and M. Kristiansen, "Five wavelength DFB fiber laser source for WDM systems," *Electron. Lett.*, vol. 33, pp. 139–140, Jan. 1997.

[11] S. Huang, M. LeBlanc, M. M. Ohn, and R. M. Measures, "Bragg intragrating structural sensing," *Appl. Opt.*, vol. 34, pp. 5003–5009, Aug. 1995.

[12] S. Huang, M. M. Ohn, and R. M. Measures, "Phase-based Bragg intragrating distributed strain sensor," *Appl. Opt.*, vol. 35, pp. 1135–1142, Mar. 1996.

[13] J. Skaar and H. E. Engan, "Distributed intragrating sensing using phase retrieval," in *13th International Conference on Optical Fiber Sensors* (B. Y. Kim and K. Hotate, eds.), vol. 3746 of *Proceedings of SPIE*, (Kuongju, South Korea), pp. 466–469, 1999.

[14] J. Skaar, "Measuring the group delay of fiber Bragg gratings by use of end-reflection interference," *Opt. Lett.*, vol. 24, pp. 1020–1022, Aug. 1999.

[15] H. A. Haus and C. V. Shank, "Antisymmetric taper of distributed feedback lasers," *IEEE J. Quantum Electron.*, vol. 12, pp. 532–539, Sept. 1976.

[16] R. C. Alferness, C. H. Joyner, M. D. Divino, M. J. R. Martyak, and L. L. Buhl, "Narrowband grating resonator filters in InGaAsP/InP waveguides," *Appl. Phys. Lett.*, vol. 49, pp. 125–127, July 1986.

[17] H. A. Haus and Y. Lai, "Theory of cascaded quarter wave shifted distributed feedback resonators," *J. Lightwave Technol.*, vol. 28, pp. 205–213, Jan. 1992.

[18] G. P. Agrawal and S. Radic, "Phase-shifted fiber Bragg gratings and their application for wavelength demultiplexing," *IEEE Photon. Technol. Lett.*, vol. 6, pp. 995–997, Aug. 1994.

[19] J. Canning and M. G. Sceats, "π-phase-shifted periodic distributed structures in optical fibres by UV post-processing," *Electron. Lett.*, vol. 30, pp. 1344–1345, Aug. 1994.

[20] D. Y. Stepanov, J. Canning, and Z. Brodzeli, "High-resolution measurements of fibre Bragg grating transmission spectra," in *Proceedings of ECOC'98-24th European Conference on Optical Communication*, vol. 1, (Madrid, Spain), pp. 407–408, IEEE, Sept. 1998.

[21] M. LeBlanc, S. T. Vohra, T. E. Tsai, and E. J. Friebele, "Transverse load sensing by use of pi-phase-shifted fiber Bragg gratings," *Opt. Lett.*, vol. 24, pp. 1091–1093, Aug. 1999.

[22] J. T. Kringlebotn, J. Archambault, L. Reekie, and D. N. Payne, "Er^{3+}:Yb^{3+}-codoped fiber distributed feedback laser," *Opt. Lett.*, vol. 19, pp. 2101–2103, Dec. 1994.

[23] M. Ibsen, E. Rønnekleiv, G. J. Cowle, M. O. Berendt, O. Hadeler, M. N. Zervas, and R. I. Laming, "Robust high-power (>20 mW) all-fibre DFB lasers with unidirectional and truly single polarisation outputs," in *Proc. Conf. Lasers and Electro-Optics (CLEO) 1999*, (Baltimore, MD, USA), pp. 245–246, 1999.

[24] J. T. Kringlebotn, "Optical fiber distributed feedback laser." US patent 5,844,927.

[25] E. Rønnekleiv, M. Ibsen, M. N. Zervas, and R. I. Laming, "Characterization of fiber distributed-feedback lasers with an index-perturbation method," *Appl. Opt.*, vol. 38, pp. 4558–4565, July 1999.

[26] M. Ibsen, M. K. Durkin, M. J. Cole, and R. I. Laming, "Sinc-sampled fiber Bragg gratings for identical multiple wavelength operation," *IEEE Photon. Technol. Lett.*, vol. 10, pp. 842–844, June 1998.

[27] M. Ibsen, E. Rønnekleiv, G. J. Cowle, M. N. Zervas, and R. I. Laming, "Multiple wavelength all-fibre DFB lasers," *Electron. Lett.*, vol. 36, pp. 143–144, Jan. 2000.

[28] S. W. Løvseth and D. Y. Stepanov, "Analysis of multiple wavelength DFB fiber lasers," *IEEE J. Quantum Electron.*, vol. 37, pp. 770–780, June 2001.

[29] W. H. Loh, J. P. de Sandro, G. J. Cowle, B. N. Samson, and A. D. Ellis, "40 GHz optical-millimetre wave generation with a dual polarisation distributed feedback fibre laser," *Electron. Lett.*, vol. 33, pp. 594–595, Mar. 1997.

[30] O. Hadeler, M. Ibsen, and M. N. Zervas, "Distributed feedback fibre laser sensor for simultaneous strain and temperature measurements in the RF domain," in *14^{th} International Conference on Optical Fiber Sensors* (A. G. Mignani and H. C. Lefèvre, eds.), vol. 4185 of *Proceedings of SPIE*, pp. 588–591, 2000.

[31] E. Rønnekleiv, J. T. Kringlebotn, and D. Thingbø, "800 GHz continously tunable fiber DFB laser for high speed high accuracy spectral characterization." To be presented at *Topical Meeting on Bragg Gratings, Photosensitivity and Poling in Glass Waveguide (BGGP)*, (Stresa, Italy), paper BWB2, July 2001.

[32] H. Kogelnik and C. V. Shank, "Coupled-wave theory of distributed feedback lasers," *J. Appl. Phys.*, vol. 43, pp. 2327–35, May 1972.

[33] P. J. Lemaire, R. M. Atkins, V. Mizrahi, and W. A. Reed, "High pressure H_2 loading as a technique for acheiving ultrahigh UV photosensitivity and thermal sensitivity in GeO_2 doped optical fibres," *Electron. Lett.*, vol. 29, pp. 1191–1193, June 1993.

[34] D. L. Williams, B. J. Ainslie, J. R. Armitage, R. Kashyap, and R. J. Campbell, "Enhanced UV photosensitivity in boron codoped germanosilicate fibres," *Electron. Lett.*, vol. 29, pp. 45–47, Jan. 1993.

[35] L. Dong, W. H. Loh, J. E. Caplen, J. D. Minelly, K. Hsu, and L. Reekie, "Efficient single-frequency fiber lasers with novel photosensitive Er/Yb optical fibers," *Opt. Lett.*, vol. 22, pp. 694–696, May 1997.

[36] S. Takahashi and S. Shibita, "Thermal variation of attenuiation for optical fibers," *J. Non-Crystalline Solids*, vol. 30, pp. 359–370, 1978.

[37] A. Bertholds and R. Dändliker, "Determination of the individual strain-optic coefficient in single-mode optical fibers," *J. Lightwave Technol.*, vol. 6, pp. 17–20, 1988.

[38] S. W. Løvseth, E. Rønnekleiv, J. T. Kringlebotn, and K. Bløtekjær, "Fiber distributed-feedback lasers used as acoustic sensors in air," *Appl. Opt.*, vol. 38, pp. 4821–4830, Aug. 1999.

[39] W. H. Loh and R. I. Laming, "1.55 μm phase-shifted distributed feedback fibre laser," *Electron. Lett.*, vol. 31, pp. 1440–1442, Aug. 1995.

[40] E. Rønnekleiv, "Frequency and intensity noise of single frequency fiber Bragg grating lasers." To appear in Opt. Fiber Technol., vol. 7, 2001.

[41] V. C. Lauridsen, J. H. Povlsen, and P. Varming, "Optimising erbium-doped DFB fibre laser length with respect to maximum output power," *Electron. Lett.*, vol. 35, pp. 300–302, Feb. 1999.

[42] V. C. Lauridsen, J. H. Povlsen, and P. Varming, "Design of DFB fibre lasers," *Electron. Lett.*, vol. 34, pp. 2028–2030, Oct. 1998.

[43] S. W. Løvseth and D. Y. Stepanov, "Dynamic analysis of multiple wavelength DFB fiber lasers." To be published in *IEEE J. Quantum Electron.*. Date of acceptance June 2001.

[44] S. W. Løvseth and E. Rønnekleiv, "Effects of grating errors in distributed feedback fiber lasers." To be presented at *Topical Meeting on Bragg Gratings, Photosensitivity, and Poling in Glass Waveguides (BGPP)*, (Stresa, Italy), paper BThB5, July 2001.

[45] E. Rønnekleiv, *Private communications with author*, 2000-2001.

Chapter 9

Fiber Distributed-Feedback Lasers Used as Acoustic Sensors in Air

Authors: Sigurd Weidemann Løvseth, Erlend Rønnekleiv, Jon Thomas Kringlebotn and Kjell Bløtekjær.

Published in *Applied Optics*, vol. 38, pp. 4821–4830, Aug. 1999.

Chaper 9 is not included due to copyright

Chapter 10

Conclusions and future work

This thesis is written as a collection of articles, and all chapters except the introductory ones have their individual concluding sections. The reader is thus referred to these or the thesis abstract for summaries of the results obtained. The aim of this chapter is to evaluate implications of the results given herein and elsewhere for the use of distributed feedback fiber lasers (DFB-FLs) in sensing and other applications, and point out some of the problems and challenges that remain to be addressed.

With their narrow linewidths and small size, DFB-FL sensors are promising candidates for a range of applications, although the technology does not seem to have matured enough yet to be commercially viable. For instance, a noise equivalent pressure as low as 13 dB re. 20 μPa/$\sqrt{\text{Hz}}$ in water is reported for an acoustic DFB-FL sensor with an elasto-plastic coating [1], opening up applications in underwater seismic systems and military surveillance. However, as discussed in Chapter 3, feedback from long delay lines due to Rayleigh scattering or discrete reflectors could destabilize the DFB-FLs in such applications. The tolerable feedback decreases with decreasing mirror reflectivities, longer feedback delay compared with the effective roundtrip time of the solitary laser, and increasing linewidth enhancement factor [2]. The latter value depends both on both the laser wavelength and saturation level of the gain medium [3]. A method is developed to measure the linewidth enhancement factor [4], but further systematic investigations should be made for this important laser characteristic. In any case, a wavelength selective optical attenuator between the DFB-FL and the lead fiber may ease the problems caused by external optical feedback, but in addition the laser should have a long and strong grating.

Unfortunately, stronger gratings can also enable higher order modes to lase, as reported in [5] and Chapter 3. These modes may have a higher output power than the fundamental mode, but are less stable and, because of their lower effective cavity finesse, they are more vulnerable to optical feedback, and the calculations of Chapter 7 indicate that they also generally

have a higher relative intensity noise (RIN) level. Unless the gain is high, the higher order modes could probably be avoided by writing error free gratings, as discussed in Chapter 4. It is especially important to minimize quadratic chirp. It may also be possible to increase the higher order mode threshold by apodizing the grating [6]. It is probably even better to window the gain distribution to fit the fundamental mode, as proposed in Chapter 5 , since this approach dramatically increases the higher order mode threshold without compromising the grating strength. More experimental work has to be done in order to determine if such lasers can be fabricated with high enough grating quality.

As is evident from [7] and Chapter 6, background loss leads to an exponential decrease of fundamental mode output power for high and increasing grating strength. The loss thus puts another limit to how much the grating strength could be increased. As discussed in Chapter 4, it can also be seen that low background loss would increase the threshold margin between higher order and fundamental modes. Unfortunately, UV exposure increases the loss at 1550 nm [8]. In addition, UV radiation seems to induce a spontaneous lifetime quenching of some of the Er^{3+} ions [9, 10]. As shown in Chapter 7, such quenching leads to an increased relative intensity noise (RIN) level and lower output power. The physical mechanisms behind UV induced lifetime quenching is poorly understood, and better knowledge about how the quenching is affected by grating fabrication and annealing conditions may potentially help reducing this problem.

If the lead fiber is short, the tolerable feedback level is higher and most of the problems mentioned above are not an issue. Fortunately, this will be the case in many potential sensor applications, for instance in structural monitoring, hostile industrial environments, and medicine.

Using a DFB-FL as a source for telecommunication networks or passive fiber sensors is in many ways less complicated than using it as a sensor, as an optical isolator can be put in front of the DFB-FL. However, in order to utilize the full potential of the narrow DFB-FL linewidth in sensor applications, it is important to shield the laser against environmental fluctuations, like for instance acoustic pressure and temperature waves, whose influence on unshielded DFB-FLs were discussed in Chapter 9. For telecom applications narrow linewidth is usually less important, but still it is probably advantageous to use some kind of temperature compensation to avoid drift.

The new breed of DFB-FLs with multiple fundamental modes, which are called multiple Λ or multiple wavelength DFB-FLs (MW-DFB-FLs) in this thesis, are exciting for a number of reasons. In Chapter 7 the calculated RIN spectra of DFB-FLs with up to five modes were shown. There was some increase of low frequency RIN with increasing number of modes, but the total RIN level was still low. Since the wavelengths of MW-DFB-FLs can be set both flexibly and accurately during production, a few cm of a single fiber can be used as a compact source for several channels simultaneously

in a WDM network. These lasers also have potential for microwave and soliton generation because of their stable beat frequency. However, MW-FBGs may have applications in other fields than telecommunications as well. DFB-FLs have most of their power distribution, and thus sensitivity to a measurand, concentrated around their grating phase shifts. Chapter 8 presented a new type of MW-DFB-FL sensor design, that utilizes this by superimposing multiple DFB-FL gratings with their phase shifts slightly spatially separated relative to each other. Such gratings can also be written in fibers without gain, and interrogated as passive gratings. In any case, they may provide high resolution both in space and measurand.

So far only dual fundamental longitudinal mode DFB-FLs have been reported experimentally [11]. As pointed out in Chapter 6, saturation of the UV induced refractive index shift might be a problem for MW-DFB-FLs, especially because it will cause the different wavelengths of the laser to see different reflectivities. It is not straightforward to implement a compensation measure since it has to take into account that the decay of the grating during annealing and aging varies with the UV saturation level. The potential of detrimental saturation effects increases with more than two wavelengths, but fortunately the required index shift scales only with about the square root of the number of channels when the relative phases between the subgratings are optimized. However, to fully utilize the potential of controlling the phase, the laser grating has to be written in one scan of the UV source, which will be difficult with known technology if the frequency separation between the gratings is large.

Recently, a DFB photonic crystal fiber laser was proposed [12]. A photonic crystal fiber has a microstructured cross section. Typically small air tubes are oriented parallel to the fiber axis in a quasi-periodic pattern. These holes offer high refractive index contrast with the surrounding glass, which enables engineering of the mode field distribution by inserting defects in the pattern. For instance, it is possible to make fibers with very small mode field diameter, and if an erbium-doped material is used there is hence potential for DFB-FLs with very low pump power threshold. Alternatively, fibers with very large mode field diameters can be engineered, which would enable high power DFB-FLs. The technology of photonic crystal fibers is still in its infancy, and at the moment these fibers are far too lossy to be good hosts for DFB-FLs. However, all the new design ideas for DFB-FLs indicate that fiber lasers will continue to be an exciting field full of challenges also in the coming years, even if almost 40 years of development has passed since the first fiber laser lit up the world.

References

[1] D. J. Hill and P. J. Nash, "In-water acoustic response of a coated DFB fibre laser sensor," in *14th International Conference on Optical Fiber Sensors* (A. G. Mignani and H. C. Lefèvre, eds.), vol. 4185 of *Proceedings of SPIE*, pp. 33–36, 2000.

[2] K. Petermann, "External optical feedback phenomena in semiconductor laser," *IEEE J. of Selected Topics in Q. Elect.*, vol. l, no. 2, pp. 480–487, 1995.

[3] K. E. Alameh, R. A. Minasian, and Y. Zhao, "A numerical model for the complex susceptibility of saturated erbium-doped amplifiers," *J. Lightwave Technol.*, vol. 33, pp. 855–860, Apr. 1997.

[4] E. Rønnekleiv, "Frequency and intensity noise of single frequency fiber Bragg grating lasers." To appear in Opt. Fiber Technol., vol. 7, 2001.

[5] E. Rønnekleiv, M. Ibsen, M. N. Zervas, and R. I. Laming, "Characterization of fiber distributed-feedback lasers with an index-perturbation method," *Appl. Opt.*, vol. 38, pp. 4558–4565, July 1999.

[6] D. Y. Stepanov, J. Canning, L. Poladian, R. Wyatt, G. Maxwell, R. Smith, and R. Kashyap, "Apodized distributed-feedback fiber laser," *Opt. Fiber Technol.*, vol. 5, pp. 209–214, 1999.

[7] V. C. Lauridsen, J. H. Povlsen, and P. Varming, "Optimising erbium-doped DFB fibre laser length with respect to maximum output power," *Electron. Lett.*, vol. 35, pp. 300–302, Feb. 1999.

[8] G. Meltz and W. W. Morey, "Bragg grating formation and germanosilicate fiber photosensitivity," in *Photoinduced Self-Organization Effects in Optical Fiber* (F. Oullette, ed.), vol. 1516 of *Proc. SPIE*, pp. 185–199, Dec. 1991.

[9] J. Hübner, T. Feuchter, C. V. Poulsen, and M. Kristensen, "Directly UV-written erbium doped waveguides," in *Photosensitivity and Quadratic Nonlinearity in Glass Waveguides: Fundamentals and Applications*, vol. 22 of *OSA Technical Digest Series*, 1995.

[10] E. Rønnekleiv, O. Hadeler, and G. Vienne, "Stability of an Er-Yb-doped fiber distributed-feedback laser with external reflections," *Opt. Lett.*, vol. 24, pp. 617–619, May 1999.

[11] M. Ibsen, E. Rønnekleiv, G. J. Cowle, M. N. Zervas, and R. I. Laming, "Multiple wavelength all-fibre DFB lasers," *Electron. Lett.*, vol. 36, pp. 143–144, Jan. 2000.

[12] T. Søndergaard, "Photonic crystal distributed feedback fiber lasers with bragg gratings," *J. Lightwave Technol.*, vol. 18, pp. 589–597, Apr. 2000.

Appendix A

Errata

One error have been found in each of the two published journal papers included in the thesis. The correct expression and value were used to calculate the presented results.

Chapter 6: Analysis of Multiple Wavelength DFB Fiber Lasers

A complex conjugation of κ is omitted in the second line of the transfer matrix given in equation (6b). The correct matrix is given below:

$$T_m^{q,q-1} = \begin{bmatrix} r_m + d_m s_m, & (g_2^* + j\kappa)\, s_m \\ -(g_2 + j\kappa^*)\, s_m, & r_m - d_m s_m \end{bmatrix} \tag{6b}$$

Chapter 9: Fiber Distributed-Feedback Lasers Used as Acoustic Sensors in Air

In Section 3, third paragraph, it is stated that an interferometer imbalance of 66 cm corresponds to a fringe sensitivity of 20 μrad/Hz. The correct value is 20 rad/GHz.

Appendix B

Table of Symbols and Acronyms

The chapters of this thesis are written independently, and there is some variation in notation. In addition, the acronyms used may be confusing to a novice in the field. Hopefully, the table of symbols and acronyms given here can help a confused reader. The table is alphabetically organized. Greek characters and other special symbols are categorized after their first letter in their English spelling. For instance, the symbol ϕ is found with the letter "p". Chapter references are not given for acronyms as these have the same meaning throughout the thesis. Only symbols that are referenced in the text are listed systematically. I.e., not all symbols used as intermediate values in mathematical expressions are mentioned, if they do not have a clear physical interpretation.

Symbol/ Acronym	**Chapter**	**Definition**
$*$	2,6,7	Complex conjugation
$\angle F_m$	6	Phase of feedback parameter F_m
A	2	Amplitude of right traveling wave
$\alpha = \frac{\Delta n_{\mathrm{unsat}}(z)}{\Delta n_{\mathrm{sat}}}$	6	Saturation parameter of UV induced index change.
α	9	Thermal expansion coefficient of the fiber material
a_0	4,6,7	Background loss
α_0	6	Average value of the saturation parameter α
α_1	6	Amplitude of sinusoidal modulation of the saturation parameter α
A_m	6,7	Amplitude of right traveling wave of laser mode m

Symbol/ Acronym	Chapter	Definition
$A_{m,q}$	6,7	A_m at the end of section q
a_p	4,6,7	Pump absorption at zero inversion
a_{pump}	6,7	Pump absorption at actual inversion
a_s	4,6,7	Signal absorption at zero inversion
B	2	Amplitude of left traveling wave
B	8	Birefringence
β	2	Optical propagation constant
$\bar{\beta}$	6,7	Average Bragg wave number of subgratings in a multiple wavelength structure
B_m	6,7	Amplitude of left traveling wave of laser mode m
$B_{m,q}$	6,7	B_m at the end of section q
c	8	Speed of light
c	9	Speed of sound
$C_{1,2,3,4}$	9	Constants in differential equation solution found by boundary conditions
C_g	7	Group velocity of fiber mode
c_p	9	Specific heat capacity of air at constant p
c_V	9	Specific heat capacity of air at constant volume
CW		Continuous wave
D	9	Fiber diameter
D_2	9	Empiric constant
$\delta = \beta - K$	2	Detuning (of prop. constant)
$\delta_{B,\max}$	4	Detuning between center and edge of grating (in frequency)
DBR		Distributed Bragg reflector
δ_{corr}	6	Correction in detuning due to saturation of the UV induced refractive index change
DFB		Distributed feedback
DFB-FL		Distributed-feedback fiber laser
ΔK	8	Nearest neighbor subgrating Bragg wavenumber difference
d_m	6,7	Parameter in coupled mode equations ($d_m = g_0 - a_o - j\delta_m$)
δ_m	6,7	Detuning of the propagation constant of mode m from $\bar{\beta}$
Δn	8	Refractive index modulation amplitude
$\Delta\nu$	6,7	Frequency difference between subgratings
$\Delta\nu$	9	Acoustically induced frequency shift

Symbol/ Acronym	Chapter	Definition
$\delta\nu_B$	4	Detuning between mean and local Bragg frequency of a grating
$\Delta\nu_B$	8	Nearest neighbor subgrating Bragg frequency difference
$\delta\nu_{B,\mathrm{RMS}}$	4	RMS detuning between mean and local grating Bragg frequency
Δn_i	9	Temperature and strain induced change of refractive index in polarization i
Δn_{loc}	6	Actual local UV induced index change
Δn_{max}	8	Maximum achievable UV induced refractive index modulation amplitude
$\Delta\nu_{q,r}$	8	Difference between the Bragg frequencies of subgrating q and r
Δn_{sat}	6	Saturation level of UV induced index change
$\Delta\nu_{\mathrm{tot}}$	9	Total laser frequency shift (both from temperature and pressure)
$\Delta n_{\mathrm{unsat}}(z)$	6	Intended local index change assuming linear UV response
$\Delta p(\boldsymbol{r})$	9	Harmonically varying acoustic pressure amplitude at position $\boldsymbol{r}$
$\Delta\phi$	6,7	Phase difference between subgratings at center
$\Delta\phi_{\mathrm{center}}$	4	Center phase shift value
$\Delta\phi_{\mathrm{err}}$	4	Grating phase error value
$\Delta\phi_{q,r}$	8	Phase difference between subgrating q and r
dq_{conv}	9	Heat transfer due to convection
D_s	2	UV spot size diameter
$D_{T_{\mathrm{air}}}$	9	Thermal diffusivity of air
Δt	7	Length of time step
ΔT	9	Amplitude of the harmonic temperature variation at the acoustic frequency
ΔT_0	9	Amplitude of adiabatic contribution from the acoustic wave of the harmonic temperature variation
$\Delta T(\boldsymbol{r})$	9	Harmonically varying acoustic temperature amplitude
$D_{T_{\mathrm{silica}}}$	9	Thermal diffusivity of fused silica
Δz	7	Length of grating section
$\Delta z_{\mathrm{res,max}}$	8	Highest achievable resolution
Δz_q	6,7	Length of section q of grating
E	9	Young's modulus
$\vec{E}$	8	Electric field of incoming optical wave

Symbol/ Acronym	Chapter	Definition
EDFA		Erbium doped fiber amplifier
ϵ_i	9	The ith strain vector element in the contracted matrix notation (See Ref. 31 of Chapter 9)
$\epsilon_{kl;i}$	9	Element (k,l) of the strain tensor in concentric layer i of the fiber
$E_m(z,t)$	6,7	Total local field of mode m at position z and time t
ϵ_{rr}	9	Radial strain
$\epsilon_{\theta\theta}$	9	Azimuthal strain
ϵ_{zz}	9	Longitudinal strain (as subscript it means constant ϵ_{zz})
f	9	Acoustic frequency
FBG		Fiber Bragg grating
f_L	7	Center frequency of the anti-phase intensity oscillation closest to the main relaxation oscillation peak
$F_m = g_2 \frac{A_m}{B_m}$	6	Feedback parameter of mode m
FWHM		Full width half maximum
f_R	7	Relaxation oscillation center frequency
g	9	Acceleration due to gravity
G	5	Gain apodizing function
γ	2	Damping parameter in transfer matrix
$\gamma = c_p/c_V$	9	Adiabatic constant (in air)
g_0	2,6,7	Amplitude gain coefficient
g_2	2,6,7	Gain grating coefficient
g_{2r}	6,7	$2r$'th order Fourier component of gain with respect to $\bar{\beta}$
$g_{k,0}$	6,7	Amplitude gain coefficient of gain medium k
$g_{k,2}$	6,7	Gain grating coefficient of gain medium k
$g_{k,2r}$	6,7	$2r$'th order Fourier component of gain with respect to $\bar{\beta}$ for gain medium k
g_{loc}	7	Total local gain amplitude
$g_{\mathrm{loc},k}$	7	Local gain amplitude of gain medium k
γ_m	6,7	Damping parameter in transfer matrix of mode m
g_p	4,6,7	Pump gain at full inversion
g_s	4,6,7	Signal gain at full inversion
$g_{\mathrm{ss},k,2n}$	7	Steady state $2n$'th order Fourier component of gain with respect to $\bar{\beta}$ for gain medium k

Symbol/ Acronym	Chapter	Definition
$g_{\mathrm{ss,loc},k}$	7	Steady state local gain amplitude of gain medium k
$g_{\mathrm{unsat},k}$	6,7	Unsaturated gain of gain medium k
$\hbar$	7	Planck's constant divided by 2π
$h_{\mathrm{beat}/2} = \frac{l}{l_{\mathrm{beat}/2}}$	6	Number of half beat lengths between subgratings
$H_i^{(2)}$	9	The second Hankel function of order i
$i_{f,m}$	7	Spontaneous emission amplitude into the forward mode
$i_{b,m}$	7	Spontaneous emission amplitude into the backward mode
I	7	Inversion
I_i	6	The modified Bessel function of the first kind and order i
ISO		(Optical) isolator
j	2,6-9	Imaginary unit
J_i	9	Bessel function of the first kind and order i
k	2	Boltzmann's constant
K	2	Bragg wave number
κ	2-7,9	(Complex) Refractive index coupling coefficient
κ	9	Thermal conductivity
$K_{B,i}$	7	Bragg wave number of subgrating i
$K_{1,2,3;i}$	9	Constants of the Lamé solution in concentric fiber layer i
K_i	6	Bragg wave number of subgrating i
κ_i	6-8	Coupling coefficient of subgrating i
$\kappa_{\max}$	8	Maximum coupling coefficient
$\kappa_{\mathrm{sat}} = \frac{\kappa_{\mathrm{unsat}}}{\alpha_1}$	6	Saturated coupling coefficient
$\kappa_{\mathrm{tot}}(z)$	8	Total complex coupling coefficient
κ_{th}	4	Threshold coupling coefficient
κ_{unsat}	6	Coupling coefficient expected from a linear response to UV
l	2-4,6	Total grating length
L	5	Total grating length
Λ	6-8,10	Bragg grating pitch
λ_B	1,8	Bragg wavelength
$l_{\mathrm{beat}/2}$	6	Half beat length between subgratings
λ_{B_i}	8	Bragg frequency in polarization i
l_{eff}	4	Effective cavity length
Λ_{err}	4	Pitch of detuning error

Symbol/ Acronym	Chapter	Definition
Λ_g	1,2	Bragg grating pitch
Λ_i	6,7	Pitch of subgrating i
λ_p	8	Pump wavelength
LPF		Low pass filter
Λ_{pm}	2	Phase mask pitch
M	8	Amplitude of any measurand
μ	9	Poisson ratio
MFD		Mode field diameter
μ_m^+	7	Time derivative of A_m normalized with respect to A_m and C_g
μ_m^-	7	Time derivative of B_m normalized with respect to B_m and C_g
MW-DFB-FL		Multiple wavelength DFB-FL
MW-FBG		Multiple wavelength FBG
MZ		Mach-Zehnder interferometer
n	6,9	Effective (average) refractive index
N	8	An integer
ν	9	Laser frequency
n_1	9	Empiric constant
∇^2	9	Laplace operator
ν_B	8	Bragg frequency of grating
ν_{B_i}	8	Bragg frequency of grating in polarization i
n_{eff}	1,7	Effective refractive index
NEP		Noise equivalent power
N_g	6-8	Number of subgratings
N_{gm}	4,6,7	Number of gain media
n_i	8,9	Effective index in polarization i
N_{last}	7	Number of gain Fourier coefficients calculated
N_m	6,7	Total number of modes
ν_q	8	Laser/transmission notch frequency in subgrating number q
N_s	6,7	Total number of segments in transfer matrix calculations
Nu_D	9	Nusselt number with respect to D
$\overline{\text{Nu}_D}$	9	Nusselt number averaged over the fiber surface
ω	9	Acoustic angular frequency
OCDR		Optical coherence domain reflectometry
OFDR		Optical frequency domain reflectometry
ω_m	6,7	Angular optical frequency of mode m
OSA		Optical spectrum analyzer

Symbol/ Acronym	Chapter	Definition
OTDR		Optical time domain reflectometry
p	9	Pressure (as subscript it means constant p)
$\Phi_0(z)$	6	Intended phase of complex coupling function ignoring saturation effects
PC		Polarization controller
P_c	6,7	Standing wave phasor
ϕ_i	6-8	Phase of subgrating i
p_{ij}	9	The (i,j)'th element of the elasto-optical tensor of silica in the contracted matrix notation (See Ref. 31 of Chapter 9)
P_p	1,4,6,7	Pump power
P_q	8	Power distribution at the notch (main resonance) frequency of subgrating q
Pr	9	Prandtl number
P_s	7	Local total signal (DFB-FL) power
$P_{\mathrm{sat},k}$	6,7	Saturation power, gain medium k
$P_{s,l}$	1	Left signal power
P_{sp}	4,6,7	Spontaneous emission power per length
PS_q	8	Phase shift of subgrating q
$P_{s,r}$	1	Right signal power
p_{static}	9	Static pressure (i.e. not varying at the acoustic frequency)
P_{tot}	6,7	Sum power of the backward and forward traveling waves for all laser modes. (Total average power)
PZT		Piezoelectric translator/lead zirconate titanate
q	9	Heat per unit volume
r	9	Distance from fiber axis
$\boldsymbol{r}$	9	Spatial position vector
R	4	Mirror reflectivity
R	7	Spontaneous emission energy per length
R	9	Fiber radius
ρ	9	Density of mass
Ra_D	9	Rayleigh number with respect to D
Re_D	9	Reynolds number with respect to D
RIN		Relative intensity noise
RIN_p	7	Relative intensity noise of pump
RMS		Root mean square
$R(\nu)$	8	Reflectivity as a function of optical frequency ν

Symbol/ Acronym	Chapter	Definition
r_{wl}	4,6,7	Pump to signal wavelength ratio
t	2	Transmission coefficient
t	7,9	Time
T	2,9	Temperature (as subscript it means constant T)
T	2	Transfer matrix
τ	7	Unquenched spontaneous emission life time
$T_{a,b}$	2	Element of a'th row and b'th column of matrix T
$T(\nu)$	8	Transmissivity as a function of optical frequency ν
$T_m^{q_2,q_1}$	6	Transfer matrix of mode m from the end of section q_1 to the end of section q_2
$(T_m^{q_2,q_1})_{a,b}$	6	(a,b)'th element of matrix $T_m^{q_2,q_1}$
T_{static}	9	Static temperature (i.e. not varying with the acoustic frequency)
UV		Ultra violet
v	9	Kinematic viscosity
V	9	Volume
V	9	Cross flow velocity
VA		Variable attenuator
v_{drift}	9	Convection drift velocity
v_{ref}	9	Reference velocity which v_{drift} should be compared to
w	5	Gain window width
WDM		Wavelength division multiplexing/multiplexer
WLS		White light source
ξ	9	Thermo-optic coefficient of the fiber material
$x_{s,1}$, $x_{s,2}$	7	Gaussian, normalized variables ($< x_{s,1}^2 > + < x_{s,2}^2 >= 1$)
ξ_k	4,6,7	Fraction of erbium ions belonging to gain medium k
Y_i	9	Bessel function of the second kind of order i
z	4-8	Position along grating axis
ζ_k	4,6,7	Spontaneous emission quenching factor of gain medium k
z_{err}	4	Phase error position
σ_{err}	4	Spatial frequency of detuning error
z_q	8	Position of phase shift in subgrating q
σ_{zz}	9	Longitudinal stress (as subscript it means constant σ_{zz})

Publication List

Journal publications

1. S. W. Løvseth and E. Rønnekleiv, "Fundamental and higher order mode thresholds of DFB fiber lasers." Submitted to *J. Lightwave Technol.*, May 2001.[1]

2. S. W. Løvseth and D. Yu. Stepanov, "Dynamic analysis of multiple wavelength DFB fiber lasers." To be published in *IEEE J. Quantum Electron.*. Date of acceptance June 2001.[1]

3. S. W. Løvseth and D. Yu. Stepanov, "Analysis of multiple wavelength DFB fiber lasers," *IEEE J. Quantum Electron.*, vol. 37, pp. 770–780, June 2001.[1]

4. C. Laliew, S. W. Løvseth, X. Zhang, and A. Gopinath, "A linearized optical directional-coupler modulator at 1.3 μm," *J. Lightwave Technol.*, vol. 18, pp. 1244–1249, September 2000.

5. S. W. Løvseth, E. Rønnekleiv, J. T. Kringlebotn, and K. Bløtekjær, "Fiber distributed-feedback lasers used as acoustic sensors in air," *Appl. Opt.*, vol. 38, pp. 4821–4830, Aug. 1999.[1]

Conference publications

6. S. W. Løvseth and E. Rønnekleiv, "Effects of grating errors in distributed feedback fiber lasers." To be presented at *Topical Meeting on Bragg Gratings, Photosensitivity, and Poling in Glass Waveguides (BGPP)*, Stresa, Italy, paper BThB5, July 2001.

7. M. A. Englund, S. W. Løvseth, D. Yu. Stepanov, and E. C. Mägi, "Selective gain tuning in erbium doped fibres." Submitted to the postdeadline session of *OECC / IOOC 2001 Conference - Incorporating ACOFT*, (Sydney, Australia), July 2001.[1]

8. S. W. Løvseth and D. Yu. Stepanov, "Multiple wavelength operation of distributed feedback fiber lasers," in *2000 Conference on Lasers*

and Electro-Optics Europe Conference Digest, p. 317 (paper CThE51), IEEE, Sept. 2000.

9. S. W. Løvseth and D. Yu. Stepanov, "Analysis of DFB fiber laser multiple wavelength operation," in *25th Australian Conference on Optical Fibre Technology - Program and Proceedings*, (Canberra), pp. 77–79, Australian National University, June 2000.

10. S. W. Løvseth and E. Rønnekleiv, "Stability of distributed feedback fiber lasers with optical feedback," in *Technical Digest of Norwegian Electrooptics Meeting 1999*, p. 19, Optics Section of Norwegian Physical Society, 1999.

11. E. Rønnekleiv and S. W. Løvseth, "Stability of distributed feedback fiber lasers with optical feedback," in *13th International Conference on Optical Fiber Sensors* (B. Y. Kim and K. Hotate, eds.), vol. 3746 of *Proceedings of SPIE*, pp. 466–469, 1999.[1]

12. S. W. Løvseth, K. Bløtekjær, and J. T. Kringlebotn, "Contributions to wavelength shifts of DFB fiber lasers used as acoustic sensors in air.," in *European Workshop on Optical Fiber Sensors* (B. Culshaw and J. D. C. Jones, eds.), vol. 3483 of *Proceedings of SPIE*, pp. 69–73, 1998.

13. C. Laliew, S. W. Løvseth, X. Zhang, and A. Gopinath, "Synthesis of the optical modulator response," in *International Topical Meeting on Microwave Photonics. Technical Digest*, pp. 40–41 (paper MC4), IEEE, 1998.

14. S. W. Løvseth, C. Laliew, and A. Gopinath, "Synthesis of amplitude response of optical directional coupler modulators," in *1997 IEEE MTT-S INTERNATIONAL MICROWAVE SYMPOSIUM DIGEST* (G. A. Koepf, ed.), vol. 3, (New York, USA), pp. 1717–1720 (paper TH3F–59), Institute of Electrical and Electronics Engineers, 1997.

15. S. W. Løvseth, C. Laliew, and A. Gopinath, "Amplitude response of optical directional coupler modulators by Fourier transform technique," in *Proceedings 8th European Conference on Integrated Optics (ECIO'97)*, (Stockholm, Sweden), pp. 230–233 (paper EThC4), Royal Institute of Technology, 1997.

Thesis

16. S. W. Løvseth, "Directional coupler using the linear electrooptic effect for use as modulators or filters," Diploma Thesis, Physics Department, Norwegian Institute of Technology, Trondheim, Norway, 1996.

Media Coverage

17. S. Harris, "Fibre lasers make optoelectronic ears," *Opto & Laser Europe*, no. 67, p. 17, 1999.

18. S. Harris, "DFB fibre lasers hear sounds in air." in http://optics.org, Aug. 1999.

[1]The paper is included in this thesis.